Does KSHV induce virus specific specialised ribosomes during infection?

James Murphy

Submitted in accordance with the requirements for the degree of

Doctor of Philosophy

The University of Leeds

Faculty of Biological Sciences

School of Molecular and Cellular Biology

June 2021

The candidate confirms that the work submitted is his own and that appropriate credit has been given where reference has been made to the work of others.

Acknowledgements

I would firstly like to express my gratitude to my supervisors, Prof. Adrian Whitehouse and Dr. Julie Aspden for their incredible guidance, support, and trust throughout my PhD. Both Ade and Julie are the most engaging and inspiring supervisors that I've been lucky enough to have worked for. They have always made whatever time is needed to support my research and have always had an open door for advice and I could not have asked for better mentors or supervisors.

Secondly, I would like to express a huge appreciation to all my colleagues and friends in the Whitehouse and Aspden groups. Both groups are a wonderful place to work with such an amazing collaborative and friendly environment. You have all made the PhD so much more fun and enjoyable and thank you for all the help and advice you've all given me along the way.

Most importantly, I would like to give an enormous thank you to Dr. Sophie Schumann and Ms. Elena Harrington, a.k.a 'Team Ribo'. Sophie has help to guide and develop me as a scientist throughout my PhD by generously passing on her wisdom and expertise. Ellie is one of the most dependable and hardworking people I know. I am so grateful for the team environment we have as we collaborate and help each other out, from the day-to-day experiments to long term planning and analysis. I would like to acknowledge Sophie for carrying out the pre-ribosomal complex pulldowns which were sent for quantitative mass spectrometry and to Ellie for carrying out the final viral genome replication and reinfection assays.

Many thanks to Dr. Elton Vasconcelos for all the analysis that he performed on the ribosome profiling next generation sequencing data.

I am grateful to the Wellcome Trust for funding my PhD and enabling the first-year rotation projects and the flexibility in design of my main PhD project.

I would also like the express an enormous appreciation to my brother and parents. They are all so supportive and encouraging of everything I do and I am so grateful for the opportunities my parents have given me that put me in a position which I have been able to pursue a PhD.

Last but definably not least, I am so grateful for my wonderful wife, Kat, who is the most kind, supportive, and loving person I know and is always there for me in the best times and the hardest. You have made this journey so much easier and more enjoyable.

Abstract

Historically, ribosomes have been viewed as unchanged homogeneous units with no intrinsic regulatory capacity for mRNA translation. However, over the last 20 years many reports have shown heterogeneity in the ribosome population of cells and more recently studies have demonstrated phenotypic relevance of these specialised ribosomes. Gene expression is controlled at every level from, mRNA transcription through to protein turnover. Ribosome specialisation offers another option for the regulation of gene expression whereby distinct subpopulations of ribosomes preferentially translate specific groups of mRNAs.

No virus encodes machinery to translate its own proteins. Furthermore, viruses have been shown to co-opt and manipulate all areas of cellular life to enhance their replication. Emerging evidence has started to reveal that viruses can target ribosomes to create virus-specific specialised ribosomes during infection.

This thesis therefore investigates whether Kaposi's sarcoma-associated herpesvirus (KSHV) alters host cell ribosome composition to enhance the production of viral proteins. KSHV was identified to target pre-40S ribosome subunits for modification during ribosome biogenesis. KSHV increases the association of two ribosome biogenesis factor complexes, BUD23-TRMT112 and NOC4L-NOP14-EMG1, with pre-40S ribosome subunits. The KSHV protein ORF11 also binds to pre-40S ribosome subunits, most likely facilitating the above increased interactions.

Following these findings BUD23 was demonstrated to be essential for the productive and efficient lytic replication of KSHV and more precisely the translation of late lytic genes. Using the powerful technique of ribosome profiling BUD23 was identified to increase the translation of KSHV upstream open reading frames in late lytic KSHV genes or genes involved in late gene expression.

Overall, this thesis provides evidence that KSHV manipulates ribosome biogenesis during lytic replication to create ribosomes that are specialised for the effective translation of its late lytic mRNAs.

Contents

List of figures

List of tables

Abbreviations

< less than

> greater than

~ approximately

3D three dimensional

α alpha

Ψ pseudouridine

aa amino acid

aa-tRNA aminoacyl-tRNA

ABCE1 ABC-type ATPase

Acp aminocarboxypropylation

ADP adenosine diphosphate

AIDS acquired immune deficiency syndrome

ANOVA analysis of variance

AP-1 activator protein 1

APS ammonium persulfate

ATP adenosine triphosphate

AZIN1 antizyme inhibitor 1

β beta

BCA bicinchoninic acid

BCBL body cavity based lymphoma

Bcl2 B-cell lymphoma 2

bp base pair

BSA bovine serum albumin

BST2 bone marrow stromal cell antigen 2

bZIP basic leucine zipper domain

CAML calcium modulating ligand

CATC capsid associated tegument complex

Casp3 caspase 3

CDK cyclin-dependent kinase

cDNA complementary DNA

CDS coding sequence

CP central protuberance

CRM1 chromosomal region maintenance 1

CT cycle threshold

DAPI 4', 6-diamidino-2-phenylindole

DBA Diamond-Blackfan anemia

DC-SIGN dendritic cell-specific intercellular adhesion molecule-3-grabbing non-integrin

dH_20 distilled water

DIMT1 dimethyladenosine transferase 1

DKC1 dyskerin pseudouridine synthase 1

DMEM Dulbecco's modified Eagles medium

DMSO dimethyl sulphoxide

DNA deoxyribonucleic acid

DNA-PK DNA-dependent protein kinase

DNase deoxyribonuclease

dNTP deoxyribonucleoside (5'-) triphosphate

DRG1 developmentally regulated GTP binding protein 1

ds double stranded

DT differential translation

DTT dithiothreitol

DUSP12 dual specificity phosphatase 12

EBPα enhancer binding protein alpha

EBV Epstein-Barr virus

ECL enhanced chemiluminescence

EDTA ethylenediaminetetraacetic acid disodium salt

eEF eukaryotic elongation factor

EFL1 elongation factor like GTPase 1

eIF eukaryotic initiation factor

EM electron microscopy

EMG1 essential for mitotic growth 1

ENP1 essential nuclear protein 1

eRF eukaryotic release factor

ERI1 exoribonuclease 1

ERK extracellular signal-regulated kinase

ETS external transcribed spacer

FBS foetal bovine serum

FDR false discovery rate

FGARAT formyl-glycinamide-phosphoribosyl-amidotransferase

FLIP FLICE-inhibitory protein

FP foot print

GAPDH glyceraldehyde 3-phosphate dehydrogenase

gB glycoprotein B

GCN2 general control nonderepressible 2

GDP guanosine diphosphate

gH glycoprotein H

gL glycoprotein L

gp glycoprotein

GNL2 GTP-binding nucleolar protein 2

GTP guanosine triphosphate

h helix

HAART highly active antiretroviral therapy

HBV hepatitis B virus

HCl hydrochloric acid

HCMV human cytomegalovirus

HCV hepatitis C virus

Hey1 hairy/enhancer-of-split related with YRPW motif 1

HHV human herpesvirus

HIC human I-mfa domain-containing protein

HIF hypoxia-inducible factor

HIV human immunodeficiency virus

hNIC human notch intracellular

Hog1 high osmolarity glycerol 1

Hox homeobox

HRP horseradish peroxidase

HSC70 heat shock protein 70

HSP90 heat shock protein 90

hTREX human transcription/export complex

HSV-1/2 herpes simplex virus 1/2

HVS herpesvirus saimiri

IAP inhibitors of apoptosis

ICAM-1 intercellular adhesion molecule-1

IF immunofluorescence

IFN interferon

IgG immunoglobulin G

IL-6 interleukin-6

IR internal repeat

IRES internal ribosome entry site

IRF interferon regulatory factor

ISRE interferon-stimulated response element

ITAF IRES-transacting factor

ITAM immunoreceptor tyrosine-based activation motif

ISG20L2 interferon-stimulated 20 kDa exonuclease-like 2

ITS internal transcribed spacer

JNK c-Jun aminoterminal kinase

KAP1 Krüppel-associated box domain-associated protein 1

KCl potassium chloride

KS Kaposi's Sarcoma

KSHV Kaposi's Sarcoma associated herpesvirus

LANA latency-associated nuclear antigen

LC liquid chromatography

LF left foot

lncRNA long non-coding RNA

LSU large subunit

m methylation

m^7G 7-methyl-guanine

MCD multicentric Castleman's disease

MCP minor capsid protein

MDM1 mouse double-minute 1

MEK mitogen-activated protein kinase kinase

Met-$tRNA^{Met}_i$ initiator tRNA

$MgCl_2$ magnesium chloride

MHC major histocompatibility complex

MHV-68 murine gammaherpesvirus 68

MICB MHC class I chain-related protein B

MIP macrophage inflammatory protein

miRNA microRNA

mRNA messenger RNA

MRTO4 mRNA turnover protein 4 homolog

MS mass spectrometry

N sample size

Na_2CO_3 sodium carbonate

$NaBH_4$ sodium borohydride

NaCl sodium chloride

$NaHCO_3$ bicarbonate of soda

NAT10 N-acetyltransferase 10

ncRNA non-coding RNA

NEB New England Biolabs

NF-κB nuclear factor kappaB

NGS next generation sequencing

NLS nuclear localisation signal

NMD3 nonsense-mediated mRNA decay protein 3

NOP nucleolar protein

NOC4L nucleolar complex associated 4 homolog

NP nucleoprotein

NP40 tergitol-type NP-40

NPC nuclear pore complex

NPP nascent polypeptide

NSUN NOP2/Sun RNA methyltransferase

Oct-1 octamer-binding protein 1

ORF open reading frame

ori-Lyt lytic origin of DNA replication

ori-P latent origin of DNA replication

p p-value

PABP polyadenylate binding protein

PABPC1 polyadenylate-binding protein cytoplasmic 1

PAGE polyacrylamide gel electrophoresis

PAN polyadenylated nuclear

PARP-1 poly(ADP-ribose) polymerase I

PBS phosphate buffered saline

PCR polymerase chain reaction

PD pulldown

PDCD2L programmed cell death 2 like

PEL primary effusion lymphoma

PELP1 proline, glutamate and leucine rich Protein 1

PERK protein kinase R-like endoplasmic reticulum kinase

PET peptide exit tunnel

PI3K phosphoinositide 3-kinase

Pim proviral integration site for Moloney murine leukemia virus

PML promyelocytic leukemia

PNO1 partner of NOB1

PNK polynucleotide kinase

POL polymerase

polyA polyadenylated

Puro puromycin

PTC peptidyl- transferase centre

PTM post-translational modification

QC quality control

qPCR quantitative PCR

QV quality value

Raf rapidly accelerated fibrosarcoma

Rb retinoblastoma

RBF ribosome biogenesis factor

Rbl2 retinoblastoma-like protein 2

RBP-jκ recombination signal-binding protein 1 for J-kappa

RCA regulator of complement activation

RecQL RecQ like helicase

RF right foot

RIG-I retinoic acid-inducible gene I

RIM101 regulator of IME2 protein 1

RNA ribonucleic acid

RNase ribonuclease

RNP ribonucleoprotein particles

ROS reactive oxygen species

RPL large ribosomal subunit protein

RPMI Roswell Park Memorial Institute medium

RPS small subunit ribosomal protein

RRE RTA response element

rRNA ribosomal RNA

RRP ribosomal RNA-processing protein

RSK ribosomal S6 kinase

RSL24D1 ribosomal L24 domain containing 1

RT reverse transcriptase

RTA replication and transcription activator

SAF-A scaffold attachment factor A

SBDS Shwachman-Bodian-Diamond syndrome protein

SCP smallest capsid protein

Scr scrambled

SD standard deviation

SDS sodium dodecyl sulphate

shRNA small hairpin RNA

siRNA small interfering RNA

SNORA14 snoRNA 14

snoRNA small nucleolar RNA

snoRNP small nucleolar ribonucleoprotein

snRNA small nuclear RNA

sORF small open reading frame

SOX shutoff and exonuclease

ssDNA single stranded DNA

SSU subunit

SUMO small ubiquitin-like modifier

T Triangulation number

TBS-T tris buffered-saline and tween-20

TC ternary complex

TEMED N-N-N’-N’-tetramethylethylenediamine

TEX10 testis expressed 10

TMT tandem mass tagging

Topo topoisomerases

TLR toll-like receptors

TR terminal repeat

Tris tris(hydroxymethyl)aminoethane

tRNA transfer RNA

U unit

uAUG uORF AUG start site

uORF upstream open reading frame

US United States of America

UTP U3 small nucleolar RNA-associated protein

UTR untranslated region

UV ultraviolet

V volts

VSV vesicular stomatitis virus

v/v volume per volume

vCCL viral CC-chemokine ligands

VEGF vascular endothelial growth factor

vFLIP viral FLICE inhibitory protein

VGF nerve growth factor inducible

vGPCR viral G protein-coupled receptors

vIL-6 viral interleukin 6

vIRF viral interferon regulatory factor

VPS34 vacuolar protein sorting 34

VZV varicella-zoster virus

WCL whole cell lysate

WDR18 WD repeat domain 18

w/v weight per volume

XRN2 5'-3' Exoribonuclease 2

ZCCHC4 zinc finger CCHC-type containing 4

Units

% percentage

°C degrees Celsius

Å angstrom

g gram

g gravitational force

h hours

kDa kilodalton

Kb kilobase

Kbp kilobase pair

M molar

ml millilitre

mM millimolar

mm millimetre

min minute

µg microgram

µl microlitre

µm micrometre

µM micromolar

ng nanogram

nm nanometre

nM nanomolar

S svedberg

Bases

A adenine

C cytosine

G guanine

T thymine

Chapter One

~

Introduction

1 Introduction

1.1 Herpesviridae

The *Herpesviridae* is a family of large, enveloped viruses containing a tegument layer surrounding an icosahedral capsid (T=16) which holds a large linear double stranded DNA genome (125-290 kb). Herpesviruses form persistent dormant infections in the host, termed latency, but can reactivate into a lytic replication cycle where new virus particles are produced to propagate and maintain the infection. The *Herpesviridae* family belongs to the order *Herpesvirales*, whose common ancestor dates back about 400 million years[1] and comprises three families, three subfamilies, 19 genera, and 122 species[2]. The three families of the *Herpesvirales* are: the *Alloherpesviridae*, which infect fish and amphibians, the *Herpesviridae*, including all mammalian, avian and reptilian herpesviruses, and the *Malacoherpesviridae*, which cause disease in invertebrates[3]. The only genetic element to share total conservation across the order is the ATPase subunit of the DNA terminase, a protein involved in the packaging of DNA during virion maturation[4]. Although viruses are generally classified based on their phenotypic properties, the advent of genome sequencing has proven a powerful tool for taxonomy and identification of novel viruses[5].

The *Herpesviridae* is by far the largest family in the *Herpesvirales* order and was further divided into three subfamilies in 1979, *Alpha-, Beta-* and *Gammaherpesvirinae* (Figure 1.1)[6]. Over 100 species have been classified in the *Herpesvirales* family which share a total of 40 conserved genes mainly involved in capsid structure and DNA replication[1,2].

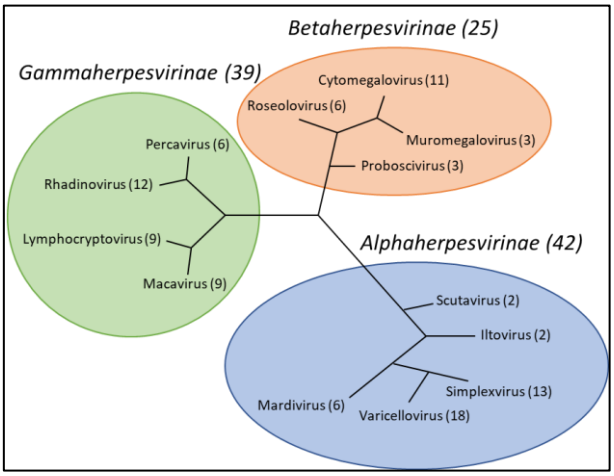

Figure 1.1 Herpesviridae family structure. Values represent the number of viral species classified into each subfamily and genus.

1.1.1 Alphaherpesvirinae

The *Alphaherpesvirinae* is the largest subfamily in the *Herpesviridae* with 42 classified members across five genera, and it is the most divergent of the subfamilies (Figure 1.1). This subfamily of herpesviruses establishes latent infection primarily in neuronal sensory ganglia cells, with outbreaks of lytic replication normally occurring in epidermal cells[7]. The members

of the *Alphaherpesvirinae* subfamily are distinct due to their relatively short replication cycle and rapid spread in cultured cells[8]. Alphaherpesviruses have a broad host range covering mammals, reptiles, and birds[2]. There are three *Alphaherpesviruses* that infect humans: herpes simplex virus type I and II (HSV-1/2) from the *simplexvirus* genus and varicella zoster virus (VZV) from the *varicellovirus* genus. These viruses are also known as human herpesvirus (HHV) type 1, 2, and 3 (HSV-1, HSV-2, and VZV respectively).

1.1.2 Betaherpesvirinae

Within the Herpesviridae the *betaherpesvirinae* subfamily is the smallest, with 25 classified members across four genera (Figure 1.1). These viruses primarily establish a latent infection within progenitor lymphoreticular cells, most commonly monocytes and T cells, with lytic replication occurring in more differentiated lymphoreticular cells[9]. *Betaherpesviruses* have a long reproductive cycle and therefore infections progress slowly *in vitro*, frequently forming enlarged cells termed cytomegalic cells[10]. There are three *betaherpesviruses* that infect humans: HHV-5, also known as human cytomegalovirus (HCMV) from the genus *cytomegalovirus*, and HHV-6 and HHV-7 from the genus *roseolovirus*.

1.1.3 Gammaherpesvirinae

The *gammaherpesvirinae* subfamily includes 39 classified members across four genera (Figure 1.1), with members having a restricted host range limited to species only of the order or family of their natural host[8]. *Gammaherpesviruses* latently infect lymphoblastoid cells, with most viruses specific for either B or T lymphocytes, whereas species mostly lytically replicate in epithelial and endothelial cells[11,12]. Only two *gammaherpesviruses* have been identified to infect humans: Epstein-Barr virus (EBV, HHV-4) of the *lymphocryptovirus* genus and Kaposi's sarcoma-associated herpesvirus (KSHV, HHV-8) of the *rhadinovirus*.

1.2 Kaposi's sarcoma-associated herpesvirus (KSHV)

This thesis focuses on the herpes virus KSHV which is the most recently identified HHV, discovered by Chang and Moore in 1994 who initially isolated herpes-like DNA fragments from Kaposi's sarcoma (KS) lesions. This along with many further studies has categorised KSHV as one of the seven human oncoviruses[13–15].

1.2.1 Associated diseases

KSHV is the aetiological agent of the endothelial tumor KS in addition to two lymphoproliferative disorders: primary effusion lymphoma (PEL) and multicentric Castleman's disease (MCD)[16,17].

The global distribution of these KSHV-associated diseases are closely correlated with the prevalence of acquired immune deficiency syndrome (AIDS), as these diseases typically only develop in immunocompromised patients[16]. KS is the most widely studied of the three KSHV-associated diseases; in sub-Saharan Africa where KSHV and AIDS are endemic the incidence of KS is very high with age standardised rates of >0.59 per 100,000 (Figure 1.2). In addition to sub-Saharan Africa there is also a high prevalence of KS in South America and Mediterranean countries (Figure 1.2). However, in much of the rest of the world the prevalence of KS in the general community is relatively low (Figure 1.2). Notably in regions of high incidence, specific communities do account for the higher prevalence of KSHV and its associated cancers, such as elderly men, migrants from endemic areas, and men who have sex with men[18]. However, the main cause of these cancers in non-endemic regions are immunosuppressive therapies mainly taken by patients after organ transplants or for chemotherapy.

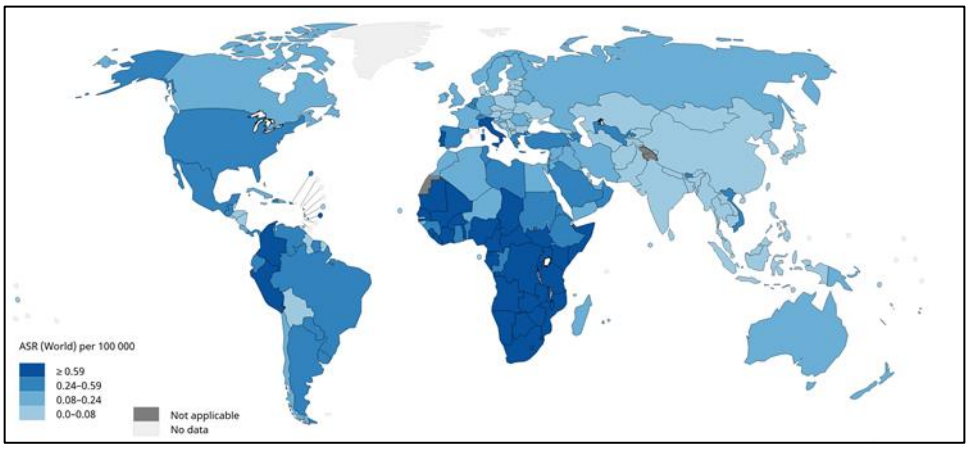

Figure 1.2 Global incidence rates of KS in 2018. Age standardised rates (ASR) per 100,000 population of each country. Data provided by GLOBACAN.

KSHV has been shown to be present in saliva, blood, semen, and cervico-vaginal secretions with transmission usually occurring via saliva exchange and sexually[19–23]. In endemic regions the transmission of KSHV more frequently occurs through saliva exchange during childhood[24]. However, in areas where KSHV is not endemic sexual transmission of the virus is more common[24].

Uniquely for KSHV, both the latent and lytic replication cycles play important roles in the development and progression of these KSHV-associated cancers[25]. Most of the latently-expressed viral proteins and miRNAs have been implicated in cancer development and progression[26–29]. However, lytic replication enables the dissemination of new virus particles from the B cell reservoir to other cell types, including endothelial cells, where these cancers develop. Furthermore, at disease sites lytic replication maintains episome copy numbers[30]. Finally, abortive lytic replication in KSHV associated tumours, where only the early KSHV genes are expressed, promotes tumor growth[31].

Despite the considerable advances in understanding of the KSHV life cycle and related pathologies since its discovery, presently there are still no vaccines or effective directly targeted therapeutic options available for the prevention or treatment of KSHV-associated cancers. At present, most treatment options aim to restore the patient's immune system to limit tumor progression.

1.2.1.1 Kaposi's Sarcoma (KS)

KS was first described in 1872, a long time before its aetiological agent was discovered in 1994[32]. A Hungarian dermatologist, Moritz Kaposi, first described the ''brownish red–to–bluish-red cutaneous nodules that tended to enlarge into dome-shaped tumours.'' Originally, he studied five patients over two to three years, all of whom died from the disease. He described the disease as neoplasms throughout the body especially on the mucosa, larynx, trachea, stomach, liver, and colon.

KS Type	Epidemiology	Clinical Distribution	Behaviour
Classical	Elderly males, generally in the Mediterranean.	Skin of the lower extremities, but mucosal and visceral lesions may develop.	Indolent
Epidemic	AIDS associated children and adults, global but high prevalence in Sub Saharan Africa.	Disseminated mucocutaneous and visceral involvement.	Aggressive
Endemic	Children and adults, in equatorial Africa.	Multiple localized skin tumours, involving lower extremities and/or lymph nodes.	Progressive
Iatrogenic	Immunosuppressed patients.	Localised mucocutaneous or disseminated KS, with possible visceral lesions.	Variable

Table 1.1 Clinical categories of KS and associated traits.

The geographical distribution of KS and its association with immunosuppression meant that by the 1960s it was suggested that its cause might be an infectious agent[33,34]. Due to the onset of the AIDS epidemic in 1989, KS morbidity drastically increased, with 15% of AIDS patients in the US described as presenting with KS[35]. This drastic increase in prevalence and mortality of KS led to intense research into its aetiology and ultimately its discovery in 1994.

KS is split into four clinical categories: classical, epidemic, endemic, and iatrogenic (Table 1.1)[36]. These distinct categories each have a clear epidemiology, phenotype, and prognosis which in turn guides different treatment options. A competent immune system is the most effective aspect to control KS. As both epidemic and iatrogenic KS have a clear mechanism by which the immune system is compromised, as such therapies to treat these types of KS aim to restore the patients' immune systems. For epidemic KS this is achieved through highly active antiretroviral therapy (HAART) which aims to reduce and clear the patient's HIV infection[37]. For iatrogenic KS, patients are taken off immunosuppressant therapies however this can lead to complications such as graft rejection[38]. Classical KS typically develops with old age as the immune system deteriorates and unfortunately there are currently no therapies to prevent this deterioration. Consequently, for both classical and endemic KS only non-targeted cancer treatments are used, such as radiotherapy, surgery, and chemotherapy[39].

1.2.1.2 Primary effusion lymphoma (PEL)

PEL is a rare Hodgkin's lymphoma with similar epidemiology to KS, mainly occurring in AIDS patients but can also be iatrogenic and found in otherwise heathy patients in equatorial Africa where KSHV is endemic[40]. PEL develops as malignant B-cells enter serosal cavities of the body and establish lymphomatic growth[40]. Treatment options for PEL are limited with no direct therapeutic options and focus on restoring a patient's immune system, similarly to KS treatment[41]. Due to the lack of direct therapeutics and the low efficacy of available treatments the prognosis of PEL patients is poor, with a median survival of <1 year[42].

1.2.1.3 Multicentric Castleman's disease (MCD)

About half of all MCD patients are infected with KSHV[43]. KSHV-associated MCD again has the same epidemiology as KS and PEL, with most patients having a weakened immune system due to AIDS or immunosuppressive therapies[44,45]. KSHV negative (idiopathic) MCD has a complex etiology which is not fully understood[43]. In KSHV-associated MCD the virus

infects lymph node plasmablasts and drives the production of viral interleukin (IL) 6, human IL-6, and several other proinflammatory proteins[46]. This cocktail of cytokines induces B cell and plasma cell, proliferation and angiogenesis[46]. Due to the importance of IL-6 in driving the progression of MCD, two anti-IL-6 therapies are clinical available for its treatment: Tocilizumab (anti-human IL-6 receptor) and Siltuximab (anti-IL6 chimeric monoclonal antibody)[47,48]. Furthermore, Rituximab (anti-CD20) is also clinically approved for treatment of MCD[49]. Due to these direct acting therapeutics the prognosis of KSHV-associated MCD is very good, with a one year survival rate of >85%[46].

1.2.2 Genome organisation

KSHV has a large double stranded DNA genome of 170 kb with over 95 genes encoding for 78 viral proteins (Figure 1.3 and Table 1.2,Table **1.3** andTable **1.4**), four long noncoding RNAs (lncRNAs) and 13 microRNAs (miRNAs). The four lncRNAs include Pan and three circular RNAs, circVIRF4, kcirc55, kcirc97[50,51]. Pan also contains three small open reading frames (sORFs) which are translated[52]. The 13 primary miRNA genes encode 25 functionally mature miRNAs which target and regulate both viral and host gene expression[53,54].

Most of the KSHV genome is unique and encodes for viral genes, however this is flanked by approximately 30 kb of terminal repeat (TR) sequences. These TRs consist of an 801 bp sequence that is repeated and is highly GC rich. In the virion the genome is linear, however upon initial infection the genome circularises by fusion of the flanking TR regions to create a stable episome[55].

Like most other herpesviruses, KSHV has acquired genes from its host cell to regulate cellular mechanisms and pathways in favour of the virus. At least 14 of KSHV-encoded genes are cellular orthologues including both protein coding and miRNA genes[56].

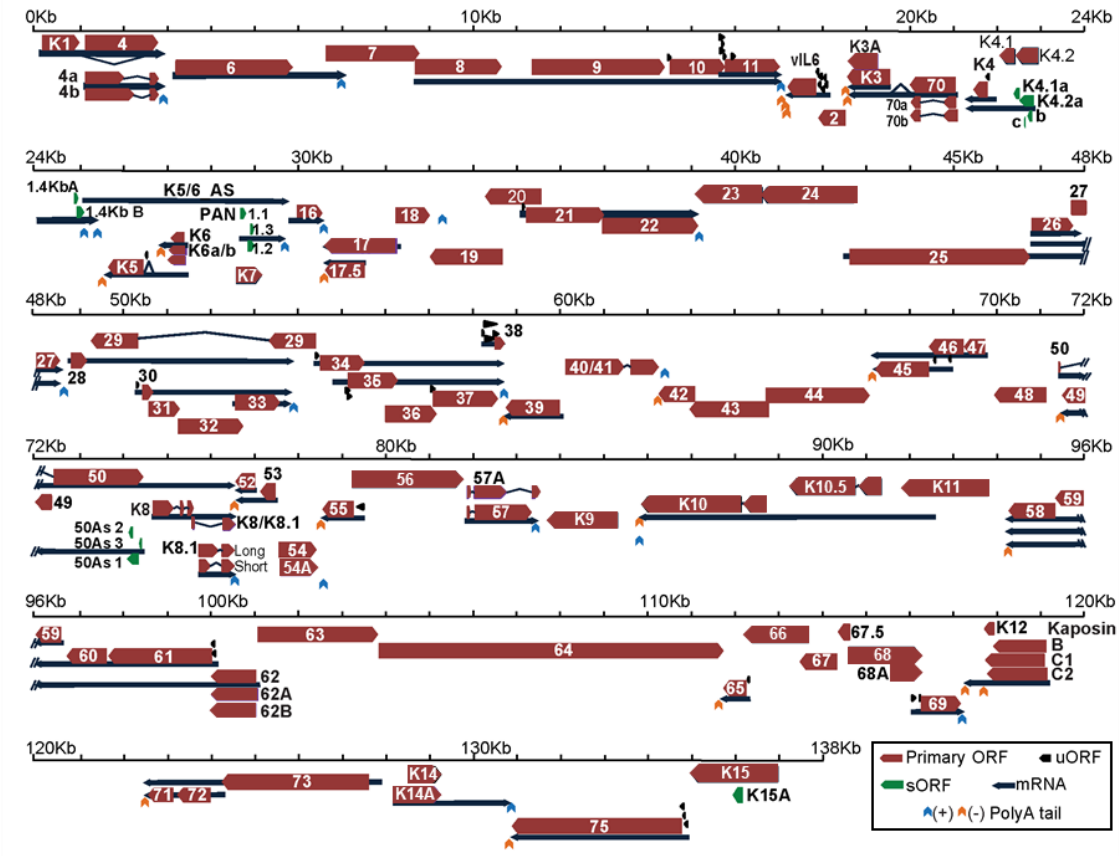

Figure 1.3 KSHV genome map. Linear map of all KSHV genomic features, adapted from Arias et al. 2014.

Gene	Translation	Timing	Function
ORFK1		Latent	ITAM homologue
vIL6	uORF	Latent	viral Interleukine 6 homolog
ORFK12	Alt. Start	Latent	Kaposin
ORF71		Latent	vFLIP
ORF72	uORF	Latent	vCyclin
ORF73		Latent	LANA

Table 1.2 Latently expressed KSHV proteins. Non-canonical translation events: upstream open reading frame (uORF); alternative start site (Alt. Start); short open reading frame (sORF).

Gene	Translation	Timing	Function
ORF6	uORF	8 h	ssDNA Binding protein
ORF11	uORF	8 h	Ribsome biogenesis/Cell membrane
ORFK3	Internal	8 h	Immune modulator
ORF70		8 h	Thymidylate synthase
ORFK4	uORF	8 h	vMIP2
1.4kb	sORF	8 h	Unknown
ORFK5	uORF	8 h	RING-CH E3 Ubiquitin ligase
ORFK6		8 h	vMIP3
ORFK7		8h	Viral Inhibitor of Apoptosis
PAN	sORF	8 h	Late gene expression
ORF16		8 h	Bcl2 homolog
ORF45	uORF	8 h	Tegument protein and RSK activator
ORF50		8 h	RTA
ORF57		8 h	mRNA export/splicing
ORF4		24 h	Complement binding/Envelope protein
ORF17.5		24 h	Capsid scaffold protein
ORF18		24 h	Late gene regulation
ORF46		24 h	Uracil deglycosylase
ORF47	uORF	24 h	Envelope glycoprotein L
ORF48		24 h	Unknown
ORF49		24h	Activates JNK/p38
ORF58		24 h	EBV BMRF2 homologue
ORF59		24 h	Processivity factor
ORF2		24-48h	Dihydrofolate reductase
ORF34	uORF	24-48 h	Late gene expression
ORF35	uORF	24-48 h	Unknown
ORF36		24-48 h	Serine protein kinase
ORF37	uORF	24-48 h	Sox
ORF38	uORF	24-48 h	Viral maturation and egress/Tegument
ORF39		24-48 h	Envelope glycoprotein M
ORFK8		24-48 h	bZip
ORF60		24-48 h	Ribonucleoprotein reductase
ORF61	uORF	24-48 h	Ribonucleoprotein reductase
ORF63		24-48 h	Inflammasome NLRP1 homolog
ORFK14		24-48 h	vOX2
ORF74		24-48 h	vGPCR
ORFK3A		24-48 h	Immune modulator

Table 1.3 Immediate early and early expressed KSHV proteins. Non-canonical translation events: upstream open reading frame (uORF); alternative start site (Alt. Start); short open reading frame (sORF).

Gene	Translation	Timing	Function
ORF17		48 h	Capsid protease
ORF19		48 h	Capsid associated tegument complex
ORFK8.1		48 h	Envelope glycoprotein
ORF64		48 h	Capsid associated tegument complex
ORF7		48-72 h	Terminase subunit
ORF8		48-72 h	Envelope glycoprotein B
ORF9		48-72 h	DNA polymerase
ORF10	uORF	48-72 h	Regulator of interferon function
ORF21	uORF	48-72 h	Thymidine Kinase
ORF22		48-72 h	Envelope glycoprotein H
ORF23		48-72 h	Late gene expression
ORF24		48-72 h	Late gene expression
ORF25		48-72 h	Major capsid protein
ORF26		48-72 h	Minor capsid protein/Tri2
ORF27		48-72 h	Glycoprotein
ORF28	uORF	48-72 h	BDLF3 EBV homolog
ORF29		48-72 h	Terminase subunit
ORF30	uORF	48-72 h	Late gene regulation
ORF31		48-72 h	Late gene expression
ORF32	Internal	48-72 h	Capsid associated tegument complex
ORF33		48-72 h	Tegument protein
ORF40/41		48-72 h	Helicase-primase
ORF42		48-72 h	Unknown
ORF43		48-72 h	Portal protein (capsid)
ORF44		48-72 h	Helicase
ORF52		48-72 h	Tegument protein
ORF53		48-72 h	Enevlope glycoprotein N
ORF54	Alt. Start	48-72 h	dUTPase/Immunmodulator
ORF55	uORF	48-72 h	Tegument protein
ORF56		48-72 h	Primase
ORFK9		48-72 h	vIRF1
ORFK10		48-72 h	vIRF4
ORFK10.5		48-72 h	vIRF3
ORFK11		48-72 h	vIRF2
ORF62	Alt. Start	48-72 h	Capsid protein Tri1
ORF65	uORF	48-72 h	Smallest capsid protein
ORF66		48-72 h	Late gene expression
ORF67		48-72 h	Nuclear egress complex
ORF67.5		48-72 h	Terminase subunit
ORF68	Internal	48-72 h	Genome packaging
ORF69	uORF	48-72 h	BRLF2 Nuclear egress
ORF75	uORF	48-72 h	FGARAT enzyme
ORFK15	Internal	48-72 h	Glycoprotein

Table 1.4 Late expressed KSHV proteins. Non-canonical translation events: upstream open reading frame (uORF); alternative start site (Alt. Start); short open reading frame (sORF).

1.2.3 Virion architecture

KSHV is composed of a large spherical virion with an icosahedral capsid at the centre encasing the genome, surrounded by a tegument layer and finally the envelope (Figure 1.4). The mature virion has an average diameter of 200 nm but varies depending on the thickness of the tegument layer[57].

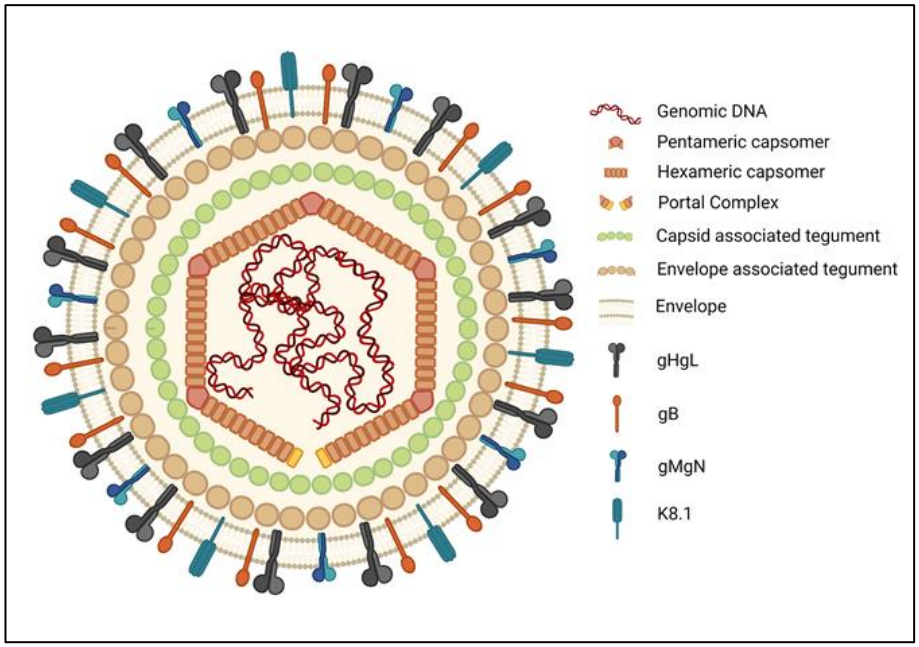

Figure 1.4 KSHV Virion Structure.

The icosahedral capsid is assembled from 162 capsomers with a T = 16 symmetry consisting of pentameric and hexameric major capsid proteins (MCP, ORF25), with a total capsid diameter of 130 nm[58]. The capsomers are held securely together with the help of the smallest capsid protein (SCP, ORF65) and heterotrimeric triplexes composed of a Tri1 (ORF62) and two Tri2 [Minor Capsid protein, ORF26] proteins[58]. In each capsid one pentameric capsomer is replaced with a dodecameric portal complex (ORF43) which nucleates the formation of the rest of the capsid[59]. The portal complex facilitates the packaging and release of the viral genome into and out of the capsid[59].

The tegument layer of the KSHV virion is a dense proteinaceous region consisting of at least 13 viral proteins which are organised into an inner capsid associated layer and an outer envelope associated layer[60]. A distinctive pentameric capsid associated tegument complex (CATC) has been defined which binds to capsid vertices. The complex contains, two copies of ORF19, two copies of ORF64, and one copy of ORF32[59]. The CATC interacts with Tri1-Tri2

complexes of the capsid through ORF32 and functions mainly structurally but is also involved in genome packaging an release[59]. Other tegument proteins include ORF6, 7, 11, 21, 33, 45, 50, 52, 55, 63 and 75, these are involved in a diverse range of functions from viral egress and ingress, to immune evasion and early replication events[60]. One of the most well characterised tegument specific proteins is ORF45, which is involved in viral egress through binding microtubules and immune evasion though inhibition of IRF-7[61,62]. A number of host cell proteins have also been reported to be specifically packaged into the tegument layer of the virion that potentially offer a range of benefits to the virus early in infection[63]. These include the cellular chaperons Hsc70 and Hsp90 which facilitate virus replication and protein folding, respectively[64,65].

The final virion envelope is gained from the inner cellular membranes, most likely by trafficking through the Golgi apparatus[66]. Glycoproteins found in the virus envelope include, gB (ORF8), gH (ORF22), gL (ORF47), gM (ORF39), and gN (ORF53), which are all conserved across other herpesviruses. Envelope glycoproteins unique to KSHV include ORF4 and K8.1[63,67–70]. The glycoproteins gH and gL form complexes and along with gB, K8.1, and ORF4, all redundantly bind heparan sulphate proteoglycans on the cell surface[71]. gHgL, gB and possibly other envelope glycoproteins are also responsible for cell tropism and binding of entry receptors, such as ephrin receptors on endothelial and epithelial cells, and DC-SIGN receptors on immune cells[72]. The glycoproteins gM and gN also form a heterodimer, however their roles in the virion are not understood[67].

1.2.4 Life cycles

Like all herpesviruses, KSHV has a biphasic life cycle comprising latent and lytic replication programmes. During latency, KSHV exists in a dormant state where only a subset of viral genes are expressed facilitating the episomal persistence of the viral genome[55]. Changes in physiological conditions including hypoxia, co-infection, oxidative stress and inflammatory cytokines have been reported to result in the induction of lytic reactivation[73–76]. This results in a tightly controlled temporal cascade of full lytic gene expression leading to genome replication, virion assembly and egress[52]. In addition to these two distinct life cycles, KSHV can importantly undergo abortive lytic reactivation[25]. This results in the expression of early lytic genes without subsequent genome replication, virion assembly and cell lysis.

All aspects of the KSHV life cycle are important for the virus to thrive in the host and greater population. Latency enables the virus to exist in the host undetected for long periods of time. Complete lytic replication is required for the virus to maintain high copy numbers in the host and importantly infect new hosts. An abortive lytic cycle enables the virus to express important early lytic genes which contribute to disease progression and maintenance of a favourable environment for KSHV to exist.

1.2.4.1 Primary infection

The KSHV envelope glycoproteins gHgL, gB, K8.1 and ORF4 all bind heparan sulphate proteoglycans on the cell surface. This brings the virion into close proximity with the cell so the virion can bind its entry receptors, which are also cell type specific. KSHV has a broad tropism and can infect a wide range of different cell types including, endothelial, epithelial, fibroblasts, monocytes, macrophages, dendrocytes and B cells[77–80].

The envelope glycoprotein gB is responsible for binding integrins and DC-SIGN for cell entry and gHgL binds the main entry receptors, ephrin receptors[77,78,80]. The envelope protein K8.1 is also required for entry into B cells, the main host cell reservoir, however its role in this process is still to be elucidated[79]. The binding of entry receptors activates signalling from the receptor triggering endocytic entry. KSHV has been shown to activate several endocytic pathways to enable entry including, clathrin-mediated, caveolin-mediated and micropinocytosis[81–83]. As virions are trafficked through the endocytic pathway the pH of the compartment lowers, this is thought to trigger the fusion process of the virion envelope with the endocytic membrane[84]. The mechanism of fusion has not been fully realised in KSHV however for the closely related gamma-herpesvirus EBV, gB has been shown to be the key fusogen[85]. Due to the sequence similarity of the KSHV gB to EBV gB it is though that this too is the main glycoprotein for KSHV fusion[72].

Upon membrane fusion, the virion capsid is released into the cytoplasm. KSHV actively utilises microtubule polymerisation and dynein motor ATP-dependent retrograde transport to traffic to the nucleus[86]. These pathways are activated through Rho-GTPases in a PI3K dependant manner during KSHV entry through integrin signalling[86]. The CATC on the virion capsid docks with the nuclear pore and facilities translocation of the genome out of the capsid through the portal complex and into the nucleus through the nuclear pore[59]. The major protein to facilitate this whole process is ORF19.

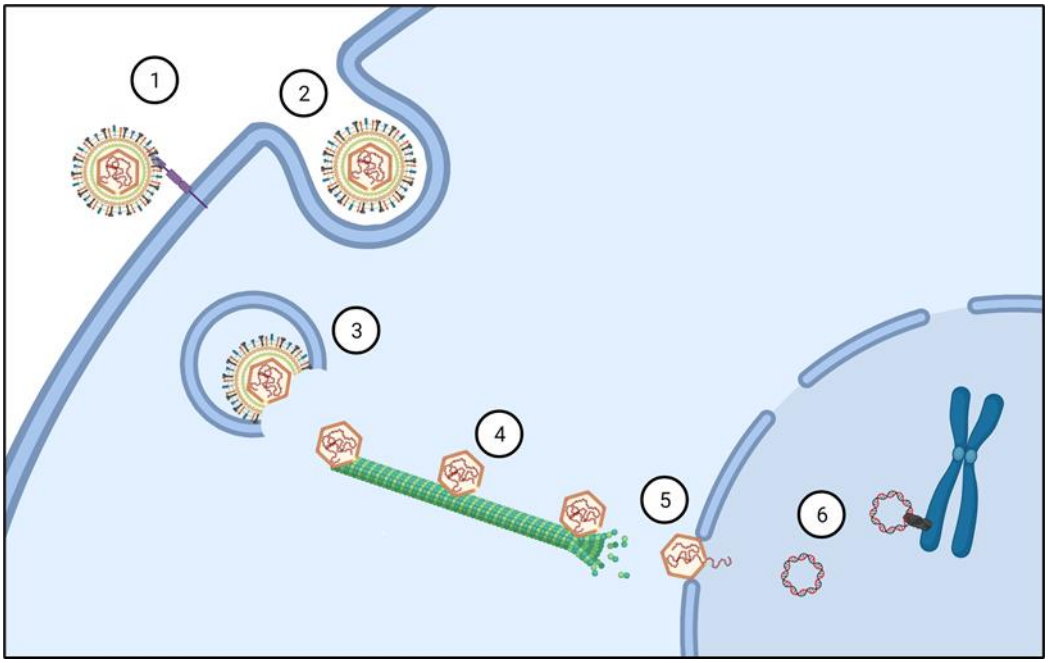

Figure 1.5 KSHV primary infection. Attachment and binding of KSHV virion **(1)**. Receptor mediated endocytosis **(2)**. KSHV envelope fusion with endocytic membrane **(3)**. Microtubule trafficking of KSHV capsids to the nuclear pore **(4)**. Release of KSHV genome through capsid portal complex into the nucleus **(5)**. Circularisation of KSHV genome and tethering to host chromosome by LANA **(6)**.

Once in the nucleus, the linear genome undergoes circularisation and chromatinisation[87]. The mechanism of KSHV genome circularisation is not fully understood. However, closely related linear EBV genomes activate the DNA damage response pathway to recruit these cellular proteins for genome circularisation which is thought to involve DNA end-processing and homologous recombination followed by ligation[88,89]. Circularisation of the KSHV genome is essential to generate the episome maintenance element consisting of multiple terminal repeats sequences[90]. In addition, circularisation is required for rolling-circle genome replication, episome stability and immune suppression[87]. The chromatinisation of the KSHV episome is also carried out by cellular proteins however, like circularisation this mechanism is not fully understood. The virion tegument protein ORF75 does play an important role though in the regulating the chromatinisation of the episome[87]. ORF75 negatively regulates PML nuclear bodies to prevent transcriptionally repressive chromatinisation resulting in poor gene expression[91].

1.2.4.2 Latency

The default replication cycle of KSHV is latency, where only a small subset of the viral genes are expressed and the virus maintains its copy numbers by replicating once every cell

division. This enables KSHV to establish a lifelong infection in the host while subverting the innate and adaptive immune surveillance mechanisms, enhancing cell survival and virus persistence. Alongside sporadic abortive lytic cycles these latent characteristics causes the development of KSHV-associated diseases. The viral latency associated gene locus encodes four protein coding genes, LANA (ORF73), vCyclin (ORF72), vFilp (ORF71), and kaposin (ORFK12), and 13 miRNAs all of which are highly expressed during latency[92]. A number of other genes are also expressed to low levels during latency compared to their high expression during lytic reactivation, vGPCR (ORF74), vOX (ORFK14), vIRF1-4 (ORFK9, 10, 10.5 and 11) and vIL6[92]. The expression of these genes are thought to be a product of abortive lytic reactivation in latent cell populations[25].

The major KSHV latent protein is LANA (ORF73) which is essential for KSHV episomal replication, maintenance, and efficient segregation of episomal DNA into the daughter cells during mitosis[93,94]. LANA is a highly multifunctional protein that binds both, cellular and viral, proteins and DNA[28,95–97]. LANA is required and sufficient for KSHV genome replication and maintenance, however it also regulates a wide variety of host cell signalling pathways to facilitate an optimal cellular environment for latency (Figure 1.6)[98–100]. LANA binds directly to the TR region of the circularised episome and tethers it to host chromosomes through binding chromatin proteins, including H2A/B, H3 and H4[101,102]. This tethering enables the faithful separation of episomes into daughter cells during cell division allowing long term persistence[103].

LANA tightly controls KSHV genome replication which occurs once every cell cycle for each episome during the S phase, similarly to the host genomic DNA[104]. Genome replication initiates at a number of different sites throughout the episome, however the dominate genome replication site during latency is *ori-P*, present in the TR region[94,105]. LANA binds *ori-P* at adjacent LANA binding sites causing a conformation change in the episome at this region[106]. Furthermore, LANA recruits the host cell DNA pre-replication complex which in turn recruits DNA replication licensing factors in the same way as host cell DNA replication events occur[107,108]. Replication folk complex proteins are then recruited alongside topoisomerase II generating double stranded DNA breaks to make the episome accessible for replication[109,110]. Finally, DNA primases and polymerases are recruited, and replication commences bi-directionally.

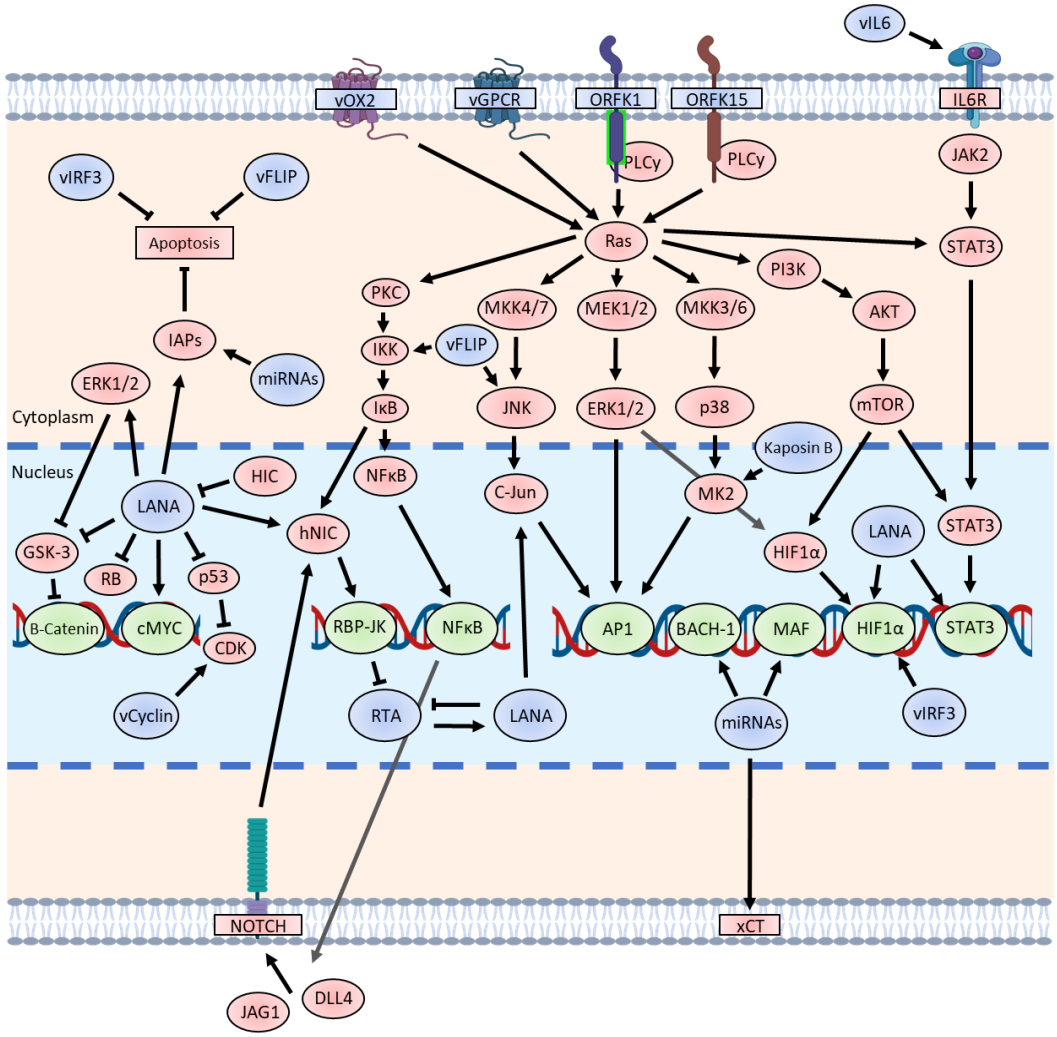

Figure 1.6 Latent KSHV cell signalling manipulation. Red markers are cellular signalling molecules, receptors, and processes. Green markers are cellular transcription factors. Blue markers are viral proteins and miRNAs. Abbreviations: Inhibitors of Apoptosis (IAPs); human Notch Intracellular (hNIC); human I-mfa domain-containing protein (HIC); Cyclin-Dependent Kinase (CDK).

LANA also negatively regulates lytic reactivation through transcriptional repression of the replication and transcription activator (RTA, ORF50) promoter. RTA is the viral latent-lytic switch protien, discussed below (Section 1.2.4.3). LANA binds the cellular recombination signal sequence-binding protein Jκ (RBP-Jκ) allowing it to be recruited to the RTA promoter, leading to transcriptional silencing of the gene[111,112]. In addition, LANA recruits the cellular transcriptional repressor Krüppel-associated box domain-associated protein 1 (KAP1) to lytic promoter regions[96]. Furthermore, LANA recruits SUMO-2, a cellular histone SUMOylation complex, which regulates chromatin mediated gene silencing[113].

To help establish a successful environment for KSHV latency LANA manipulates a number of host cell signalling pathways to repress KSHV reactivation, escape the host immune surveillance and promote cell proliferation and survival (Figure 1.6)[28,98,99,114–116]. The rest of

the proteins present during latency also contribute to the manipulation of these pathways (Figure 1.6)[25,117–121]. The genes LANA, vCyclin, vFlip, K12 and the KSHV miRNAs, encoded on the latency locus, are most highly expressed during latency and therefore have a major contribution to maintaining a successful latent environment. Briefly, vFLIP (ORF71/K13), the viral homologue of the cellular fas-associated death domain (FADD)-like interleukin-1 beta-converting enzyme inhibitory protein, activates the NF-κB pathway to promote cell proliferation and survival[122]. The latent KSHV protein vCyclin (ORF72), a homologue of cellular cyclin D, forms an active kinase complex with cellular cyclin-dependent kinase 6 (CDK6) and regulates cell cycle and cell proliferation by phosphorylating pRb[123]. The latent ORFK12 gene expresses three Kaposin proteins, A, B and C. All three proteins stimulate a pro-inflammatory environment and Kaposin B has been reported to bind MK2 activating the pro-inflammatory MAPK pathway[124].

The KSHV latency locus also encodes 13 pre-miRNAs which yields 25 functionally active mature miRNAs. These miRNAs play a key role in regulating both viral and cellular gene expression to maintain latency. Including regulating expression of RTA, the viral latent-lytic switch protein, and regulating cellular functions such as, apoptosis (caspase 3, casp3), immune evasion (MHC class I chain-related protein B, MICB) and epigenetic regulation (retinoblastoma-like protein 2, Rbl2)[125–127].

The manipulation and dysregulation of these pathways during viral latency and abortive lytic induction ultimately result in the development of KSHV-associated diseases[25,128].

1.2.4.3 Lytic replication

The balance for control of which life cycle KSHV undergoes is controlled by a battle between LANA and RTA. The default and dominate result of this battle is greatly in favour of LANA and latency. However, upon changes to the cellular environment this battle can be pushed into the favour of RTA resulting in the temporal cascade of lytic gene expression (Figure 1.7). These environmental changes can include hypoxia, co-infection, oxidative stress and inflammatory cytokines. Hypoxia-induced transcription factors, such as HIF-1, bind the RTA promoter and induce its expression[76]. The reactive oxygen species hydrogen peroxide activates the ERK1/2 and JNK pathways leading to the expression of RTA and lytic reactivation[129]. Similarly, INF-γ can stimulate KSHV-infected cells to express RTA and induce

lytic reactivation[130]. The HIV-1 transactivator Tat is also thought to induce expression of RTA[131].

The primary function of RTA is as a transcription factor for KSHV immediate early and early lytic genes, many of which contain RTA response elements[132]. However, RTA can also function indirectly by binding cellular transcription factors, such as RBP-Jκ, C/EBPα and Oct-1, which then allows RTA to associate with promoters lacking RTA-binding sites[133,134]. Upon the RTA N-terminal binding gene promoters, the host transcriptional machinery is then efficiently recruited, via its C-terminal transcriptional activation domain, and RNA polymerase (POL) II starts transcription[135,136]. In a positive feedback mechanism RTA recruits transcriptions factors Oct-1 and RBP-Jκ to its own promoter region furthering the robust activation of the lytic replication cycle[137,138].

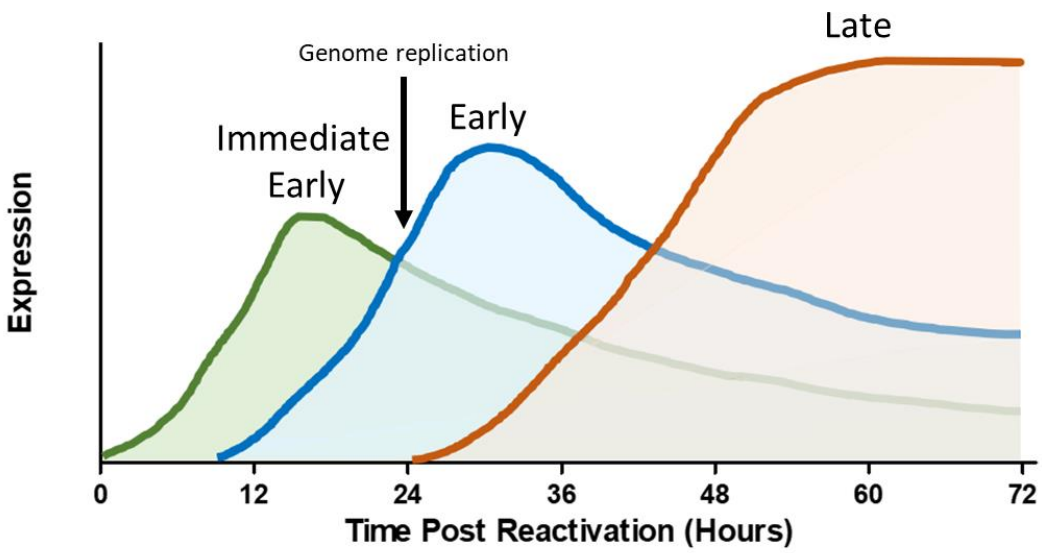

Figure 1.7 Expression profile of KSHV lytic genes. Green immediate early genes include lytic induction proteins and modulators of the host cell. Blue early genes include genome replication factors and late lytic expression factors. Orange late genes include structural, packaging and egress proteins. KSHV genome replication starts from 24 hours.

In addition to the transactivation activity of RTA, it also exhibits ubiquitin E3 ligase activity, targeting a variety of cellular proteins for proteasome-mediated degradation. These targeted proteins inhibit lytic activation and are involved in processes such as the immune response and gene regulation. For example, RTA targets IRF-7 due to the repressive function of IFN signalling during lytic replication and the transcriptional repressor Hey1, which inhibits[139,140].

As the cascade of lytic genes starts one of the earliest and most integral KSHV proteins for continued lytic replication and infectious virus production is ORF57[141]. ORF57 is an RNA

binding protein and is highly multifunctional with roles in RNA processing namely; splicing, stability and polyadenylation, and nuclear export of viral RNAs[142–144]. A large number of both viral and cellular mRNAs are bound by ORF57, some of which have a conserved ORF57 responsive element[145]. Most KSHVs genes lack introns and therefore do not associate with the human transcription/export (hTREX) complex during splicing for mRNA nuclear export[52]. However, ORF57 is one of the first lytic proteins to be expressed and contains an intron at its 5' end so its mRNA is therefore efficiently processed and exported via the host machinery[52]. ORF57 the binds intronless mRNAs and enhances their nuclear export enabling the downstream lytic cascade of viral gene expression. Malik et al. showed that ORF57 facilitates export by direct recruitment of the cellular export adaptor Aly to nascent viral mRNAs forming a ribonucleoprotein particle[146]. Subsequently, the complete hTREX complex is recruited to these ribonucleoprotein particles for efficient mRNA nuclear export[147].

The onset of lytic induction is accompanied by the rapid, global degradation of host mRNA transcripts in a process termed host shutoff. This process is mediated by the early lytic gene SOX (ORF37) which functions as an alkaline endo and exonuclease[148]. Host shutoff promotes immune evasion, frees up the host cell gene expression machinery and results in an 80% degradation of host transcripts[149]. A combination of consensus site sequence and structure enables SOX to identify its mRNA targets. One such site includes unpaired adenine nucleotides located 5′ to the incision site within the context of a stem loop structure[150].

The most highly expressed KSHV gene during lytic replication encodes the lncRNA PAN, accounting for 80% of the viral transcriptome. However, interestingly it is not fully understood what the role of PAN is during the lytic replication cycle. Two roles have been proposed that both drive late viral gene expression. Firstly, PAN has been shown to recruit the histone demethylases, UTX and JMJD3, to remove the repressive markers H3K27me3 from histones silencing KSHV late lytic genes[151]. Secondly and most interestingly Campbell and Izumiya proposed a model were the extraordinarily high transcription of PAN acts to physical trap and localise RNA POL II in close proximity to the rest of the viral genome enabling the efficient transcription of distal genes[152]. Interestingly PAN also expresses three sORFs from its transcript. To date, little is known about the function of these sORFs, however they are also very highly translated compared to the rest of the viral proteome.

Many host cell signalling pathways and factors are required to initiate and maintain the KSHV lytic replication cycle. Activation of the transcription factor AP-1 via the Raf/MEK/ERK

pathway occurs during lytic induction as KSHV genes including RTA, ORF57 and bZIP (ORFK8) contain AP-1 promoter binding sites[134]. The cellular kinases Pim-1 and 3 are upregulated during reactivation and inhibit LANA activity via phosphorylation[153]. A major pathway that is activated during lytic induction is calcineurin signalling through activation of intracellular calcium transport[154]. The activation of this pathway is essential for KSHV reactivation, although the full role of calcineurin signalling is still not known.

KSHV Gene(s)	KSHV Protein(s)	Function
ORFK3/5	Modulator of immune recognition (MIR1/MIR2)	Viral E3 ligases capable of ubiquitinating MHC-I, ICAM-1, B7-2, Tetherin (CD317/BST2), DC-SIGN, and DC-SIGNR[155]
ORFK4/4.1/6	Viral CC-Chemokine Ligands (vCCLs)	Homologues of cellular chemokines: viral CC-chemokine ligand 1 vCCL1 (vMIP1), vCCL2 (vMIP2), and vCCL3 (vMIP3), respectively. Blocks signaling through chemokine receptors[156].
ORFK7	Viral Inhibitor of Apoptosis (vIAP)	Interacts with cellular proteins, PLIC1, caspase 3/Bcl-2, CAML, Vps34, and promote cell survival during lytic replication[157].
ORF4	Complement control protein (and envelope protein)	Homologue to cellular RCA. Regulates complement activation by increasing the decay of the classical C3 convertase[158].
ORF45	ORF45	Inhibit type-1 IFN induction by sequestering IRF7 to cytoplasm[159].
ORF63	ORF63	Homologue to cellular inflammasome complex NLRP1[160].
ORF64	Viral deubiquitinase	A non-specific deubiquitinase, shown to deubiquitinate RIG-I to suppress RIG-I-mediated activation of the IFNβ[161].
ORF75	ORF75	A viral effector for the degradation of ND10 proteins[162].

Table 1.5 Lytic KSHV immune modulators.

KSHV has several lytic specific proteins that modulate the immune system, on top of the proteins mentioned above that are also expressed to some extent during latency (Table 1.5). It is also important for KSHV to evade the immune system during lytic replication allowing KSHV time to produce large amounts of new infectious virions.

Once all immediately early and early genes have started to be expressed, KSHV then moves onto the replication of its genome. Unlike latent genome replication, lytic genome replication initiates from *ori-Lyt* of which two sites have been identified, *ori-Lyt* (L) and (R)[163].

Furthermore, lytic genome replication proceeds via a rolling-circle mechanism producing a long concatemer of genomic DNA that is subsequently cleaved into 170 kb long genomes prior to packaging[164]. Lytic genome replication also mainly utilises viral factors including a viral polymerase compared to host machinery in latent replication.

The *ori-Lyt* contains an RTA response element which RTA binds and subsequently recruits bZIP to the *ori-Lyt*[165]. bZIP also binds the *ori-Lyt* further upstream of RTA causing the episome to loop out, resulting in the bending and distortion of the *ori-Lyt* DNA, which facilitates unwinding of the site[165]. This complex is termed the pre-initiation complex which can then recruit the rest of the genome replication machinery. The core proteins of the viral replication complex include the DNA polymerase (ORF9), a polymerase processivity factor (ORF59), single-stranded DNA binding proteins (ORF6), a helicase (ORF44), a primase (ORF56), and primase-associated factors (ORF40/41)[166]. Cellular components are also incorporated into the replication complex many of which are essential for replication. These cellular factors include; topoisomerases (Topo) I and II, RecQL, poly(ADP-ribose) polymerase I (PARP-1), DNA-PK, Ku86/70 autoantigens, MSH2/6, and scaffold attachment factor A (SAF-A)[167,168]. RecQL is recruited during the formation of the pre-initiation replication complex, however the rest of the cellular factors join after the formation of the core viral replication complex[167]. For example, SAF-A does not bind the replication complex but associates with the looped out *ori-Lyt* DNA anchoring it to the nuclear matrix for efficient DNA replication[167].

The KSHV late structural, packaging and egress genes are not expressed until viral genomic replication has been initiated[169]. The mechanism for this regulation is not fully understood however, it has been proposed that replication of the viral genome causes structural changes to the chromatin which opens up the locus of late lytic genes for their expression[164]. Proteins expressed at the early stage of the lytic cascade form a late gene transcription preinitiation complex, these proteins include ORFs 18, 23, 24, 30, 31, 34, and 66[170]. The viral protein ORF24 binds to newly revealed TATA sequences in the late gene promoters[171]. ORF24 then recruits RNA Pol II and the late preinitiation complex through interactions with ORF34, resulting in the efficient transcription of late lytic genes[172].

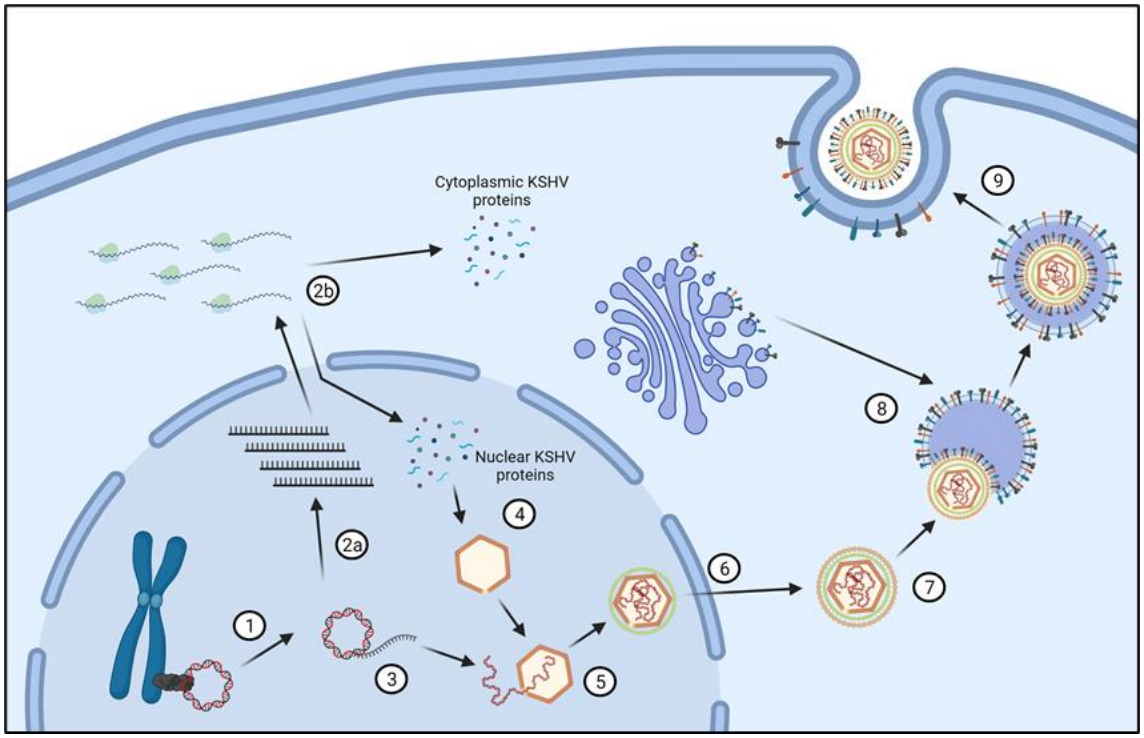

Figure 1.8 KSHV lytic infection. Lytic reactivation **(1)**. Transcription of KSHV lytic genes **(2a)**. Translation of KSHV lytic genes **(2b)**. Rolling-circle KSHV genome replication **(3)**. Capsid assembly **(4)**. Packing of genome into nascent capsids and accumulation of capsid associated tegument proteins **(5)**. Nuclear export of capsids via budding through the nuclear membranes **(6)**. Accumulation of final tegument proteins on capsids **(7)**. Budding of capsids into trans-Golgi network derived vesicles studded with virion glycoproteins **(8)**. Final egress occurs as the trans-Golgi network derived vesicle fuses with the cell membrane **(9)**.

As capsid proteins are expressed they are trafficked into the nucleus where they are thought to self-assemble[173]. Little research has focused on the formation of KSHV capsids and therefore most information and models are based on HSV-1 studies. The MCP firstly forms penton and hexon capsomers[174]. HSV-1 has then been shown to form protomer capsids consisting of Tri1-Tri2 complexes surrounded by three MCP capsomers[175]. These protomers then assembly around a nucleating portal protein decorated with multiple scaffold proteins (ORF17.5) forming porous circular procapsids[59,173]. The circular procapsids angularises and solidify into icosahedrons through the joining of SCPs[173]. The capsid protease, ORF17 then cleaves the scaffold proteins from inside the procapsids. Finally, CATCs form on the procapsid vertices and portal complex making them ready for genome packaging[176].

Again, little research has focused on the packaging of genomes into KSHV procapsids and therefore most information and models are again based on HSV-1 studies. The terminase complex, comprised of ORFs 7, 29 and 67.5, forms on the end of replicating genomic concatemers[177]. It then associates with CATC proteins on a procapsid portal and acts as an

ATP-dependent motor to thread a single KSHV genome into the capsid through the portal complex[177]. The viral proteins ORF29 and 68 cleave the genome from the long concatemer once it has been packaged and the terminase complex dissociates from the fully formed capsid[178].

The capsid now begins the process of egress through which it accumulates a tegument layer and finally a glycoprotein-rich envelope. As with capsid formation and packaging the process and mechanisms of KSHV egress has been less well studied compared to alphaherpesviruses like HSV-1, therefore much of this process is inferred from those studies. Firstly, the capsid needs to exit the nucleus which it does so by budding through the inner nuclear membrane into the perinuclear space and then fuses with the outer nuclear membrane to be released into the cytoplasm[179]. Once in the cytoplasm herpes viruses then acquire the rest of their tegument layers including both viral and cellular proteins[174]. The CATC protein ORF64 is essential and thought to be the main regulator for tegument recruitment and organisation[180,181]. The tegument covered virus particles then gain their final lipid envelope though budding into vesicles derived from the trans-Golgi network that are studded with the virion glycoproteins[182,183]. One of the main functions of the herpes virus gMgN glycoprotein complex is thought to be recruitment and organisation of the rest of the virion glycoproteins in the trans-Golgi vesicles ready for envelopment[184,185]. The envelopment process is, at least in part, regulated by the tegument protein ORF45[186]. Very little is known about how the final stages of egress proceed, although the trans-Golgi network vesicles containing nascent virions are trafficked to and fuse with the cell membrane releasing the infectious virions out of the cell[174].

1.3 The ribosome

The mammalian ribosome is a large macromolecular machine consisting of two subunits, the larger 60S subunit and the smaller 40S subunit, which together constitute a 4.3 megadalton 80S ribosome[187]. The main function of the ribosome is the synthesis of proteins through translation which, in the simplest terms, involves the decoding of mRNA by the small subunit coupled with the formation of peptide bonds by the large subunit. These processes are linked by tRNA molecules which are the true translators in this translation process.

The majority of eukaryotic ribosomal biology was first carried out in yeast, due to the simplicity of the system, and a lot of mammalian ribosome biology is inferred from these studies[188]. While the study of yeast ribosomal biology has given a comprehensive insight into eukaryotic ribosomal biology there are subtle but important differences across the kingdom. In recent years more mammalian specific studies have been carried out which have highlighted some of these differences and enable a greater understanding of the biogenesis, structure, and mechanics of human ribosomes[187,189–191].

Cells have two main types of ribosomes, the majority are cytoplasmic and the second smaller class are mitochondrial ribosomes[192,193]. Cytoplasmic ribosomes translate mRNAs derived from nuclear genes whereas mitochondrial ribosomes translate mRNAs derived from the mitochondrial DNA. All mitochondrial mRNAs encode membrane bound proteins involved in the electron transport chain[194]. Mitochondrial ribosomes differ structurally, due to differences in their RNA and protein composition to cytoplasmic ribosomes, as they are specialised towards the synthesis of these membrane proteins[195–198]. These structural differences in turn allow functional changes in how the mitochondrial ribosomes decode mitochondrial mRNAs and produce proteins[199–201]. Although, mitochondrial ribosomes represent a highly specialised type of ribosome specific to the translation of membrane bound proteins of the electron transport chain, the rest of this thesis will focus on the main cytoplasmic ribosomes and their specialisation.

1.3.1 Structure

At the core of each ribosomal subunit is the rRNA species contained within that subunit. The ribosomal proteins can be thought to decorate the rRNA, with most of these proteins at or near the surface of each subunit. The cytoplasmic large ribosomal subunit consists of the 28S, 5S and 5.8S rRNAs and 47 proteins, while the small subunit comprises a single 18S rRNA chain and 33 proteins[187]. In addition to the rRNA and proteins the human ribosome also contains ~240 Mg^{2+} ions and vast number of K^{+} ions that are integral to maintaining the stable yet dynamic structure of the ribosome[187].

The region at which the two subunits come together is termed the interface and mainly consists of rRNA, the core interaction is between helix H69 of the 28S rRNA and helix h44 of the 18S rRNA[187]. At this interface the 40S subunit binds the mRNA strand in a cleft between the 'head' and 'body' of the small subunit and the codons of the mRNA strand interact with anticodons of the tRNA molecules (Figure 1.9). These tRNA molecules occupy three sites in the ribosome, the A, P and E sites (Figure 1.9). The first site is the A site which binds the incoming aminoacyl-tRNA (aa-tRNA), the second is the P site which contains the peptidyl-tRNA bound to the nascent polypeptide chain, and finally the E (exit) site holds the deacylated tRNA before its ejection from the ribosome (Figure 1.9). The 3' ends of the tRNA molecules sit in the 60S subunit whereby the P- and A-site tRNAs are in close proximity to the peptidyl-transferase centre (PTC), and the 3' end of the E site tRNA is angled away from the PTC towards the L1 stalk (Figure 1.9).

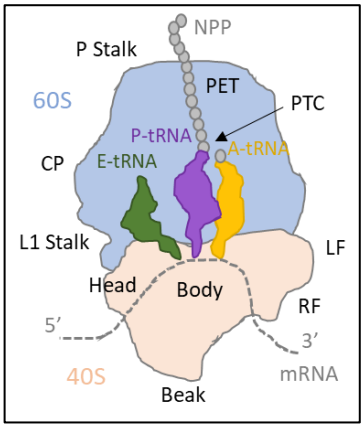

Figure 1.9 Schematic of the ribosome structure. Large 60S subunit blue and small 40S subunit orange. mRNA grey dashed line; NPP, nascent polypeptide; PET, peptide exit tunnel; PTC, peptidyl-transferase centre; CP, central protuberance; LF, left foot; RF, right foot.

The 60S subunit, and more specifically the PTC, is the catalytic centre of the ribosome where peptide bond formation occurs. The PTC consists mainly of rRNA which is highly conserved across all domains and kingdoms of life, supporting the idea that the core mechanism of protein synthesis is universal[202]. While the 60S subunit is the catalytic centre of the ribosome the 40S subunit undergoes large conformational changes which drives the process of translocation. Overall the 40S subunit undergoes three major conformational changes during translation, a universal rotation, parallel to the 60S subunit, described as 'ratcheting' in bacterial ribosomes[203], a pivot movement of the head and beak regions towards the 60S subunit L1 stalk[187], and a rotation of the small subunit perpendicular to the universal rotation axis termed 'subunit rolling'[204].

The ribosomal rRNAs contain 228 modification sites with 14 different posttranscriptional modifications[205]. In addition, the ribosomal proteins are widely and dynamically posttranslationally modified mainly though phosphorylation and ubiquitylation[206]. The best resolution structure of the human 80S ribosome to date has a global average of 2.9 Å in

which the authors are able to map 130 distinct rRNA modifications[189]. These modifications can alter the ribosome both structurally and functionally.

1.3.2 Translation

There are four main processes involved in translation: initiation, elongation, termination, and recycling of the ribosome (Figure 1.10). Elongation is the fastest step in the process taking just 1/6th of a second, whereas initiation is the rate-limiting step taking the longest to complete[207]. The cell has a vast array of mechanisms to regulate translation at each step, furthermore these mechanisms are dysregulated and exploited through disease and by pathogens[208–212].

1.3.2.1 Initiation

Translation initiation is the process by which elongation competent 80S ribosomes are assembled and the P site is occupied by the initiator tRNA (Met-tRNA$^{Met}_i$), which is base paired with the mRNA start codon (AUG). Canonical translation initiation requires at least nine eukaryotic initiation factors (eIFs) and consist of four main steps, mRNA activation, formation of the 43S pre-initiation complex, followed by formation of the 48S initiation complex and, finally the joining of the 60S subunit.

Canonical translation initiation starts with mRNA activation through the binding of the eIF4F complex to the 5' m^{7}G mRNA cap[213–215]. The eIF4F complex consists of eIF4A, eIF4E and eIF4G which associates and unwinds the 5' terminal secondary RNA structure in an ATP-dependent manner with eIF4B[216]. Unwinding the mRNA allows the association of the 43S preinitiation complex with the 5' mRNA UTR (untranslated region)[217]. The 43S preinitiation complex comprises a 40S subunit, the eIF2–GTP:Met-tRNA$^{Met}_i$ ternary complex (eIF2 TC), eIF3, eIF1, eIF1A and probably eIF5, this complex then scans the 5' UTR of the mRNA in the 5' to 3' direction[218]. The preinitiation complex scans the 5' UTR until it recognises the AUG initiation codon usually flanked on its 5' end by a Kozak sequence[219,220]. The Met-tRNA$^{Met}_i$ then base pairs with the initiation codon inducing a conformational change including the hydrolysis of eIF2-GTP causing its partial release and leaving behind the now translation committed 48S initiation complex[221,222]. The association of the 60S subunit with the initiation complex is mediated by eIF5B-GTP which causes the full dissociation of all initiation factors (eIF1, eIF2-GDP, eIF3 and eIF5) apart from eIF1A[222,223]. Finally, hydrolysis of eIF5B-

GTP leads to its release from the 80S ribosome along with eIF1A giving way for translation of the mRNA open reading frame (ORF)[224].

A second mechanism of translation initiation is mediated through internal ribosome entry sites (IRESs), these are RNA elements that facilitate end-independent ribosomal recruitment to internal 5' UTR locations in the mRNA. IRES structures where first discovered in 1988 by two groups independently in viruses of the *Picornaviridae* family, poliovirus and encephalomyocarditis virus[225,226]. Since the late 1980's many more viral IRES elements have now been discovered[227–231]. Although, viral IRES elements lack sequence homology they can be divided into four distinct groups based on RNA secondary structure and mechanism of translation initiation[211]. A latent KSHV transcript contains a group one/two like IRES element for the translation of vFLIP[232]. The transcript is bicistronic with the IRES element located in the ORF of the upstream gene vCyclin[232].

Some human mRNAs also contain IRES elements, many of these mRNAs encode proteins required in the stress response to conditions such as apoptosis, mitosis, hypoxia, and nutrient limitation[233]. Like viral IRES elements cellular IRES elements have low sequence homology in addition they also share little structural homology making classification difficult. However, cellular IRES elements can be generally separated into two classifications based on the mechanisms of ribosome recruitment. Type one cellular IRES elements recruit IRES-transacting factors (ITAFs) which in turn either directly recruit 40S ribosomal subunits or recruit 40S ribosomal subunits through eIFs as bridging factors[233–235]. Type two cellular IRES elements recruit 40S ribosomal subunits directly through base pairing with the 18S rRNA[236].

1.3.2.2 Elongation

Translation elongation requires two eukaryotic elongation factors (eEFs) and consists of three main steps, mRNA decoding, peptide bond formation and, translocation. Translation initiation culminates with the Met-tRNA$^{Met}_{i}$ occupying the ribosome P site with its anticodon base paired with the initiation codon. Therefore, at the start of elongation the second codon in the mRNA ORF is in the A site.

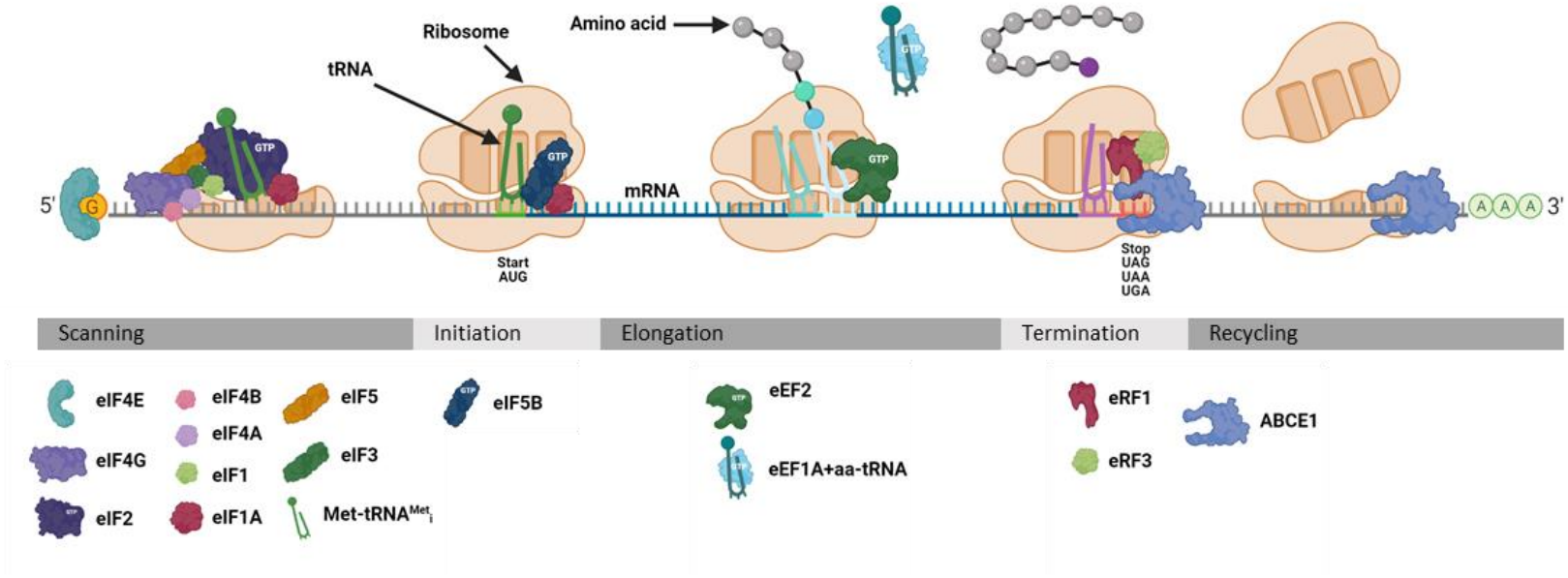

Figure 1.10 Translation overview.

The first step of the elongation cycle involves decoding the mRNA codon in the A site. Free aa-tRNAs are bound by eEF1A-GTP in a ternary complex (eEF1A TC), these ternary complexes are recruited to the elongating ribosome by eEF1A[237]. A cognate eEF1A TC stably base pairs with the codon present in the ribosome A site triggering hydrolysis of eEF1A-GTP and its release from the aa-tRNA[238]. The aa-tRNA therefore becomes fully incorporated into the ribosome A site[238].

A peptide bound is then rapidly formed between the specific amino acid on the A site aa-tRNA and the nascent polypeptide chain, which transfers the protein chain from the P site tRNA to the A site tRNA[202]. The 40S subunit then undergoes a universal rotation as described above. This rotation causes the movement of the P and A site tRNAs from the classical state into a hybrid state. In this hybrid state the anticodon ends of the tRNA molecules stay in the original P and A sites but the acceptor ends move along to the E and P sites respectively[239]. eEF2-GTP then binds and stabilises the ribosome in this rotated state[240].

Translocation of the mRNA through the ribosome then moves the hybrid tRNA molecules into the classical E and P sites, directed by the hydrolysis of eEF2-GTP and its conformational changes[241]. eEF2 directs the pivot movement of the 40S subunit head and beak region as described above driving the movement of mRNA through the ribosome by exactly one codon length[242]. Upon hydrolysis eEF2 is released from the ribosome which results in the reversal of structural changes that occur during elongation back to the decoding state[243]. The final step in the elongation cycle is for the deacylated tRNA present in the E site to be ejected from the ribosome[244]. The elongation cycle continues until the ribosome has translated the entire length of the mRNA ORF.

1.3.2.3 Termination

Translation termination occurs as the ribosome comes to the end of the mRNA ORF, signified when the A site is occupied by a stop codon (UAA, UGA, or UAG), and requires the collaborative action of two eukaryotic release factors (eRFs), eRF1 and eRF3.

Firstly, eRF1 binds to the ribosome A site recognising the termination codon which it archives due to its highly similar structure to a tRNA molecule[210,245]. eRF1, like tRNA molecules, is in a complex with a specialised GTPase, eRF3-GTP which is closely related to eEF1A[246,247]. Binding of eRF1 to the termination codon stimulates the hydrolysis of eRF3-GTP leading to its release from the complex. After eRF3 release the eRF1 catalytic domain

Gly–Gly–Gln (GGQ) swings into the PTC and is positioned to coordinate a water molecule that hydrolyses the nascent peptide chain resulting in its release from the peptidyl-tRNA[245,248].

1.3.2.4 Recycling

The final stage of translation is recycling the terminated ribosome into its separate subunits ready for another round of translation. Recycling is orchestrated by the ABC-type ATPase, ABCE1[249]. ABCE1 recycles ribosomes that have either undergone canonical translation termination, as described above, or recognition of stalled and vacant ribosomes by mRNA surveillance factors[250].

The post termination ribosome still holds eRF1 in the A site and a deacetylated tRNA in the P site or hybrid P/E site. ABCE1 binds these ribosomes at the exposed site of eRF1 and may also facilitate nascent polypeptide release, this complex is termed the pre-splitting complex[251]. Upon ribosome binding ABCE1 undergoes multiple rounds of ATP binding and hydrolyses which drives its structural reorganisation causing ribosome subunit splitting[252]. After subunit splitting the large subunit, eRF1, mRNA and deacetylated tRNA dissociate leaving ABCE1 bound to the small subunit, this complex is called the post-splitting complex[253]. ABCE1 remains bound to the small ribosome subunit during the initial stages of translation initiation with the formation of the 43S initiation complex and may also facilitate this process[253].

1.3.2.5 Upstream open reading frames (uORFs)

Along with IRESs and other mRNA secondary structures, uORFs offer another mechanism for translational control encoded by an mRNA. uORFs are regulatory elements in the 5’ UTR of mRNAs that modulate the translation initiation rate of downstream coding sequences (CDSs) by sequestering ribosomes. Compared with transcriptional control, translational regulation enables a more direct response to adjust the protein abundance upon cellular signals or environmental stimuli in a variety of biological processes.

Based on the position of the start and stop codons relative to the CDS, uORFs can be split into three categories: non-overlapping, out-of-frame overlapping and alternative start sites (Figure 1.11). Several scenarios can occur during translation initiation and termination of mRNAs containing a uORF (Figure 1.11). Firstly, during scanning the preinitiation complex can fail to recognise the uORF AUG start site (uAUG) due to its unfavourable location without

a Kozak sequence. The preinitiation complex then continues scanning along the 5' UTR until it reaches the canonical CDS start site allowing normal translation and expression of the mRNA CDS, this process is termed 'leaky scanning'. Alternatively, the preinitiation complex can recognise the uAUG and initiate translation, this intern can block other preinitiation complexes that are scanning for the CDS AUG[254]. After termination of uORF translation there are three possible outcomes for the ribosome. Firstly, the 40S subunit may stay bound to the 5' UTR, forming another preinitiation complex and continuing to scan for the CDS start site to re-initiate translation resulting in an overall reduction in translation of the CDS. However, the other two possibilities are that during termination both the 40S and 60S subunit dissociates from the mRNA or the ribosome stalls and triggers nonsense-mediated decay[255]. These later two outcomes result in total loss of expression of the CDS.

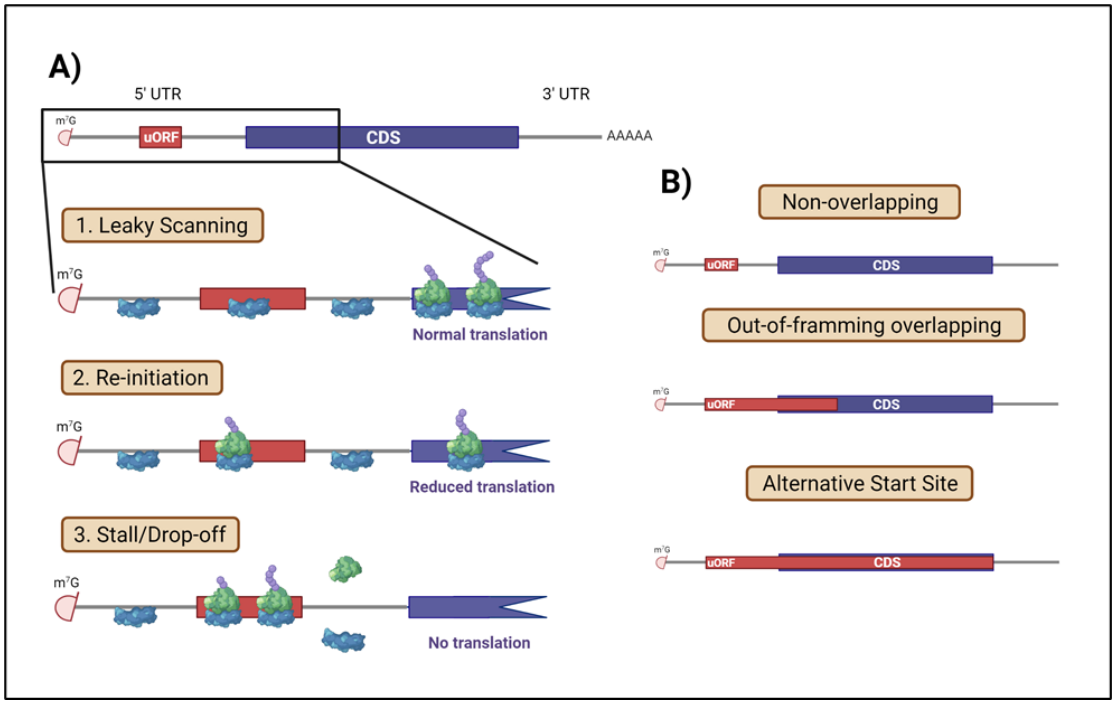

Figure 1.11 uORF Translation regulation. Mechanisms of uORF translation and the downstream effect of the CDS translation (A). The three categories of uORF based on the position of the start and stop codons relative to the CDS (B).

The regulation and utilisation of uORFs in response to cell stress have been well investigated. During cell stress, kinases such as GCN2 or PERK phosphorylate eIF2 reducing the formation of the 43S preinitiation complex[256]. With the reduction of 43S preinitiation complexes, the CDS translation of mRNAs with multiple uORFs is enhanced. This is because the first uORF is translated but after translation termination the 43S preinitiation complex is not quickly formed again resulting in the leaky scanning of downstream uORFs[257].

However, by the time the scanning 40S subunit reaches the start codon of the CDS the preinitiation complex has had time to form again so efficient translation of the CDS occurs[258].

Furthermore, the protein antizyme inhibitor 1 (AZIN1) is required for polyamine synthesis from ornithine, and its translation is regulated by a uORF in a negative feedback loop. When the cellular polyamine level is low, translation of the AZIN1 uORF is negligible due to its unfavourable start codon and Kozak context[259]. However, when the concentration of polyamines is high, ribosomes become stalled at the PPW tripeptide motif near the stop codon of the AZIN1 uORF because polyamines compete for binding sites with the translation factor eIF5A[260]. Ribosome stalling in the AZIN1 uORF therefore prevents the translation of AZIN1 CDS in addition to causing queuing of upstream scanning ribosomes allowing them more time to initiate translation of the AZIN1 uORF further reducing the translation of the CDS[260].

KSHV mRNAs are remarkably similar to human mRNAs, containing a 5' 7-methylguanylate cap and UTR and 3' UTR and polyadenylated tail[52,261]. However, interestingly 25 KSHV mRNAs contain uORFs and two of its lncRNAs contain sORFs (Table 1.2Table 1.3Table 1.4). The functionally or mechanisms of these KSHV uORFs has not to date been investigated.

1.4 Ribosome biogenesis

Eukaryotic ribosome biogenesis is a highly orchestrated process requiring the coordinated activity of all three RNA polymerases and over 400 transiently associated ribosome biogenesis factors (RBFs) (Figure 1.12)[262]. In addition, it is one of the most energy-consuming cellular processes, with approximately 7,500 new ribosomal subunits synthesised per minute in actively growing HeLa cells[263]. The process is both continuous and dynamic from the start of rRNA transcription to the final maturation steps in the cytoplasm.

Saccharomyces cerevisiae has been used extensively as a model organism for eukaryotic ribosome biogenesis. However, while the basics of the pathway are conserved across the domain, human ribosome biogenesis is considerably more complex due to the increased number of ribosomal proteins, modifications, and regulatory networks. More recently, proteomic and RNAi studies have revealed these extra layers of complexity to human ribosomes and their biogenesis[264–266].

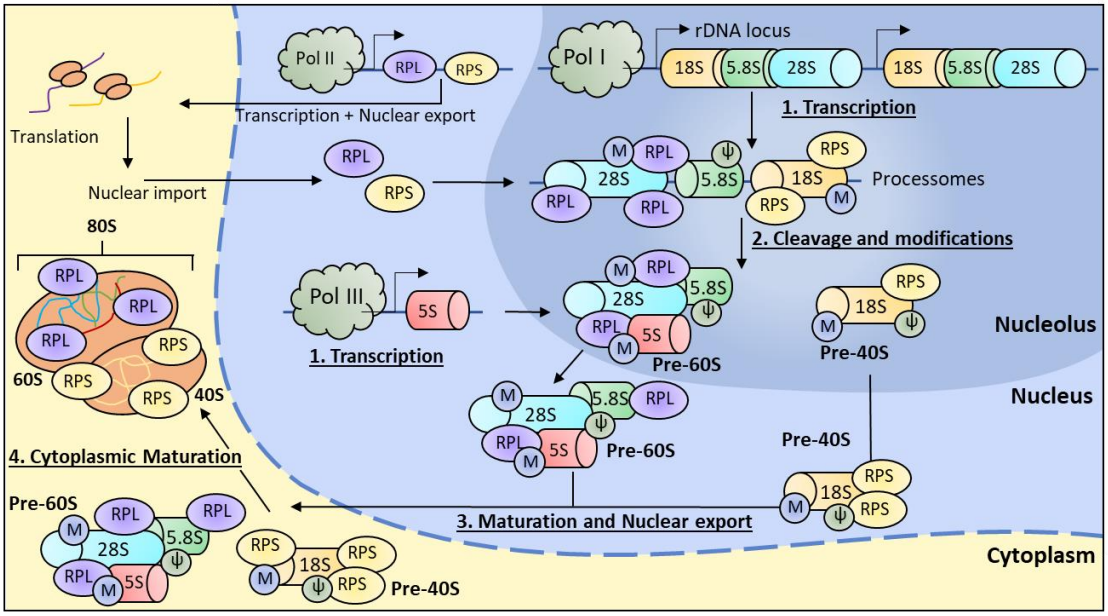

Figure 1.12 Eukaryotic ribosome Biogenesis. Three of the four ribosomal RNAs (rRNAs), 18S, 5.8S and 28S, are transcribed as a single 47S pre-mRNA by RNA Pol I, in the nucleolus. The fourth 5S rRNA is transcribed in the nucleus by Pol II. snoRNAs organise the co-transcriptional methylation and pseudouridylation of over 100 rRNA nucleotides. The core ribosomal protein genes are transcribed by Pol II and translated in the cytoplasm. The proteins are imported back into the nucleus and many assembled onto pre-rRNAs cotranscriptionally forming the SSU and LSU processomes. The 47S rRNA is cleavage forming the pre-60S and pre-40S complexes. Further modifications of each complex occurs through the nucleoplasm before the tightly regulated process of their nuclear export. Final maturation steps of each subunit take place in the cytoplasm before they associate together during translation initiation. **Ψ, pseudouridylation; M, methylation; Pol, polymerase; RPL, large subunit RPs; RPS, small subunit RPs.**

RBFs include both proteins and small nucleolar RNAs (snoRNAs), which can have enzymatic, co-factor and structural roles in ribosome biogenesis. Humans have a vast number of different enzymatic RBFs including, nucleases, GTPases, ATPases, RNA helicases, protein and RNA methyltransferase, pseudouridine synthases and acetyltransferases. RBF co-factors include many proteins and snoRNAs. The snoRNAs specifically guide chemical modifications of the rRNAs and the protein co-factors facilitate many other enzymatic processes in ribosome biogenesis. Structural RBFs facilitate biogenesis functionally as scaffolds to mould and regulate the formation of the pre-ribosome complexes. Many RBFs have multiple roles during ribosome biogenesis which can pose difficulties when trying to identify each individual RBF's function. This is further complicated as although RBFs can associate with pre-ribosome complexes independently, a large number also form modular complexes that function together to further ribosome biogenesis.

The incorporation of ribosomal proteins into maturing pre-ribosomal subunits occurs in an ordered and hierarchical major, leading to the sequential assembly of particular domains[267]. Furthermore, many ribosomal proteins are initially tethered to the maturing pre-ribosomal subunits before been fully incorporated at later stages of ribosome biogenesis[262].

1.4.1 Pre-ribosome processomes

Ribosome biogenesis starts with the transcription of the rDNA gene locus by RNA Pol I in the nucleolus (Figure 1.13). Cotranscriptionally the rRNA is folded, modified and 40S ribosomal proteins start to bind and assemble, both processes are tightly controlled by the elongation of the rRNA and require multiple RBFs and RBF complexes (Figure 1.13). The first two complexes to form and bind the nascent rRNA chain are the UTP-A and then B complexes, binding the 5'-ETS[268]. Following this the U3 small nucleolar ribonucleoprotein (snoRNP) complex then binds further along the 5'-ETS as it is transcribed[269]. As the 18S rRNA moiety becomes co-transcriptionally available other major complexes bind including, IMP3-IMP4-MPP10, UTP-C, RCL1-BMS1 and ANN[269]. Through the transcription of the 18S rRNA many other RBFs transiently bind to shape, organise, and modify the rRNA and proteins. During the maturation of the small subunit (SSU) processome 16 of the 33 small subunit ribosomal proteins assemble to stabilise and start to form the 40S subunit. These proteins include, RPS3A, RPS4, RPS5, RPS6, RPS7, RPS8, RPS9, RPS11, RPS13, RPS14, RPS15A, RPS16, RPS23, RPS24, RPS27 and RPS28[267]. These proteins form the body and head structures of the 40S subunit (Figure 1.9). This particle defines the first step of ribosome biogenesis and is termed the SSU processome or 90S particle.

RNA Pol I continues to transcribe the rDNA locus through the IST1 linker and onto the 60S subunit 5.8S rDNA, ITS2, 28S rDNA and finally the 3'-EST resulting in the full 47S rRNA (Figure 1.13). Unlike the SSU processome, the large subunit (LSU) processome contains far less RBF factors and complexes especially compared to its size (Figure 1.13). Furthermore, only 8 of the 47 large subunit proteins are associated with the LSU processome. These proteins include, RPL3, RPL4, RPL6, RPL7, RPL7A, RPL18, RPL32 and RPL35A, and are the solvent exposed proteins of the 60S subunit[270,271]. Overall, the LSU processome is considerably less developed and structured compared to the SSU processome and therefore undergoes more stages of maturation in the nucleolus and nucleoplasm.

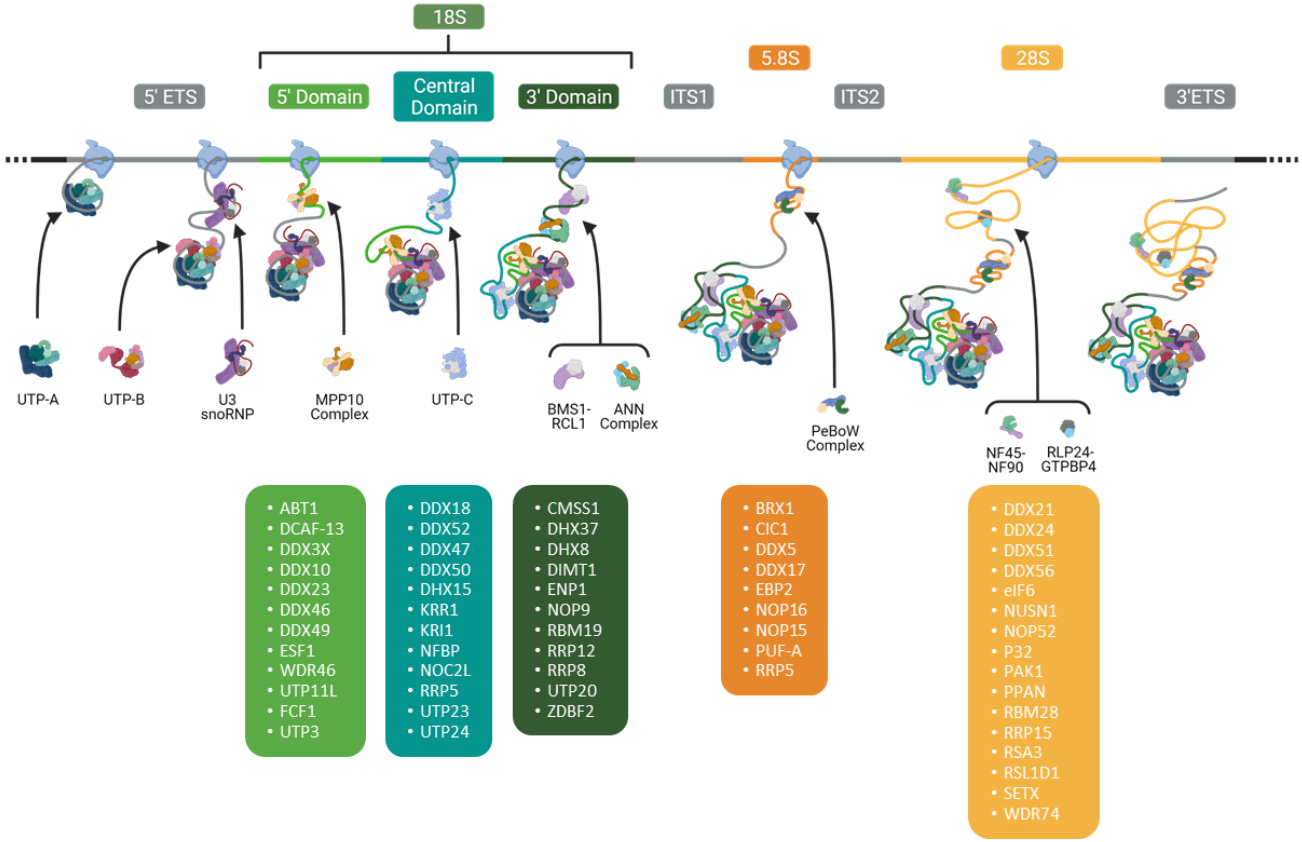

Figure 1.13 Biogenesis of the pre-ribosome processomes. UTP-A complex – HEATR1, NOL11, UTP4, UTP15, WDR43 and WDR75. UTP-B complex – PWP2, TBL3, UTP6, UTP18, WDR3 and WDR36. U3 complex – 15.5K, Fibrillarin, NOP56, NOP58, U3-55K and U3 snoRNA. MPP10 complex – MPHOSPH10, IMP3 and IMP4. UTP-C complex – NOL6 and RRP7A. ANN complex – AATF, NGDN and NOL10. PeBoW complex – BOP1, DDX27 PES1 and WDR12. Individual and transient RBFs shown in coloured boxes relative to timing of association.

Throughout the transcription of the 47S rRNA over 100 bases are modified mainly by pseudouridylation and 2'-*O*-ribose methylation[272]. Most of these modifications are guided and catalysed by two families of snoRNPs called H/ACA box (pseudouridylation) and C/D box snoRNPs (2'-*O*-ribose methylation)[273]. Each modification is performed by a particular snoRNP that combines a set of core proteins with a specific snoRNA. The catalytic pseudouridyl synthase for all H/ACA box snoRNPs is dyskerin and the methyltransferase of C/D box snoRNPs is fibrillarin[272]. In addition, some modifications are also catalysed by specific enzymes (Table 1.6).

The fate of the pre-40S and pre-60S ribosome complexes diverge at this point through rRNA processing events. Firstly, the A' and 02 sites are cleaved at the 5' and 3'-ETS respectively (Figure 1.14), the enzymes responsible for this are not yet known[274]. Two routes of rRNA processing can then occur, either the 45S rRNA can be cleaved at sites A0 and 1 before or after the cleavage at site 2 and the separation of the pre-40S and pre-60S subunits (Figure 1.14). Cleavage at these sites is carried out by UTP23, UTP24 and RMRP respectively, to generate the 21S small subunit rRNA and a 32.5S large subunit rRNA (Figure 1.14)[275–277].

While cleavage and separation of the SSU and LSU processomes means the pre-40S and pre-60S mature separately, the biogenesis of both subunits are still closely linked both spatially and temporally.

Enzyme	Modification	Base	Refernce(s)
SNORA14	Pseudouridylation	18S-U1240	278
EMG1	N^1-methylation		278
TSR3	N^3-aminocarboxypropylation		279
NAT10	N^4-acetylcytidine	18S-C1337	280
		18S-C1842	
BUD23	N^7-methylguanosine	18S-G1639	281
DIMT1	N^6N^6-dimethyladenosine	18S-A1850/1	190
NML	N^1-methyladenosine	28S-A1332	282
NSUN5	5-methylcytosine	28S-C3761	283
NSUN1	5-methylcytosine	28S-C4414	284
ZCCHC4	N^6-methyladenosine	28S-A4220	285

Table 1.6 Ribosome biogenesis rRNA modification enzymes.

1.4.2 40S Subunit

With the cleavage of the rRNA at the A0 and 1 sites the UTP-A and B, and U3 snoRNP complexes dissociate and are recycled[268]. Furthermore, rapidly after the cleavage and separation of the pre-40S and 60S subunits the EMG1-NOP14-NOC4L-UTP14A complex and the RBF PNO1 associate with pre-40S particles before they are exported to the nucleoplasm[286].

In the nucleoplasm the 3'-5' trimming of the 21S rRNA from site 2 to site E occurs by the sequential action of the nuclear exosome containing RRP6 and the poly(A)-specific ribonuclease (PARN) (Figure 1.14)[277,287]. The processing of the 21S rRNA generates the 18S-E rRNA species and is accompanied by the association of more ribosomal proteins and the association and dissociation of RBFs to make a nuclear export competent pre-40S complex (Figure 1.14). These ribosomal proteins are, RPSA, RPS2, RPS15, RPS17, RPS18, RPS19, RPS21, RPS25, RPS26 and RPS30 which form the beak of the 40S subunit (Figure 1.9)[191,267]. Most of the nucleolar specific RBFs dissociate from the pre-18S ribosome in the nucleoplasm including the EMG1-NOP14-NOC4L-UTP14A complex, however PNO1, ENP1, and RRP12 remain associated[191]. The RBF RRP12 co-ordinates important structural rearrangements of the 18S-E rRNA in the head and beak facilitating the incorporation of the above ribosomal proteins which is a critical checkpoint for quality control and nuclear export. RBFs that associate with the pre-40S ribosomal subunit in the nucleoplasm and are exported include LTV1, NOB1, BUD23, TRMT112, RIOK2, PDCD2L and TSR1[191,288]. TRMT112 is the co-factor for BUD23 which mediates the N^7-methylation of G1639 in the 18S rRNA (Table 1.6)[281]. The RBFs RIOK2 and PDCD2L are nuclear export adaptors and bind CRM1, triggering and facilitating the translocation of pre-40S ribosomal subunits across the nuclear pore[288,289].

In the cytoplasm the pre-40S ribosome undergoes distinct final maturation steps. The ribosomal proteins RACK1, RPS12, RPS27A, RPS3, RPS10, RPS20 and RPS29 are incorporated with the dissociation of RIOK2 and ENP1[191]. Final maturation steps involve the pre-40S subunit associated with PNO1, RIOK1, eIF5B, factor X and a mature 60S subunit in a proofreading translation initiation style event[191,290]. During this final event PNO1 arranges helix 44 of the 18S-E rRNA into a mature state causing its release[191]. This then enables NOB1 to cleave the final region of ITS1 sequence still present on the 18S-E rRNA at site 3, resulting in the release of all RBFs and the formation of a translation competent 18S ribosome subunit (Figure 1.14 andFigure 1.15)[291].

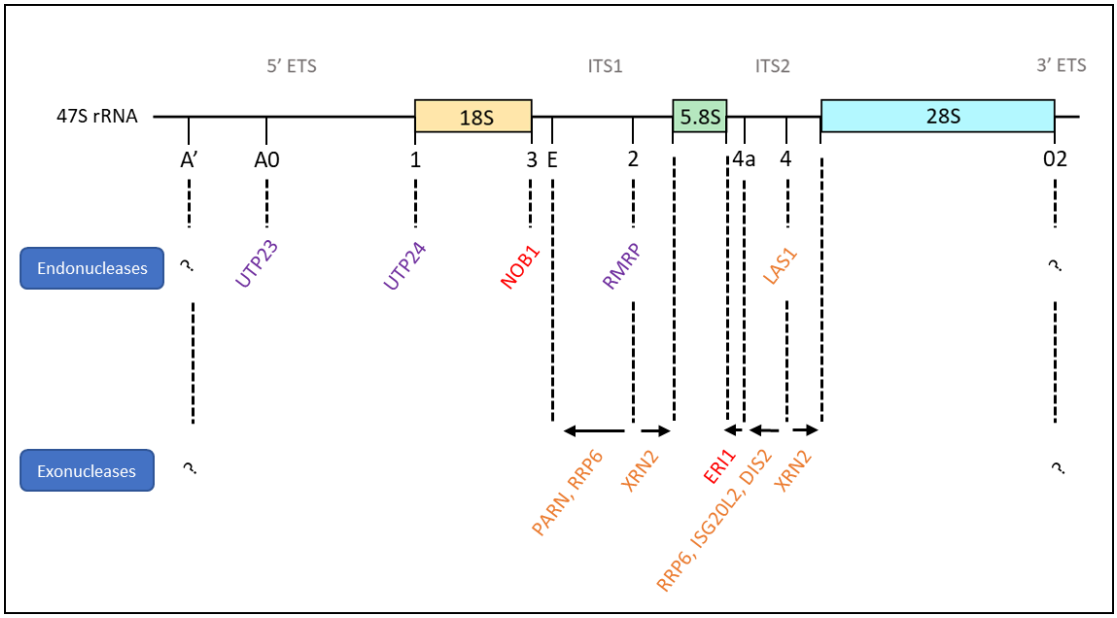

Figure 1.14 Pre-rRNA processing enzymes. The endo- and exonucleases responsible for processing the rRNA during ribosome biogenesis and the rRNA site at which they effect. Enzyme name colour represents cellular region of activity. Purple=Nucleolus, Yellow=Nucleoplasm and Red=Cytoplasm.

1.4.3 60S Subunit

After the cleavage and separation of the pre-40S and 60S subunits the 5S rRNA associates with the maturing pre-60S particle in the nucleolus. The 5S rRNA is transcribed in the nucleoplasm by RNA POL III where it recruits RPL5 and 11 to form the 5S RNP[292]. The RNP is transported to the nucleolus where it associates with the evolving pre-60S complex. Similar to yeast it is thought that the 5S RNP is only tethered to the pre-60S subunit in the nucleolus, and not until later stages of maturation in the nucleoplasm is it fully incorporated into the subunit[292]. Later stages of nucleolar maturation sees the association of a number of ribosomal proteins into the pre-60S particle including, RPL13, RPL14, RPL13A, RPL17, RPL18A, RPL23 and RPL26, which start to form the subunit interface (Figure 1.9)[271]. Furthermore, a number of important RBFs associate with the maturing pre-60S complex, RSL24D1, GNL2 and MRTO4. The RBF RSL24D1 binds the interface between domains V and VI of the 28S rRNA, acting as a space holder for the ribosomal protein RPL24[293]. GNL2 binds domain V of the 28S rRNA and, similar to the yeast homologue Nog2, is important for guiding structural arrangements of the PTC[294]. MTRO4 acts as a placeholder for the ribosomal protein P0 which forms the start of the 60S subunit L1 stalk[295]. During translocation of the pre-60S complex from the nucleolus to the nucleoplasm most of the early RBP complexes and factors dissociate[188].

After translocation from the nucleolus the final region of ITS1 on the 5' end of the 32.5S rRNA is rapidly removed by the endonuclease XRN2 (Figure 1.14 andFigure 1.15)[277]. Site 4 of ITS2 is then cleavage by the endonuclease LAS1 separating the 5.8S rRNA from the 28S rRNA, generating a 12S and 28.5S rRNA respectively (Figure 1.14 and Figure 1.15)[296]. The RBF MDM1 and the PELP1-TEX10-WDR18 complex associate with the pre-60S particle to guide the 180° rotation and full incorporation of the 5S RNP[297,298]. This incorporation event promotes a cascade of ribosomal protein binding including: RPL10A, RPL8, RPL9, RPL15, RPL19, RPL22, RPL23A, RPL27, RPL30, RPL31, RPL34, RPL35, RPL36, RPL37, RPL38 and RPL37A. Many of the proteins form the central protuberance along with the 5S RNP (Figure 1.9)[270,271]. Further trimming of the remaining ITS2 sequence at the 3' end of the 12S rRNA (pre-5.8S rRNA) and the 5' end of the 28.5S rRNA (Pre-28S rRNA) produces a 6S rRNA and mature 28S rRNA respectively. The 3' end of the 12S rRNA is trimmed down to the site 4a in a stepwise fashion by the endonucleases, DIS2, ISG20L2 and RRP6 respectively[266,299,300] (Figure 1.14 and Figure 1.15). The 5' end of the 28.5S rRNA is removed by the endonuclease XRN2[301] (Figure 1.14 and Figure 1.15). Most of the RBFs and complexes dissociate from the pre-60S particles prior to nuclear export. The departure of GNL2 from the mature PTC enables association of the nuclear export factor NMD3 which also binds the PTC[294,302]. The fact that NMD3 needs to bind a mature PTC means the maturation of this 60S subunit region is most likely a quality control checkpoint for nuclear export. Finally, just before nuclear export DUSP12 phosphorylates MRTO4 releasing it from the pre-60S complex, allowing the recruitment of the ribosomal protein P0 which forms the base of the 60S subunit L1 stalk (Figure 1.9)[295]. In addition, this sterically frees NMD3 to bind the nuclear export adaptor CRM1 triggering the translocation of pre-60S ribosomal subunits across the nuclear pore[303].

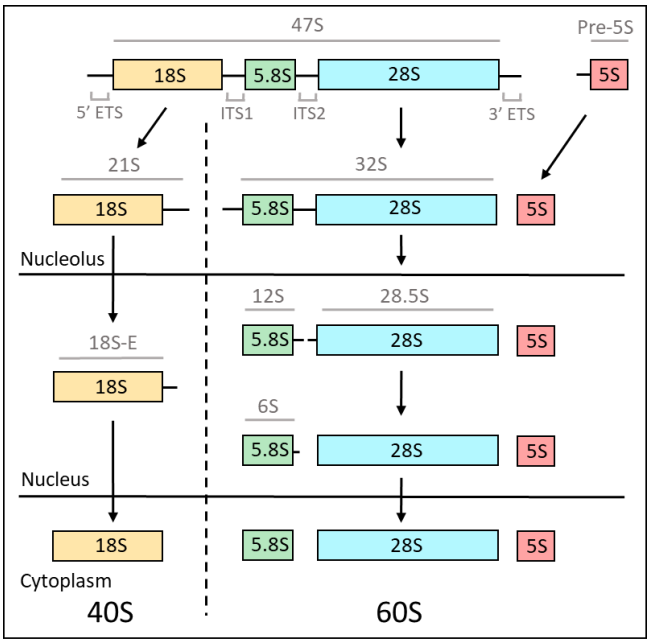

Figure 1.15 Subcellular localisation of pre-rRNA species. The various rRNA species present throughout ribosome biogenesis.

The details of 60S cytoplasmic maturation are not as well studied in humans compared to the 40S. However, the removal of the final 3' ITS2 sequence from the 6S rRNA is completed by the multifunctional enzyme ERI1 producing the mature 5.8S rRNA[304] (Figure 1.14 and Figure 1.15). The final ribosomal proteins to be incorporated into the 60S subunit include, P1, P2 RPL12, RPL21, RPL27A, RPL28, RPL29, RPL39, RPL40, RPL41 and RPL36A[270,271]. Furthermore, the RBF yeast homologue of RSL24D1 recruits and activates the GTPase DRG1, which catalyses its replacement with RPL24[305]. The final steps of maturation and proof reading of the 60S subunit involve the release of NMD3 from the PTC by the GTPase LSG1, as described in yeast[302]. The RBF SBDS then takes the place of NMD3 and can only bind if the P-site, P-stalk, and PTC are fully mature[306]. SBDS then recruits the GTPase EFL1 causing the release of eIF6 which binds during early ribosome biogenesis and acts to preventing premature translation, by impeding the association of pre-60S particles with 40S subunits (Figure 1.13)[307,308]. The release of eIF6 causes conformational changes in EFL1 activating its GTP hydrolysis and concomitant dissociation along with SBDS from the fully mature translation competent 60S subunit[308].

1.5 Ribosome Specialisation

Historically, ribosomes have been viewed as unchanged homogeneous units with no intrinsic regulatory capacity for mRNA translation. However, over the last 20 years many reports have shown heterogeneity in the ribosome population of cells and more recently studies have demonstrated phenotypic relevance of these specialised ribosomes[309–313].

Gene expression is controlled at every level from, mRNA transcription through to protein turnover. At the level of mRNA translation, protein expression can be regulated through the binding of proteins to UTRs, uORFs, structures within the mRNA itself and lncRNA-mRNA base pairing[257,314–316]. Ribosome specialisation offers another option for the regulation of gene expression whereby distinct subpopulations of ribosomes can more preferentially translate specific groups of mRNAs.

The concept of specialised ribosomes was first theorised in the 1950s when differences in ribosome size and shape were identified, and a one gene–one ribosome–one protein hypothesis was discussed by Crick[317,318]. These concepts were generally not accepted or challenged until the early 2000's with the suggestion of the "Ribosome Filter Hypothesis." This idea suggested that translation could be activated or inhibited by ribosomal subunits

depending on how they interact with specific mRNAs[319]. In 2006 and 2007 respectively concepts of "immunoribosomes" and a "ribosome code" were developed. Yewdell and Nicchitta proposed that immunoribosomes are a subset of ribosomes dedicated to the translation of antigens for presentation by MHC[320]. The "ribosome code" proposed an idea that like the histone code different ribosome protein paralogues can specify translation of distinct mRNAs[321]. All of these hypothesis have contributed to the now well-defined concept and rapidly expanding field of specialised ribosomes which has been seen over the last 10 years[322–324].

1.5.1 Ribosomopathies

Ribosomopathies are a family of genetic diseases that arise from mutations in genes encoding for ribosomal proteins and biogenesis factors (Table 1.7). These diseases manifest with a diverse set of phenotypes which tend to be tissue specific. This has helped fuel the idea that different cell types might require specific ribosomal proteins or modifications to translate cell type specific mRNAs. Ribosomopathies have therefore also been an important factor in the evolution of the specialized ribosome theory.

Due to the severe nature of ribosomopathies they are generally rare conditions. However, the most prominent and best understood example is Diamond-Blackfan anemia (DBA), which results from haploinsufficiencies in genes encoding both small and large ribosomal subunit proteins with RPS19 been the most common, mutated in 25% of patients (Table 1.7)[325]. DBA is characterised by bone marrow failure due to inhibition of hematopoietic stem cell differentiation along the erythroid lineage.

Williams-Beuren syndrome is caused by a complex multi-gene deletion on chromosome 7q11.23, and results in a variety of symptoms, most noticeably cardiovascular abnormalities[326]. One of the genes deleted is the RBF BUD23, which as described above, N^7-methylates G1639 of the 18S rRNA (Table 1.6). Baxter et al. made the phenotypic link demonstrating that the depletion in BUD23 expression in mice cardiomyocytes leads to the development of dilated cardiomyopathy and premature death[327]. In addition, they show that BUD23 promotes the translation of mitochondrial proteins and impacts oxidative phosphorylation which is required by ATP-hungry cells such as cardiomyocytes[327].

Ribosomopathy	Affected Gene(s)	Mutation(s)	Clinical Features	Reference(s)
Diamond-Blackfan anemia	RPL5, RPL11, RPL27, RPL35A, RPS7, RPS10, RPS17, RPS19, RPS24, RPS26, RPS27, RPS28, GATA1, TSR2	Various (Most prevelent in RPS19)	Anaemia, microcephaly, hypertelorism, ptosis, micrognathia, cleft palate, short, webbed neck, malformed or absent thumbs, cataracts, glaucoma, strabismus	328
Williams-Beuren syndrome	BUD23	Deletion of 1.7 Mb region of chr. 7q11.23	Hyperacusis, vascular stenosis, Hypertension, Intracardiac lesion, global cognitive impairment, hypodontia, osteopenia or osteoporosis, celiac disease, ADHD	326
5q-myelodysplastic syndrome	RPS14	Deletion of 1.5 Mb region of chr.5	Severe anaemia, thrombocytosis, dysmegakaryopoiesis	329
Isolated congenital asplenia	RPSA	pP199Sfs*25, pQ9*, p.T54N, p.L58F, p.R180W, p.R180G, p.R186C	Lack of spleen, immunodeficiency	330
RPS23-related ribosomopathy	RPS23	p.R67K	Microcephaly, hearing loss, simian palmar creases, epicanthic folds in the eyes, foetal finger pads, extra front teeth, facial asymmetry and high palate, intellectual disability, autism spectrum disorder	331
Scleroderma	UTP14A	Gene hypermethylation – decreased expression	Hardened/thickened skin, ulcers/sores, swollen joints, fingers or toes, muscle weakness	332
Bowen-Conradi syndrome	EMG1	p.D86G	Growth retardation, microcephaly, micrognathia, joint abnormalities, camptodactyly, rocker-bottom feet, severe psychomotor delay	333
Dyskeratosis congenita	DKC1, TERC, TERT, NOP10, NHP2, TINF2	Various (Most prevalent Dyskerin p.A353V)	Mucocutaneous abnormalities, pulmonary fibrosis, bone marrow failure, immunodeficiency	334–336
Cartilage-hair hypoplasia	RMRP	Various	Short stature, bone deformities, hair growth abnormalities	337
North American Indian childhood cirrhosis	UTP4, NOL11	Various (Most prevalent NOL11 p.R565W)	Biliary cirrhosis, portal hypertension	338,339
X-linked intellectual disability, cerebellar hypoplasia and spondyloepiphyseal dysplasia	RPL10	p.A64V	Intellectual disability, cerebellar hypoplasia and spondyloepiphyseal dysplasia	340

Table 1.7 Ribosomopathies, causes and phenotypes.

Rather than the tissue specific phenotypes observed in ribosomopathies being due to specialisation of ribosomes and translation of tissue specific mRNAs, some authors have proposed a more general model of p53 stabilisation leading to cell-cycle arrest and apoptosis[341,342]. Mutations of ribosomal proteins and RBFs cause disruptions in ribosome

biogenesis, which in turn leads to the stabilisation of p53. It has therefore been suggested that variations in the threshold or extent of p53 activation in different cell types may contribute to tissue specificity in some ribosomopathies. Furthermore, an overall reduction in ribosome biogenesis can occur due to mutations in ribosomal proteins or RBFs leading to a reduction of available ribosomes for translation[343]. Therefore, in fast-proliferating cell types or tissues this can lead to the reduction in translation of specific mRNAs due the number of ribosomes becoming limiting. Overall, this suggests that some of the symptoms exhibited in ribosomopathies may be dosage dependent. The likelihood is that all three mechanisms described have varying roles to play in different ribosomopathies.

1.5.2 Mechanisms and phenotypes

Six different types of mechanisms have been reported leading to ribosome specialisation including, changes in ribosomal protein stoichiometry, paralogues and posttranslational modifications, addition of ribosome-associated proteins and changes in rRNA genetic variation and modifications. Specialised ribosomes have been most extensively studied in developmental biology however they have also been reported in, cell type specificity, cell homeostasis, cancer, and viral infection.

One of the most well characterised examples of ribosome specialisation is during mammalian body patterning and neurogenesis involving the expression of homeobox (Hox) mRNAs. The large ribosomal subunit protein RPL38 is expressed at elevated levels in the developing vertebrate and spinal core of embryonic mice[310]. Haploinsufficiency of RPL38 in developing mice results in specific defects in the formation of the axial skeleton and motor neurons[310]. For example, these mice develop an extra rib, have shorter or kinky tails and wavey or branching motor neurones. However, overall cap dependant translation is not affected in these mice and these specific phenotypes are not present in mice with other ribosomal protein depletions[310]. Hox genes have been shown to be key regulators of vertebrae segment identity, and the loss of function of specific Hox genes in mice causes very similar phenotypes to RPL38 haploinsufficient mice[344]. Furthermore, specific Hox gene expression was shown to be drastically reduced in RPL38 haploinsufficient mice due to the IRES dependent translation of these specific Hox mRNAs[345]. Overall, this demonstrates a detailed mechanism were RPL38 can specialise ribosomes for the translation of specific Hox gene IRES containing mRNAs.

Furthermore, a fantastic example of ribosome specialisation during cell homeostasis is a yeast response to salt or pH stress with the down regulation of Rps26[311]. The small subunit ribosomal protein Rps26 is required for the faithful translation initiation of strong Kozak sequence start sites. Yeast stress response genes, such as Hog1 and Rim101, contain unfavourable Kozak sequences and are therefore less well translated during homeostatic cell conditions. However, upon yeast cell salt or pH stress, Rps26 is depleted, increasing the pool of ribosomes that lack Rps26 which can therefore more efficiently translate these stress response genes.

Cancers have been associated with a number of ribosomal protein mutations perpetuating the idea of 'onco-ribosomes'[346–348]. Interestingly, the 18S rRNA base 1240U, which can be hypermodified with $m^1acp^3\Psi$, is unmodified in up to 45.9% of colorectal cancers (CRCs)[349]. Cells depleted of $m^1acp^3\Psi$ share the same translational signature as CRC patients with reduced 1240U $m^1acp^3\Psi$[349]. The $m^1acp^3\Psi$ modification of the 18S rRNA base 1240U is at the ribosomal P site and directly interacts with the P site tRNA and RPS16[349]. However, the mechanism for the cancer specific translational phenotype is yet to be determined.

Finally, there is also emerging reports of virus specific specialised ribosomes. For example, the large subunit ribosomal protein RPL40 is required for vesicular stomatitis virus (VSV) cap-dependent translation initiation, but not bulk cellular translation[350]. The specificity of RPL40 positive ribosomes for VSV mRNAs over cellular mRNAs is even more remarkable as VSV mRNAs are virtually indistinguishable from cellular mRNAs[350]. Furthermore, a poxvirus kinase phosphorylates serine/threonine residues in the human small ribosomal subunit protein RACK1 that are not phosphorylated in uninfected cells or cells infected by other viruses[309]. The phosphorylation of RACK1 dictates ribosome selectivity towards viral RNAs with 5' UTR polyA-leaders[309].

1.6 Thesis Aim and objectives

No virus encodes machinery to translate its own proteins. In addition, viruses have been shown to co-opt and manipulate just about every facet of cellular life. Therefore, it would seem very plausible that, as cells produce specialised ribosomes to regulate the translation of cellular mRNAs, viruses too could use this same idea to create virus specific specialised ribosomes to enhance the translation of their own viral mRNAs.

Hence, the central hypothesis of this thesis was to determine whether viruses can produce specialised ribosomes during their infection to preferentially or efficiently promote the translation of viral mRNAs.

The overall object of this thesis was to understand whether KSHV, during lytic replication, modifies ribosomes that can preferentially or efficiently translate its mRNAs. Towards this objective there were three aims:

The first aim sought to determine how KSHV could modify ribosomes during lytic replication. Hence, the composition and stoichiometry of newly emerging ribosomes undergoing ribosome biogenesis were investigated during latent and lytic replication to identify changes to this process.

Amongst other changes identified to pre-40S ribosome complexes during lytic replication, the RBF BUD23 was identified to have increased association with these complexes. The second aim was to validate and determine the importance of this observation for lytic KSHV replication.

BUD23 was shown to be important for lytic replication and specifically the efficient translation of late viral genes. The final aim was therefore to understand how the increased association of BUD23 during ribosome biogenesis in KSHV lytically replicating cells impacted the translation of viral genes using ribosome profiling.

Chapter Two

~

Materials and Methods

2 Materials and Methods

2.1 Materials

2.1.1 Chemicals, reagents, and materials

Chemical/Reagent/Material	Supplier	Catologue #
Acetic acid, 99.5%	Acros Organics	124040010
Phosphatase Inhibitor Cocktail I	Alfa Aesar	J63907.AA
Precision Plus Protein Dual Color Standards	Bio-Rad Laboratories	1610394
Xylene Cyanole		1610423
DTT	Fisher Scientific	10592945
Ethanol		12468750
HCl		10294190
Isopropanol		10315720
Methanol		10284580
NaCl		10326390
Tris		10724344
Tween-20		10485733
NaOH (1N)	Hanna Instruments	HI-70457
MagStrep type 3 XT Beads 5% Suspension	IBA Solutions For Life Science	15362006
1 Kb Plus DNA Ladder	Invitrogen	10787018
Acrylamide/Bis 19:1, 40% (w/v) solution		AM9024
EDTA (0.5 M), pH 8.0		AM9260G
GlycoBlue Coprecipitant (15 mg/mL)		AM9516
KCl		AM9640G
SUPERase-In RNase Inhibitor (20 U/uL)		AM2694
TRIzol LS Reagent		11588616
TRIzol Reagent		15596018
UltraPure™ DNase/RNase-Free Distilled Water		10977035
0.45 µm nitrocellulose blotting membrane	Life Science products Cytiva	10600002
Glycine	Melford	G0709
1M $MgCl_2$	Millipore	20-303
Skim milk powder		70166
Sucrose		1076875000
ECL Western Blotting Substrate	Promega	W1015
Nuclease-Free Water		P1199
RNasin Plus RNase Inhibitor		N2611
Acrylamide/Bis-acrylamide 30% 37.5:1	Severn Biotech	20-2100-10

TBE 10X		20-6000-50
APS	Sigma-Aldrich	215589
Biotin		14400
Bromophenol Blue sodium salt		B5525
BSA		A7906
cOmplete(TM), EDTA-free Protease Inhibit		5056489001
Cycloheximide		C4859
Formaldehyde solution, 36.0%		47608
Glycerol		G7757
Holey carbon film Supported Copper Grids		TEM-HC300CUCC
PBS tablets		P4417
Poly-L-lysine solution, 0.01%		P4707
SDS		L5750
Silver Nitrate		204390
Sodium Carbonate		71360
TEMED		T9281
Triton X-100		X100
NP-40 Surfact-Amps™ Detergent Solution	Thermo Scientific	85125
BCA Protein Assay		23227
Urea		29700
SuperSignal West Femto Chemiluminescent Substrate		34095
VECTASHIELD® Antifade Mounting Medium with DAPI	Vector Laboratories	H-1200-10
Sodium Thiosulphate	VWR	84852.23

Table 2.1 Supplier and product numbers of all chemicals, reagents, and materials used in this thesis.

2.1.2 Cell Lines

HEK-293T cells (American Type Culture Collection)

TREx BCBL1-Rta cells[351] - a gift from J. U. Jung (UCLA)

2.1.3 Cell Culture

Cell culture plasticware was purchased from the Thermo Scientific Biolite range and all other cell culture reagents listed below in Table 2.2.

Cell Culture Reagent	Supplier	Catologue #
25mm Ezee Syringe Filters, 0.45µM, PVDF, sterile	Elkay	LK25-PV45-50S
Sterile PES Syringe Filter, Pore Size: 0.2um	Fisherbrand	15206869
Dulbecco's modified Eagle's medium media with glutamine (DMEM)	Lonza	41965062
10% Fetal Bovine Serum (FBS)	Gibco	10270106
Hygromycin B (50 mg/mL)		10687010
Opti-MEM I Reduced Serum Medium		31985070
Penicillin-Streptomycin (5,000 U/mL)		15070063
Puromycin Dihydrochloride		A1113803
Roswell Park Memorial Institute 1640 growth medium with glutamine (RPMI)		21875091
Trypan Blue Solution, 0.4%		15250061
Lipofectamine 2000	Invitrogen	11668019
PBS without Calcium without Magnesium	Lonza	BE17-516F
Doxycycline Hyclate	Sigma-Aldrich	D9891
Polybrene Transfection Reagent		TR-1003

Table 2.2 Supplier and catalogue numbers of all cell culture reagents.

2.1.4 Plasmids

Fourteen pCDH-CMV-MCS-EF1-Puro plasmids were cloned and purchased from GenScript. Plasmids included: Twin-Strep-FLAG-DIMT1, Twin-Strep-FLAG-NOC4L, Twin-Strep-FLAG-PNO1, Twin-Strep-FLAG-TSR1, Twin-Strep-FLAG-LTV1, Twin-Strep-FLAG-RSL24D1, Twin-Strep-FLAG-MRTO4, Twin-Strep-FLAG-GNL2, Twin-Strep-FLAG-NMD3, Twin-Strep-FLAG-LSG1, scrambled-shRNA, shRNA1-BUD23 and shRNA2-BUD23.

The lentivector expression system packaging plasmids psPAX2 (12260) and pVSV.G (12259) were purchased from Addgene.

2.1.5 Antibodies

All primary antibodies, their working dilutions and suppliers are shown in Table 2.3. Horseradish peroxidase (HRP)-conjugated anti mouse and anti-rabbit secondary IgG, used for Western blotting at a 1:5000 dilution, were obtained from Agilent Technologies (P044701-2 and P044801-2).

Alexa Flour 488 goat anti-rabbit IgG and Alexa Flour 546 donkey anti-mouse IgG, used for immunofluorescence microscopy at a dilution of 1:500, were purchased from Life Technologies (A11008 and A10036).

Antibody	Origin	Working Dilution	Supplier	Catologue #
Anti-GAPDH	Mouse	1:5000	Proteintech Europe	60004-1-Ig
Anti-FLAG	Mouse	1:250 (IF)	Sigma-Aldrich	F1804
Anti-FLAG	Rabbit	1:5000	Sigma-Aldrich	77425
Anti-DNA Pol II	Mouse	1:500 (IF)	Sigma-Aldrich	CTD4H8
Anti-BUD23	Rabbit	1:500	Thermo Fisher Scientific	PA521698
Anti-NOC4L	Rabbit	1:500	Proteintech	17025-1-AP
Anti-RPS19	Rabbit	1:500	Proteintech	15085-1-AP
Anti-ORF57	Mouse	1:1000	Santa Cruz	sc-135747
Anti-CDK1	Mouse	1:5000	Abcam	ab18
Anti-ORF59	Rabbit	1:1000	Prof. Britt Glaunsinger, University of California, Berkeley	N/A
Anti-K8.1	Mouse	1:1000	Advanced Biotechnologies	13-212-100
Anti-ORF65	Rabbit	1:500	Cambridge Research Biochemicals	crb2005224

Table 2.3 Primary antibodies, their working dilution, and suppliers.

2.1.6 Kits and Enzymes

Kits and Enzymes	Supplier	Catologue #
DNA-free™ DNA Removal Kit	Invitrogen	AM1906
TURBO™ DNase		AM2238
LunaScript® RT SuperMix Kit	New England Biolabs	E3010L
Monarch Total RNA Miniprep Kit		T2010S
NEBNext® Multiplex Small RNA Library Prep Set for Illumina®		E7300S
NEBNext® rRNA Depletion Kit		E6310L
T4 PNK		M0201L
GoTaq® qPCR Master Mix	Promega	A6002
RNase I	Thermo Scientific	EN0601

Table 2.4 Kits and Enzymes with suppliers and catalogue numbers.

2.1.7 Primers

Primer	Direction	Sequence (5'-3')
GAPDH	Forward	TGTGGTCATGAGTCCTTCCACGAT
	Reverse	AGGGTCATCATCTCTGCCCCCTC
ORF65	Forward	AAGGTGAGAGACCCCGTGAT
	Reverse	TCCAGGGTATTCATGCGAGC
ORF57	Forward	GCCATAATCAAGCGTACTGG
	Reverse	GCAGACAAATATTGCGGTGT
ORF59	Forward	CCGATCGTGGAAAGGTAGGA
	Reverse	ATGTACTCGACGCTGGCATA
K8.1	Forward	GTTCCACACAGATTCGCACA
	Reverse	AGTTCATCCTGCCTAGCCAG
BUD23	Forward	TACGTTCGCAACTCACGGAT
	Reverse	CCAGCAGGTAACAGGGCTTA
18S rRNA Total	Forward	GATGGTAGTCGCCGTGCC
	Reverse	GCCTGCTGCCTTCCTTGG
18S rRNA G1639	Forward	GTAACCCGTTGAACCCCATT
	Reverse	CCATCCAATCGGTAGTAGCG
28S rRNA	Forward	GGGTGGTAAACTCCATCTAAGG
	Reverse	GCCCTCTTGAACTCTCTCTTC

Table 2.5 qPCR primer sets and their sequences.

2.2 Methods

2.2.1 Cell Culture

2.2.1.1 Cell Maintenance

HEK-293T cells, an embryonic kidney derived cell line was cultured in DMEM growth media, supplemented with 10% FBS, penicillin (100 U ml^{-1}), and streptomycin (100 µg ml^{-1}) at 37°C in 5% CO_2. TREx BCBL1-Rta cells, a human B-cell lymphoma cell line latently infected with KSHV, were grown in RPMI 1640 growth medium with glutamine, supplemented with 10% FBS, penicillin (100 U ml^{-1}), streptomycin (100 µg ml^{-1}) and hygromycin B (100 µg ml^{-1}) at 37°C in 5% CO_2.

2.2.1.2 Cell Passaging

Throughout this study cell lines were maintained by passaging every three to four days up to a passage number of 30. HEK-293T cells were passaged by mechanical disruption from the flask surface once reaching a confluency of 80%. The cells were diluted down in fresh DMEM growth media and reseeded at 10% confluency. TREx BCBL1-Rta cells were passaged one reaching a density of 1.5 x 10^6 cells/ml by dilution with fresh RPMI growth media and reseeded at a density of 0.1 x 10^6 cells/ml.

2.2.1.3 Cell Harvesting

After experimental treatment of 293T cells the media was aspirated and the cells washed off with PBS followed by centrifugation (500 x g, 5 min, 4°C) and the PBS discarded to collect the cell pellet. TREx BCBL1-Rta cells were thoroughly resuspended then collected by centrifugation (500 x g, 5 min, 4°C) and the media discarded. Followed by a PBS wash and final centrifugation as above to collect the cell pellet.

2.2.1.4 TREx Cell Counting

TREx BCBL1-Rta cells were thoroughly resuspended and a 20 µl sample diluted 1:1 in trypan blue solution (0.4%). The trypan blue cell dilution was incubated at room temperature for one minute before been transferred onto a hemocytometer (Hawksley, Improved Neubauer 2xBright) and viable cells counted.

2.2.1.5 Lentivector Expression and shRNA Systems

Fourteen pCDH-CMV-MCS-EF1-Puro plasmids were cloned and purchased from GenScript, eight expression plasmids and six shRNA plasmid. Each expression plasmids encoded different FLAG/Strep tagged ribosome biogenesis bait proteins, DIMT1, PNO1, NOC4L, LTV1, TSR1, MRTO4, LSG1, and NMD3. The five shRNA plasmids targeted the ribosomal biogenesis factor gene BUD23 and one shRNA plasmid contained a scrambled (Scr) sequence that doesn't target the human genome.

Sub-confluent HEK-293T cells seeded in 6 well plates were grown in DMEM without penicillin or streptomycin and transfected with lentivirus packaging plasmids and an expression or shRNA plasmid. The two packaging plasmids psPAX2 (6.5 µg/ml) and pVSV.G (6.5 µg/ml) and an expression or shRNA plasmid (12 µg/ml) were diluted in OPTI-MEM media containing lipofectamine 2000 and co-transfected into HEK-293T cells. Six hours post-transfection the media was replaced with fresh DMEM without penicillin or streptomycin. At 48 hours post-transfection, the lentiviral supernatants were collected and filtered through a 0.45 µm membrane. Then in the presence of polybrene (8 µg/ml) the filtered lentiviral supernatant was added to TREx BCBL1-Rta cells. The cells were spin-inoculated (800 × g, 1 hour, room temperature) then reseeded into six well plates. Six hours post-transduction the media was replaced with fresh RPMI media. At 48 hours post-transduction, the media was replaced with fresh selection RPMI media containing puromycin (2 µg/ml). The selection media was then changed and the cells passaged every three to four days.

2.2.1.6 Cell Growth Assay

TREx BCBL1-RTA cells expressing BUD23 specific shRNAs or Scr shRNA were seeded into a 6-well plate at 0.2 x 10^6 cells/well with 2 ml fresh RPMI selection media. The cells were grown for 48 hours and the cells counted at each 24 hour interval.

2.2.1.7 Cell Line Freezing

HEK-293T and TREx BCBL1-Rta cells were pelleted by centrifugation (500 x g, 5 min, 4°C) and the media discarded. The cells then resuspended in ice cold FBS at a density of 5 x 10^6 cells/ml and incubated on ice for ten minutes. The FBS cell suspension was supplemented with 25% freezing media (0.66 M glucose, 40% DMSO and 60% RPMI or DMEM) and stored rapidly at -80°C.

2.2.2 Lytic KSHV Assays

2.2.2.1 Lytic Induction

The TREx BCBL1-Rta cell line is latently infected with KSHV and modified to contain a doxycycline-inducible myc-RTA element for robust lytic reactivation. To induce lytic reactivation TREx BCBL1-Rta cells and lentivector modified TREx BCBL1-Rta cells, at a density of 0.5 to 1 x 10^6 cells/ml, were treated with 2 µg ml^{-1} doxycycline hyclate. Cells were collected at various timepoints after lytic induction as described above (2.2.1.3). Cell pellets were used in downstream analysis by western blotting (2.2.3), qPCR (2.2.5), bait protein pulldowns (2.2.6), and ribosome sequencing (2.2.11).

2.2.2.2 KSHV Reinfection Assay

TREx BCBL1-RTA cells expressing BUD23 specific shRNAs or Scr shRNA were seeded into a 6-well plate at 0.75 x 10^6 cells/well with 2 ml fresh RPMI growth media (without puromycin). The cells were induced with 2 µg ml^{-1} doxycycline hyclate for 72 hours. The culture medium, containing released virions, was then centrifuged to remove cells and debris and mix at a 1:1 ratio with fresh complete DMEM growth media which was incubated for 48 hours with naive HEK-293T cells at 40% confluency. The 293T cells were harvested as described above (2.2.1.3) then total RNA was extracted and reverse transcribed followed by qPCR analysis of the viral mRNA ORF57 to assess efficiency of virus reinfection (2.2.5). The final version of these experiments presented in this thesis were done by Elena Harrington.

2.2.3 Western Blotting

2.2.3.1 Whole cell lysate extraction

Cells were lysed in RIPA buffer [25 mM Tris/HCl (pH 7.4), 150 mM NaCl, 1% NP-40, 0.1% SDS and 1 × Roche protease inhibitor cocktail] for 30 minutes on ice and clarified by centrifugation (16,000 × g, 10 mins, 4°C).

2.2.3.2 Protein Concentration Assay

A bicinchoninic acid (BCA) assay was performed to determine the concentration of protein in each sample. Bovine serum albumin (BSA) standards were made up by 1:2 serial dilution from a 16 mg/ml BSA starting solution. In a 96-well plate, 2 µl of each sample and standard was mixed thoroughly with 2 µl reagent A (copper reagent) and 98 µl reagent B (BCA reagent). The plate was incubated (37°C, 20 mins) and then shaken before the absorbance was measured at 562 nm using a microplate reader (Multiskan™ FC Microplate Photometer, 51119000, Thermo Scientific). Protein sample concentration was interpolated from the BCA standard curve and equalised to the lowest sample concentration with additional RIPA buffer. Finally, the protein samples were mixed 1:1 with laemmli loading buffer [120 mM Tris/HCl (pH 6.8), 4% (w/v) SDS, 20% (v/v) glycerol, 50 mM DTT, 0.25% (w/v) bromophenol blue].

2.2.3.3 Sodium Dodecyl Sulphate – Polyacrylamide Gel Electrophoresis (SDS-PAGE)

Equal amounts of protein samples (20 µg or total pulldown sample) were separated by their molecular weight using a Mini-PROTEAN gel electrophoresis system (Biorad). Polyacrylamide gels were prepared at a range of concentrations (10%-15%) depending on the proteins of interest been investigated. These gels contained a resolving region [10%-15% (v/v) acrylamide/bis-acrylamide 37.5:1, 375 mM Tris/HCl (pH 8.8), 0.1% (w/v) SDS, 0.12% (v/v) APS, 0.012% TEMED (v/v)] and a stacking region [5% (v/v) acrylamide/bis-acrylamide 37.5:1, 125 mM Tris/HCl (pH 6.8), 0.1% (w/v) SDS, 0.08% (v/v) APS, 0.008% (v/v) TEMED] with 10 to 15 wells. Samples were boiled (95°C, 5 mins) and loaded on the gel along side a standard protein ladder. Gels were resolved in running buffer [25 mM Tris/HCl, 192 mM Glycine and 0.1 % (w/v) SDS] at 180 V until the dye front reached the end of the gel.

2.2.3.4 SDS-PAGE Transfer to Nitrocellulose Membrane

Resolved protein samples were transferred from the acrylamide gel to a 0.45 µm nitrocellulose blotting membrane by semidry transfer (Biorad, Trans-Blot Turbo Transfer System). Blotting paper and nitrocellulose membranes were pre-soaked in transfer buffer [20% (v/v) methanol, 25 mM Tris, 192 mM glycine] and a sandwich setup with a blotting paper on the cathode followed by the nitrocellulose membrane then the gel and finally another blotting paper. The proteins were transferred for 20 minutes at 25 V and 0.1 A.

2.2.3.5 Immunoblotting

To block nonspecific protein binding sites, membranes were incubated at room temperature with 5% (w/v) non-fat milk in Tris buffered saline and Tween-20 (TBS-T) [150 mM NaCl, 50 mM Tris/HCl (pH 7.5), 1% (v/v) Tween-20] on a rocking platform for 1 hour. Membranes were then probed overnight with a primary antibody against the protein of interest in 5% (w/v) non-fat milk in TBS-T at 4°C. The following day membranes were washed three times for 5 minutes in TBS-T and labelled for 1 hour at room temperature with a secondary horseradish peroxidase-conjugated IgG antibody in 5% (w/v) non-fat milk in TBS-T. The membrane was washed again as above, and the proteins detected by chemiluminescence with ECL substrate. The chemiluminescence signal was captured digitally using a G:Box Chemi XX9 imager (Alpha Metrix). Finally, membranes were washed twice for 5 minutes in TBS-T and equal loading was then determined by probing for GAPDH as described above.

2.2.3.6 Densitometry Analysis

Densitometric measurements of the western blots were performed using ImageJ software (version 1.52a, National Institute of Health, Bethesda, MD, USA). Values for each protein of interest band were normalized to GAPDH controls and then relativised to a control condition.

2.2.4 Immunofluorescence Microscopy

2.2.4.1 Cell Culture

Glass coverslips (Menzel, 631-1342) were prepared in a 24-well plate first, by washing with ethanol to sterilise them and then incubating the cover slips for 5 minutes with poly-L-lysine. The poly-L-lysine wash then aspirated, and the coverslips washed with PBS. TREx BCBL1-Rta cell lines expressing FLAG/Strep tagged ribosome biogenesis bait proteins were seeded at

0.5 x 10^6 cells/ml onto the coated glass coverslips in RPMI selection media and incubate for 24 hours at 37°C in 5% CO_2.

2.2.4.2 Fixing and Staining

The media was aspirated, and the cells washed in PBS before been fixed with 4% (v/v) formaldehyde for 10 minutes. The formaldehyde was removed, and the cells were then again washed twice in PBS before been permeabilised with 0.1% (v/v) Triton X-100 in PBS for 20 minutes. The permabilisation solution was removed and the cells again washed three times in PBS. After permeabilization, cells were then incubated in blocking solution (PBS with 1% (w/v) BSA) for 1 hour at 37°C. The blocking solution was removed, and the cells were then probed with primary antibodies FLAG and DNA POL II, diluted in PBS with 1% (w/v) BSA, for 1 h at 37°C in humidity. The primary antibody solution was aspirated, and the cells were washed four times with PBS. The cells were then incubated with fluorescently conjugated secondary antibodies, Alexa Flour 488 goat anti-rabbit IgG and Alexa Flour 546 donkey anti-mouse IgG, diluted in PBS with 1% (w/v) BSA, for 1 h at 37°C. Finally, the secondary antibody solution as removed and coverslips were washed five times with PBS again and mounted onto microscope slides with mounting media containing DAPI.

2.2.4.3 Imaging

The slides were stored in the dark at 4°C until they were visualised. Images were obtained under oil-immersion using a LSM 880 confocal microscope (Carl Zeiss) and processed using ZEN 2.3 imaging software (Carl Zeiss).

2.2.5 Two-step Reverse Transcription Quantitative PCR (RT-qPCR)

2.2.5.1 RNA Isolation

Total RNA was isolated from cell pellets using the Monarch Total RNA Miniprep Kit. All centrifugation steps in this protocol were carried out at 16,000 x g for 30 seconds and at room temperature, unless otherwise stated. Cell pellets were resuspended in 400 µl RNA Lysis Buffer and transferred to a gDNA Removal Column fitted with a collection tube. The samples were centrifuged and the column, which binds genomic DNA, discarded. The flowthrough was mixed 1:1 with ethanol and transferred to an RNA Purification Column fitted with a collection tube. The samples were again centrifuged and the flowthrough discarded. The columns were then washed with 500 µl RNA Wash Buffer, centrifuged, and the flowthrough discarded. To obtain highly pure RNA the columns were then treated with

premixed 5 µl DNase I and 75 µl DNase I Reaction Buffer for 15 minutes at room temperature. The reaction was stopped with 500 µl RNA Priming Buffer and the samples centrifuged with the flowthrough again been discarded. The RNA samples on the columns were then washed twice with 500 µl RNA Wash Buffer and centrifuged, the second centrifugation was done for 2 minutes to ensure all buffer was removed from the columns. Finally, the columns were placed into new 1.5 ml microcentrifuge tubes (Starlab, S1615-5550) and 50 µl of Nuclease-Free Water was added to each column. The RNA was eluted from the columns by centrifugation and stored at -80°C.

2.2.5.2 Reverse Transcription (RT)

To reverse transcribe the purified RNA the LunaScript® RT SuperMix Kit was used as per the manufacture's guidelines. RNA concentrations were measured using a NanoDrop ND-1000 spectrophotometer (NanoDrop Technologies). Then 1 µg of RNA was mixed with 4 µl LunaScript RT SuperMix (5X) and the reaction mix topped up to 20 µl with Nuclease-Free Water. Negative control reactions for each control condition were also performed with a No-RT Control Mix (5X). The RT reactions were carried out in a QIAamplifier 96 (QIAGEN, 9002991). The first step for primer annealing was carried out at 25°C for 2 minutes, then at 55°C for 10 minutes for cDNA synthesis and finally at 95°C for 1 minute for heat inactivation before holding at 4°C. The cDNA or no-RT samples were then stored at -20°C.

2.2.5.3 Quantitative Polymerase Chain Reaction (qPCR)

The levels of cDNA or DNA in samples was determined by qPCR using a Rotor-Gene Q platform (QIAGEN, 9001550) with sequence specific primers for each gene. Samples were analysed in duplicated with 20 µl reactions in 0.1ml 4-Strip tubes (Starlab, I1402-0400). Each reaction consisted of:

5 µl cDNA/DNA template (Diluted 1:20-1:50)
10 µl 2x GoTaq® Probe qPCR Master Mix
0.5 µl (10 µM) forward primer
0.5 µl (10 µM) reverse primer
4 µl Nuclease-Free Water

No-RT and no template control reactions were also run for the control condition of each experiment. The cycling programme used consisted of an initial 10-minute pre-incubation

step at 95°C, followed by 40 cycles of 95°C for 15 seconds (Denaturing), 60°C for 30 seconds (Annealing) and 72°C for 20 seconds (Extension). Optical fluorescence data was recorded at the end of each extension round at 470 nm. After the qPCR program a melting curve analysis was performed, to confirm amplification of a single product for each primer, between 65°C and 95°C. Unless otherwise stated, relative expression compared to control condition was calculated using the comparative ΔΔCT method with GAPDH as the housekeeping gene.

2.2.6 Isolation of Pre-ribosomes Complexes

2.2.6.1 Cell Culture

TREx BCBL1-Rta cell lines expressing FLAG/Strep tagged ribosome biogenesis bait proteins and a control TREx BCBL1-Rta cell line were seeded at 0.75 x 10^6 cells/ml in 20 ml of RPMI selection or growth media. This was done in duplicate and in half the flasks KSHV lytic replication was induced (2.2.2.1). After 24 hours incubation the cells were harvested (2.2.1.3).

2.2.6.2 Strep Tag Pulldown

Cell pellets were lysed in a ribosome friendly lysed buffer [10 mM Tris/HCl (pH 7.6), 100 mM KCl, 2 mM $MgCl_2$, 0.5% (v/v) NP-40, 1 mM DTT, 1% (v/v) Phosphatase inhibitor (v/v), and 1 × Roche protease inhibitor cocktail] for 20 minutes on ice. Just for the experiments analysing the RNA content of the pulldowns by qPCR, 10% of the input was transferred to a fresh microcentrifuge tube for RNA isolation (2.2.5.1).

For the pulldowns, magnetic Strep-Tactin®XT coated beads were equilibrated by washing 40 µl of bead slurry three times in lyses buffer not containing phosphatase or protease inhibitor. The cell lysates were then clarified by centrifugation (12,000 × g, 10 mins, 4°C) and incubated with the equilibrated beads for 1 hour on a rotator disk at 4°C. The supernatant was then removed, and the beads washed fours times in wash buffer I [10 mM Tris/HCl (pH 7.6), 100 mM KCl and 2 mM $MgCl_2$] with short a pulse vortex in between. The beads were then finally washed in wash buffer II [10 mM Tris/HCl (pH 7.6) and 2 mM $MgCl_2$] with a pules vortex.

2.2.7 Analysis of Preribosome Complexes

2.2.7.1 Silver Stain

Wash buffer II was aspirated from beads and they were resuspended in 30 µl laemmli loading buffer. The samples were then prepared, loaded, and resolved on an SDS-PAGE gel as described above (2.2.3).

Gels were first fixed in 50% (v/v) Ethanol and 10% (v/v) Acetic Acid, then 5% (v/v) Ethanol and 1% (v/v) Acetic Acid for 30 minutes and 15 minutes respectively on a shaker at room temperature. The gels were then washed three times in ultrapure water for five minutes. Next, the gels were sensitised in 0.02% (w/v) Sodium Thiosulphate for two minutes and then washed again three times in ultrapure water (Milli-Q® Advantage A10 Water Purification System, Merck) for 30 seconds. The gels were stained in 0.1% (w/v) Silver Nitrate and 0.08% (v/v) formaldehyde in the dark for 20 minutes and washed again three times in ultrapure water for 20 seconds. The gels were finally developed in 2% (w/v) Sodium Carbonate, 0.04% (v/v) Formaldehyde and 0.0004% (w/v) Sodium Thiosulphate until protein bands were visible, then the reaction stopped using 5% (v/v) Acetic Acid.

A photograph of the gel was then taken using a G:Box Chemi XX9 imager.

2.2.7.2 Total Nucleic Acid Purification

For each sample half the volume of beads in wash buffer II was transferred to a new 1.5 ml microcentrifuge tube. The wash buffer was then aspirated from the all the tubes and the beads were resuspended in 1 ml TRIzol for total nucleic acid purification. To separate the aqueous and organic phase, 200 µl of chloroform was added to each sample and the shaken vigorously for 20 seconds. The samples were then left to settle for 2 minutes at room temperature before centrifugation (12,000 × g, 15 mins, 4°C). The aqueous phase was transferred to a new 1.5 ml microcentrifuge tube and mixed 1:1 with Isopropanol. The samples were incubated at 4°C for 10 minutes to precipitate the nucleic acid. The nucleic acid was then pelleted by centrifugation (12,000 × g, 10 mins, 4°C) and the supernatant discarded. The pellets were washed in 75% (v/v) Ethanol and re-pelleted by centrifugation (7,500 × g, 5 mins, 4°C). Finally, the supernatants were again discarded, and the pellets left on ice to air dry for 10 minutes.

2.2.7.3 Denaturing Polyacrylamide Gel Electrophoresis

A Mini-PROTEAN gel electrophoresis system was used to make and resolve a denaturing polyacrylamide gel for identification of nucleic acids species present in the samples. One half of each samples nucleic acid pellet was resuspended in formamide loading dye [95% (v/v) Deionised Formamide, 20 mM EDTA, 0.05% (w/v) Xylene Cyanol, 0.05% (w/v) Bromophenol Blue] and boiled for 5 minutes at 95°C. The samples were then loaded onto a 8% denaturing urea polyacrylamide gel [50% (w/v) urea, 1 × TBE Buffer, 8% Acrylamide/Bis-acrylamide 19:1, 0.08% (v/v) APS, 0.008% (v/v) TEMED] alongside a 1 Kb Plus DNA Ladder (ThermoFisher) and resolved at 200 V for 2 hours in TBE buffer.

The gel was then stained for 20 minutes in the dark with 1:10,000 SYBR™ Gold in TBE buffer and imaged using a G:Box Chemi XX9 imager.

2.2.7.4 DNase Treatment of Pulldown Nucleic Acid for RT-qPCR

The second half of each samples nucleic acid pellet was resuspended in 20 µl Nuclease-Free Water for quantification of RNA species present by RT-qPCR. Contaminating DNA was removed from RNA samples using a DNA-free™ DNA Removal Kit. To each sample 0.1 volume of 10 x DNase I buffer and 2 units of DNase was added and the samples incubated for 30 minutes at 37°C. The reaction was stopped by treatment with 0.1 volumes of DNase inactivating reagent for 2 minutes at room temperature. The DNase inactivating reagent was pelleted by centrifugation (7,500 x g, 1.5 min, 4°C) and the RNA supernatant transferred to a new 1.5 ml microcentrifuge tube.

The pulldown RNA samples and purified input RNA samples were then reverse transcribed (2.2.5.2) and qPCR analysis (2.2.5.3) performed for 18S, 28S and GAPDH to assess the purity the pre-ribosomal complexes. The comparative ΔΔCT was performed firstly between the pulldown and input samples then between the control and bait protein samples.

2.2.7.5 Negative Stain Electron Microscopy

The wash buffer II was removed from Strep-Tactin®XT coated beads bond with MRTO4 bait protein pre-60S ribosome complexes (2.2.6.2). The MRTO4 pre-60S ribosome complexes were then competitively eluted off the beads by washing them three times in 333 µl elution buffer [50 mM biotin/NaOH (pH 7.8), 50 mM Tris/HCl (pH 7.8), 100 mM NaCl, 2 mM $MgCl_2$, 0.5% (v/v) NP-40] and collecting the buffer each time into a single 1.5 ml microcentrifuge

tube. The elution was then concentrated to 100 µl using an Ultrafiltration Centrifugal Concentrator (Vivaspin 500, 1,000,000 MWCO, Sartorius, VS0161).

MRTO4 pre-60S ribosome complexes were applied to continuous carbon grids that had been glow discharged (Pelco Easiglow, Ted Pella) for 30 seconds in air. The samples were blotted and stained with 1% uranyl acetate solution and allowed to dry in air for 5 minutes. Samples were imaged on a FEI Tecnai™ T12 transmission electron microscope, equipped with a FEI Ceta, 4k x 4x CMOS camera, a total of 107 micrographs were collected.

A total of 16,000 particles were picked by semi-automated picking using Relion (version 2.1-beta-1) with a low-pass filter at 15 Å[352]. Further 2D classification and 3D reconstruction were also performed in Relion (version 2.1-beta-1). About 60% of collected particles were lost during two rounds of 2D classification. The remaining 6,000 particles were processed through 3D reconstruction and a surface model generated in PyMOL

2.2.8 Quantitative Proteomics

Strep-Tactin®XT coated beads bond with bait protein purified pre-ribosome complexes were sent in wash buffer II to the University of Bristol Proteomics facility for tandem mass tagging (TMT), liquid chromatography (LC), mass spectrometry (MS) analysis. The final samples sent were isolated by Sophie Schumann. Samples were proteolytically digested and labelled with amine-specific isobaric tags yielding differentially labelled peptides of the same mass[353]. Labelled samples were then pooled and fractionated using Strong Anion eXchange chromatography before analysis by synchronous precursor selection MS3 on a Orbitrap Fusion Tribrid mass spectrometer (Thermo Fisher). Through the first and second round of MS each unique peptide is identified for all samples with fragmentation of peptides occurring in the second MS. However, in the third round of MS the TMT labels are fragmented from each peptide producing a unique reporter group. These reporter groups enable calculations for relative abundance of each identified peptide from each distinct sample[354].

For each sample the background abundance values for each protein from the control TREx BCBL1-Rta cell lysate pull down was taken away from the abundance value of each protein from the TREx BCBL1-Rta FLAG/Strep TAP-tagged ribosome biogenesis bait protein sample. This eliminated any non-specific binding proteins to the Strep-Tactin®XT coated beads. A cut off abundance value of 150 was then selected and all proteins with a lower value were

discarded from further analysis. This eliminated proteins with a low specificity for the pre-ribosome complexes. Log_{10} ratios for the abundance values of each protein in the latent and lytic samples were calculated for final identification of proteins with dynamic changes during KSHV infection.

2.2.9 18S rRNA 1639 m^7G Methylation Quantification

Total RNA was isolated from cell pellets of latent TREx BCBL1-Rta cells expressing a Scr shRNA or BUD23 targeting shRNAs, or latent and 24 hour, 36 hour and 48 hour lytic TREx BCBL1-Rta cells (2.2.7.2). The purified nucleic acid pellets were resuspended in 1.0M Tris-HCl (pH 8.2).

The purified RNA was first reduced, specifically at m^7G sites, with 0.2 M $NaBH_4$ for 30 minutes on ice in the dark. The reaction was stopped with a sodium acetate, isopropanol precipitation of the RNA over night at -80°C. The RNA was pelleted by centrifugation (16,000 x g, 15 min, 4°C) and washed in ethanol twice before been resuspended in 1.0M Tris-HCl (pH 8.2). Reduced m^7G sites where then cleaved by β-elimination using 1 M aniline/acetate (pH 4.5) in the presences of 50 µg m^7GTP carrier on ice in the dark for 15 minutes. The reaction was again stopped by precipitation of the RNA but for 2 hours at -80°C and the RNA purified as described above.

The purified RNA was resuspended in Nuclease-Free Water then reverse transcribed (2.2.5.2) and qPCR analysis (2.2.5.3) performed with primers specific for total 18S rRNA and primers flanking the 18S rRNA 1639 m^7G cleavage site. The comparative ΔΔCT was performed firstly between total 18S and the 18S 1639 site then between the control and experimental conditions.

2.2.10 Polysome Profiling

Sucrose solutions at 5% and 45% were prepared which contained 10 mM $MgCl_2$, 50 mM Tris/HCl (pH 7.6), 150 mM NaCl, 1 mM DTT, 100 µg/ml cycloheximide and 1× protease inhibitor cocktail. The 5% sucrose solution (6 ml) was pipetted into 14 x 95mm open-top polyclear centrifuge tubes (Senton, 7031). A blunted ended needle and syringe was used to underlay the 5% sucrose solution with a 45% sucrose solution (6 ml). The centrifuge tubes were then capped and a Gradient Master (BioComp) was used to create a continuous 5% - 45% sucrose density gradient.

A total of 50 million latent or 36 hour lytic TREx BCBL1-Rta cells expressing a Scr shRNA or shRNAs targeting BUD23 were treated with cycloheximide (100 µg/ml) for 3 minutes then harvested (2.2.1.3). The cell pellets were lysed for 45 minutes on ice in buffer containing 10 mM $MgCl_2$, 50 mM Tris (pH 7.6), 150 mM NaCl, 1mM DTT, 1% (v/v) NP40, 100 µg/ml cycloheximide, 1× protease inhibitor cocktail, 24 U/ml TURBO DNase and 180 U/ml RNasin plus. The cell lysates were clarified by centrifugation (12,000 × *g*, 10 min, 4°C) and the resulting supernatants applied to the sucrose gradients (5% − 45%). The loaded sucrose gradients were spun at 160, 000 × *g* in a Beckman SW40 rotor for 3 hours at 4°C. Twelve 1 ml fractions from each sample were collected using a Gradient Fractionator (BioComp) and the RNA profile was measured by absorbance (254 nm) across the gradient in real time using an EM-1 Econo UV Monitor (Bio-Rad).

2.2.11 Ribosome Profiling

2.2.11.1 Ribosome Footprinting

Polysome profiles were run in duplicate as described above (2.2.10) apart from 20% of the clarified cell lysate was saved as a total mRNA input for downstream processing and analysis. Total nucleic acid was extracted from the input samples using 900 µl TRIzol LS and processed as described above (2.2.7.2).

The sucrose fractions containing the 80S and polysomes were collected and pooled into a 50 ml centrifuge tube (Greiner Bio-One, 227261). The sucrose solution was diluted down to a 10% concentration with 100 mM Tris/HCl (pH 7.6), 30 mM NaCl and 10 mM $MgCl_2$. The ribosomes were then footprinted with 50 U RNase I, rotating overnight at 4°C. The reaction was then stopped with 200U SuperRNaseIN, rotating for 5 minutes at room temperature. The sucrose samples were then concentrated down to a volume of 500 µl using 30 kDa cut off, Amicon® Ultra-4 Centrifugal Filter Units (Millipore, UFC803024). The sucrose samples were then run again on sucrose gradients (2.2.10) to collect the footprinted ribosomes. This time just the fractions containing the 80S peak were collected and the RNA precipitated 1:1 Isopropanol, 300 mM NaCl and glycoblue, overnight at -80°C.

2.2.11.2 DNase Treatment

All the factions from each sample and each duplicate were resuspended and pooled in 100 µl Nuclease-Free Water, and the same was done for the mRNA input samples. RNA concentrations were measured using a NanoDrop ND-1000 spectrophotometer. The

samples were then treated with 20 U TURBO DNase per µg of RNA and 1X TURBO DNase buffer to remove any DNA impurities. To stop the reaction the RNA was precipitated by TRIzol LS (2.2.7.2).

2.2.11.3 PolyA selection and Fragmentation of Input mRNA

PolyA RNA was selected from input mRNA samples using the Dynabeads™ mRNA DIRECT™ Purification Kit. Magnetic dynabeads® Oligo $(dT)_{25}$ (200 µl) were equilibrated by washing twice with Binding Buffer. The RNA pellet of the input mRNA samples were resuspended in 100 µl Nuclease-Free Water and heated (65°C, 2 mins). The beads were resuspended in 200 µl Binding Buffer and the input RNA samples incubated with the beads for 10 minutes at room temperature while rotating. The incubation solution was then removed, and the beads washed twice in Buffer A and then twice in Buffer B. To elute the selected polyA RNA from the beads 10mM Tris (40 µl) was added and the beads heated (75°C, 2 mins). The eluted polyA RNA was transferred to a fresh 1.5 ml microcentrifuge tube.

The selection process was carried out again on the samples with the same beads to maximise the purity of the polyA RNA. The beads were washed twice in Buffer B, the eluted polyA RNA was diluted in 160 µl Binding Buffer and heated (65°C, 2 mins). The selection process was then carried out as above.

The polyA RNA was fragmented to an optimal range of 50-80 bp. Purified polyA RNA samples were incubated 1:1 with fresh fragmentation buffer (2 mM EDTA, 10mM Na_2CO_3 and 90mM $NaHCO_3$) for 20 minutes at 95°C. The reaction was stopped with 560 µl ice cold 0.7 M sodium acetate, 640 µl isopropanol and glycoblue, and the samples then left to precipitate overnight at -80°C.

2.2.11.4 Denaturing RNA Gel Purification

PolyA RNA selected samples were centrifuged (16,000 × *g*, 30 min, 4°C) to pellet the RNA, then washed twice with 70% (v/v) ethanol. The RNA pellets of both the polyA RNA selected samples and the ribosome footprinted samples were resuspended in formamide loading dye [95% (v/v) deionised formamide, 20 mM EDTA, 0.05% (w/v) xylene cyanol, 0.05% (w/v) bromophenol blue].

A 10% polyacrylamide denaturing RNA gel [50% (w/v) urea, 1 × TBE Buffer, 10% (v/v) Acrylamide/Bis-acrylamide 19:1, 0.08% (v/v) APS, 0.008% (v/v) TEMED] was prepared and

run with an omniPAGE WAVE Maxi system (Cleaver Scientific). The gel was first pre-run for 30 minutes at 300 V in TBE Buffer and the RNA samples heated (80°C, 2 min). The gel wells were then flushed out and the polyA RNA samples loaded alongside a O'RangeRuler 10 bp DNA Ladder, and the ribosome footprint RNA samples loaded alongside 28 nt and 34 nt makers diluted 1:100 in formamide loading dye. The gel was then run for 3 hours at 300 V and then stained for 30 minutes in 1:10,000 SYBR™ Gold Nucleic Acid Gel Stain diluted in TBE Buffer.

An ultraviolet light image was then captured of the gel using a G:Box Chemi XX9 imager. The ribosome footprint fragments (28-32 bp) and the polyA RNA fragments (50-80 bp) were cut out of the gel and shredded by centrifugation (16,000 × *g*, 15 min, RT) through Gel Breaker Tubes (SeqMatic, TC-200). The RNA was eluted from the shredded gel slices by incubation with elution buffer [20mM Tris-HCl (pH 7.5), 250 mM Sodium Acetate, 1 mM EDTA and 0.25% (w/v) SDS] while rotating overnight at 4°C. The next morning the gel elution mix was filtered by centrifugation (10,000 × *g*, 1 min, RT) through Spin-X Centrifuge Filters (Corning, Costar, cellulose acetate membrane, pore size 0.22 µm, SPINX8160-036). The flowthrough RNA was precipitated with Isopropanol 1:1 and glycoblue at -80°C for 2 hours.

2.2.11.5 T4 PNK Treatment

Both ends of the fragment RNAs were repaired using T4 PNK treatment to phosphorylate the 5' ends and dephosphorylate 3' ends. Both the ribosome footprint and polyA RNA samples were centrifuged (16,000 × *g*, 30 min, 4°C) to pellet the RNA. The RNA was then washed twice with 70% (v/v) Ethanol and the pellets resuspended in 10mM Tris-HCl (pH 8).

The RNA was heat (80°C, 2 mins) then treated with 1 × T4 PNK Buffer, 10 U T4 PNK and 20 U SUPERase•In™ RNase Inhibitor for 1 hour at 37°C. The T4 PNK was inactivated (70°C, 10 mins) and the RNA precipitated with 120 mM Sodium Acetate, 60% (v/v) Isopropanol and glycoblue overnight at -80°C.

2.2.11.6 rRNA Depletion of Ribosome Footprint Samples

The NEBNext rRNA depletion kit was used, as described by the manufacturer, to remove any contaminating rRNA present in the ribosome footprint samples. All incubation steps were carried out in a QIAamplifier 96 thermocycler.

The ribosome footprint RNA was pelleted by centrifugation (16,000 × *g*, 30 min, 4°C) and then washed twice with 70% (v/v) Ethanol before resuspension in Nuclease-Free Water (12 µl). Samples were then mixed with NEBNext rRNA Depletion Solution (1 µl) and probe Hybridization Buffer (2 µl). To allow the DNA rRNA probes to hybridize with the rRNA its self, the samples were then heated at 95°C for 2 minutes and cooled to 22°C at a rate of 0.1°C/sec with a final 5 minute incubation step at 22°C.

To degraded the hybridized rRNA, samples were the mixed with NEBNext RNase H (2 µl), RNase H Reaction Buffer (2 µl) and Nuclease-Free Water (1 µl). The samples were then incubated at 37°C for 30 minutes.

Finally, to remove the DNA rRNA probes the samples were mixed with DNase I Reaction Buffer (5 µl), DNase I (2.5 µl) and Nuclease-Free Water (22.5 µl). The samples were then incubated again at 37°C for 30 minutes before precipitation with 70% (v/v) Ethanol, 65 mM Sodium Acetate and glycoblue, overnight at -80°C.

2.2.11.7 Small Fragment Multiplex Next Generation Sequencing (NGS) Library Creation

The NEBNext® Multiplex Small RNA Library Prep Set for Illumina® was used to generate the libraries for NGS. All incubation and PCR steps were carried out in a QIAamplifier 96. The RNA from both the polyA selected and ribosome footprint samples was pelleted by centrifugation (16,000 × *g*, 30 min, 4°C). The supernatant was then removed and the samples washed twice in 70% (v/v) Ethanol before resuspension in Nuclease-Free Water.

Firstly, 3' SR adaptors were ligated onto the sample RNA fragments. The 3' SR adaptors were incubated with the RNA samples at 70°C for 2 minutes to reduce secondary structures. Secondly, 3' Ligation Reaction Buffer and 3' Ligation Enzyme Mix were then added to each sample and the ligation carried out for 1 hour at 25°C. Reverse Transcription primers were added to the samples and hybridised with incubation steps of 75°C for 5 minutes, 37°C for 15 minutes, 25°C for 15 minutes and finally holding at 4°C. A 5' SR adaptor was then ligated to the RNA samples. The 5' SR adaptor was first heated (70°C, 2 mins) before been added to the samples with 5' Ligation Reaction Buffer and 5' Ligation Enzyme Mix. The samples were then incubated for 1 hour at 25°C.

Samples were then reverse transcribed, First Strand Synthesis Reaction Buffer, Murine RNase Inhibitor and ProtoScript II Reverse Transcriptase were added to the samples. The

samples were then incubated at 50°C for 1 hour followed by an inactivation period of 15 minutes at 70°C.

Next the cDNA samples were prepared for PCR amplification, LongAmp Tag 2X Mastermix, an SR Primer and a sample specific Index Primer were added to each sample. The PCR program started with an initial denaturation step (94°C, 30 secs) followed by 15 cycles of 94°C for 15 seconds (Denaturing), 62°C for 30 seconds (Annealing) and 70°C for 15 seconds (Extension). A final extension step was carried out for 5 minutes at 70°C before holding at 4°C, the cDNA samples were stored at -20°C.

2.2.11.8 Post-PCR Gel Purification

The libraries were centrifuged (16,000 × *g*, 30 min, 4°C) to pellet the cDNA, then washed twice with 70% (v/v) ethanol. The cDNA pellets were then resuspended in formamide loading dye.

An 8% polyacrylamide DNA gel [1 × TBE Buffer, 8% (v/v) Acrylamide/Bis-acrylamide 19:1, 0.08% (v/v) APS, 0.008% (v/v) TEMED] was prepared and run with an omniPAGE WAVE Maxi system, as described above (2.2.11.4). The samples were loaded alongside a O'RangeRuler 10 bp DNA Ladder. Once the gel had run for 2 hours it was then stained for 30 minutes in 1:10,000 SYBR™ Gold Nucleic Acid Gel Stain diluted in TBE Buffer.

An ultraviolet light image was then captured of the gel using a G:Box Chemi XX9 imager. The ribosome footprint cDNA libraries (155-165 bp) and the polyA RNA cDNA libraries (170-200 bp) were cut out of the gel and shredded by centrifugation (16,000 × *g*, 15 min, RT) through Gel Breaker Tubes (SeqMatic, TC-200). The cDNA libraries were eluted from the gel and precipitated as described above (2.2.11.4), the only difference was no glycoblue was used in the precipitation as to not cause any problems with the downstream analysis.

2.2.11.9 NGS

The libraries were centrifuged (16,000 × *g*, 30 min, 4°C) to pellet the cDNA, then washed twice with 70% (v/v) ethanol. The cDNA pellets were then resuspended in Nuclease-Free Water.

The libraries were individually sent to Novogene for NGS analysis. Firstly, the quality and quantity of the libraries were assessed using a 2100 Bioanalyzer (Agilent). The libraries were then pooled at a 60:40 ratio for the ribosome footprint samples compared to the polyA RNA

samples. The pooled libraries were then run on a NovaSeq 6000 (Illumina) as a single end, 50 bp run.

2.2.11.10 Data Processing

The raw data was demultiplexed by Novogene and then processed by Elton Vasconcelos (Leeds Omics, Bioinformatics Research Officer). Briefly, single-end sequencing quality control was assessed through FastQC. An average of 128 million reads were sequenced per sample. Both adapters and low-quality bases (QV < 20) were trimmed from reads' extremities using Cutadapt (v3.2) with minimum read length of 25bp, and untrimmed outputs discarded for Ribo-Seq reads. All libraries were mapped against Human hg38 rRNAs (Gencode v36) and tRNA sequences (GtRNAdb 18.1) using Bowtie2 v.2.3.4.2 (--sensitive-local -N1 -k1), and then removed using Samtools v1.9 with the -f 4 option.

STAR aligner with default parameters was used for alignments of each QC-processed library against both Human (Gencode v36 - GRCh38p13 primary assembly) and KSHV (NCBI - GQ994935.1) genomes, separately. STAR-generated BAM output files were used for assigning read counts to CDS features in each genome with featureCounts, disregarding multi-mapper reads (not invoking -M option) and assigning reads to all overlapped features (invoking -O option). Gencode v36 primary assembly gtf annotation file was used for Human counts, whereas KSHV 2.0 annotation for virus[52].

Read counts' tables generated by featureCounts for each organism were then used as input for differential translation (DT) analyses with RiboRex relying on the DeSeq2 negative binomial distribution model and a 0.05 FDR threshold. Both genome-aligned read count assessments were submitted to a multi-dimensional scaling analysis using the plotMDS function from the EdgeR package. All tools described in this paragraph were run under the R environment version 4.0.4.

Chapter Three

~

Purification and Quantification of Newly Made Ribosomes During KSHV Lytic Replication

3 Purification and Quantification of Newly Made Ribosomes During KSHV Lytic Replication

3.1 Introduction

Ribosomes have long half-lives, Hirsch and Hiatt reported that in mouse liver tissue the half-life of a ribosome is up to five days[355,356]. The long ribosome half-life therefore makes it difficult to investigate dynamic changes of ribosome populations during shorter time periods due to the large ribosome pool present in the cell before the experimental condition. As a result, to analyse the changes in the ribosome population during lytic KSHV infection the newly made ribosomes were focused on by investigating pre-ribosome complexes undergoing ribosome biogenesis.

Both Pre-40S and -60S ribosomal complexes have previously been isolated at various stages of ribosome biogenesis from yeast and human cells[191,269,357–359]. Most of these studies have aimed to structurally define more stable versions of these complexes at later cytoplasmic stages of ribosome biogenesis. In all previous studies pre-ribosomal subunits were isolated by exogenously expressing tagged versions of RBFs to specifically pulldown the complexes from cell lysates.

Quantitative mass spectrometry has been used investigate the stoichiometry and composition of mature ribosomes to identify pools of specialised ribosomes in various experimental conditions[348,360,361]. However, previously to investigate RBFs and pre-ribosome complexes, studies have only used western blotting and systematic siRNA knockdown to identify ribosomal proteins and RBFs of pre-ribosome complexes at various stages of ribosome biogenesis[264,269,357,362].

In this chapter, pre-40S and pre-60S ribosome complexes were purified from KSHV latent and lytically replicating TREx BCBL1-Rta cells. The protein composition and stoichiometry of the complexes were then analysed by quantitative mass spectrometry using TMT coupled to LC-MS/MS.

3.2 Production of TREx BCBL1-Rta Cells Stably Expressing Ribosome Associated Biogenesis Bait protein

To isolate pre-ribosome complexes during latent and lytic KSHV replication, a lentivirus expression system was used stably express tagged versions of RBFs in TREx BCBL1-Rta cells. TREx BCBL1-Rta cells were transduced with FLAG-Twin-Strep-tag®-ribosome biogenesis factor bait proteins. Five cell lines were produced expressing bait proteins that associate with pre-40S ribosome complexes and five that expressed bait proteins that associated with pre-60S complexes (Figure 3.1). Multiple RBF bait proteins were used for both the pre-40S and pre-60S complexes to maximise spatial and temporal coverage of the complexes as they transition through ribosome biogenesis (Figure 3.1).

As described in chapter one the 40S subunit RBF bait proteins include, DMIT1 which associates with pre-40S complexes in the nucleolus and catalyses the N^6N^6-dimethyladenosine of bases 1850/1 of the 18S rRNA[190]. PNO1 first binds pre-40S complexes as they leave the nucleolus and is involved in structural arrangements of the pre-40S complex right until the final stages of cytoplasmic maturation[191]. NOC4L is responsible of recruiting the EMG1-NOP14-NOC4L-UTP14A complex to pre-40S complexes again as they translocate out of the nucleolus but then dissociates during nucleoplasm maturation[286]. TSR1 and LTV1 both associate with pre-40S complexes in the nucleoplasm and are involved in structural arrangements in both the nucleoplasm and cytoplasm[191].

Furthermore, as described in chapter one the 60S subunit RBF bait proteins include, RSL24D1 and MRTO4 which both bind to pre-60S complexes in the nucleolus and along with structural rearrangements acts as a placeholder for the ribosomal protein RPL24 and P0 respectively[293,295]. GNL2 binds pre-60S complexes as they translocate from the nucleolus and facilitates structural rearrangements in the nucleoplasm to guide the formation of the PTC[294]. NMD3 associates with pre-60S complexes in the nucleoplasm and functions as a nuclear export adaptor[302,303]. Finally, LSG1 is a GTPase associating with pre-60S complexes in the cytoplasm to catalyse the release of NMD3[302].

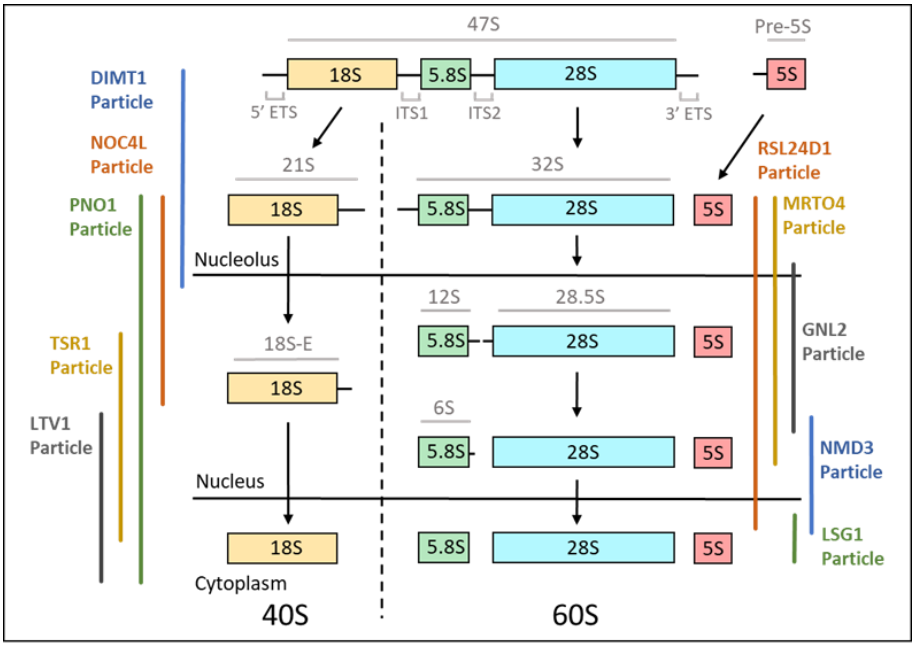

Figure 3.1 Ribosomal biogenesis bait proteins temporal association with pre-ribosomal complexes.

To confirm the successful transduction of each TREx BCBL1-Rta cell line the expression of each bait protein was assessed by immunoblotting. All bait proteins apart from the 60S subunit RBF RSL24D1 expressed to high levels (Figure 3.2). The RSL24D1 cell line was therefore excluded from the rest of the study. In addition, the GNL2 bait protein cell line proceeded to die shortly after transduction, probably due to toxic effects of GNL2 overexpression, and was therefore also excluded from the rest of the study.

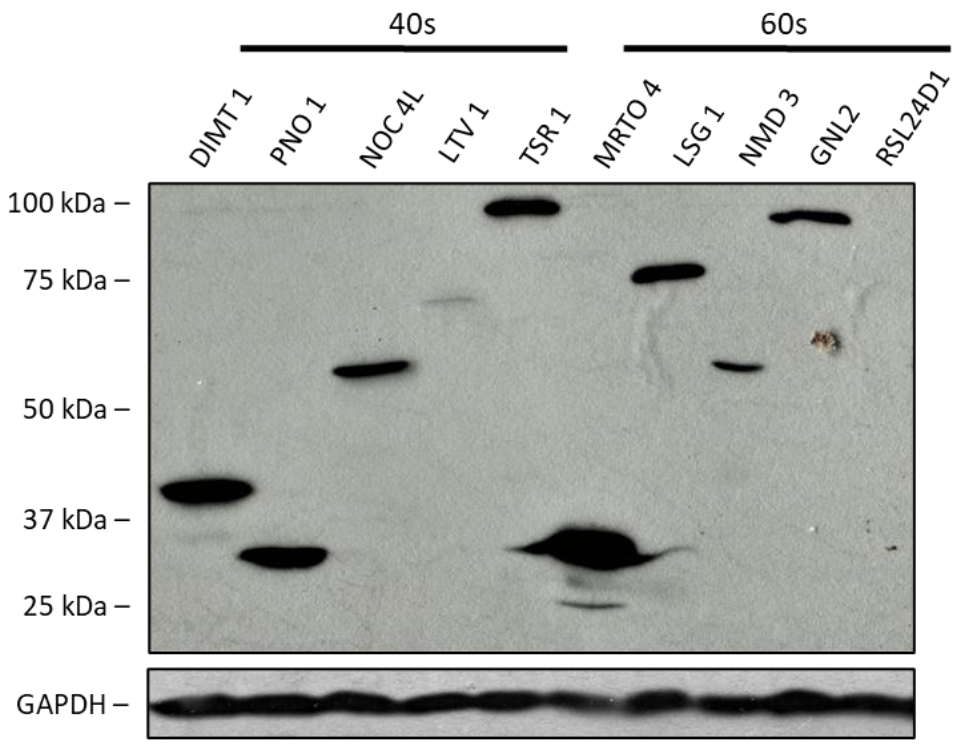

Figure 3.2 Western blot of whole cell lysates from lentivirus transduced TREx BCBL1-Rta cells lines stably expressing ribosomal biogenesis bait proteins. Bait protein N-terminal tag: FLAG-Twin-Strep-tag®. Protein's molecular weight with tag: DIMT1 (40 kDa), PNO1 (32 kDa), NOC4L (63 kDa), LTV1 (59 kDa), TSR1 (96 kDa), MRTO4 (32 kDa), LSG1 (80 kDa), NMD3 (62 kDa), GNL2 (88 kDa) and RSL24D1 (24 kDa).

Immunofluorescence microscopy was used to confirm the exogenous expression of each tagged bait protein did not affect its subcellular localisation compared to the localisation the endogenous RBF. All bait proteins had a similar subcellular localisation to the native form when compared to the human cell atlas (Figure 3.3 and Figure 3.4). Human cell atlas specified subcellular localisations of 40S subunit RBF bait proteins: DIMT1 nuclear but mainly nucleolar, PNO1 nuclear but mainly nucleolar, NOC4L nuclear but mainly nucleolar, LTV1 nuclear and cytoplasmic, and TSR1 nuclear[363]. Human cell atlas specified subcellular localisations of 60S subunit RBF bait proteins: MRTO4 nuclear, LSG1 nuclear and cytoplasmic, and NMD3 nuclear[363].

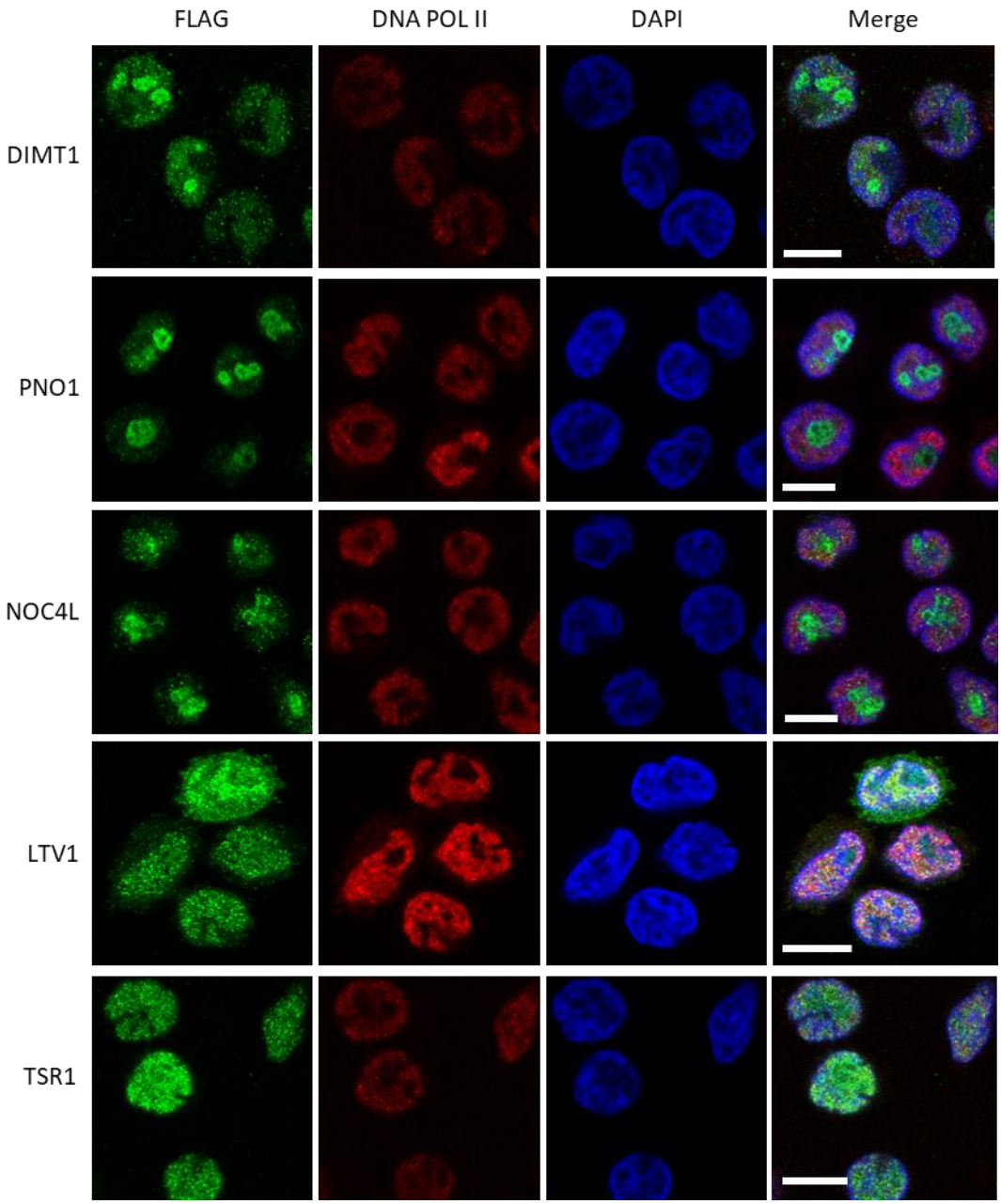

Figure 3.3 IF of lentivirus transduced TREx BCBL1-Rta cells lines stably expressing 40S subunit ribosomal biogenesis bait proteins. Cells were fixed, permeabilized, and stained for FLAG (green), DNA polymerase II (red), and the nuclear dye DAPI (blue). The cells were mounted and viewed using an LSM 880 inverted confocal microscope. Scale bars represent 10µm.

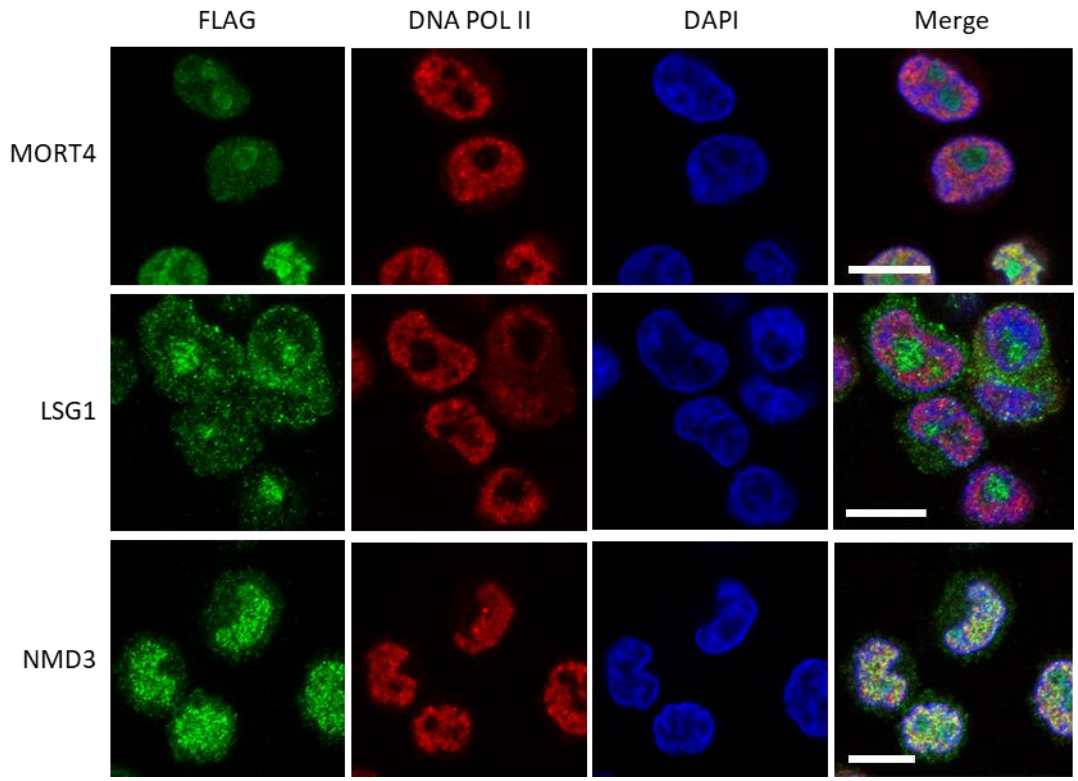

Figure 3.4 IF of lentivirus transduced TREx BCBL1-Rta cells lines stably expressing 60S subunit ribosomal biogenesis bait proteins. Cells were fixed, permeabilized, and stained for FLAG (green), DNA polymerase II (red), and the nuclear dye DAPI (blue). The cells were mounted and viewed using an LSM 880 inverted confocal microscope. Scale bars represent 10µm.

3.3 Isolation of Pre-ribosomal complexes from KSHV Latent and Lytically replicating cells

To confirm that stably expressed bait proteins can successfully precipitate pre-ribosomal complexes, pulldown assays were performed and analysed by silver stains of SDS-PAGE. Pre-40S and pre-60S ribosomal subunits were successfully purified by strep tag pulldown compared to a no bait protein control pulldown from TREx BCBL1-Rta cells latently infected with KSHV or 24 hours post lytic reactivation (Figure 3.5 A and B). For each precipitated complex multiple bands were observed representing the large number of proteins present in pre-40S and pre-60S ribosomal complexes during ribosome biogenesis. Furthermore, the strongest bands visible for each pulldown are the bait proteins themselves indicated by their molecular weights. Finally, the LTV1 strep tag pulldown is weaker than the others probably because of its lower expression levels (Figure 3.2).

To further confirm the successful isolation and purity of pre-ribosomal complexes the 18S rRNA content of PNO1-pre-40S complexes was confirmed by agarose gel electrophoresis and qPCR (Figure 3.5 C).

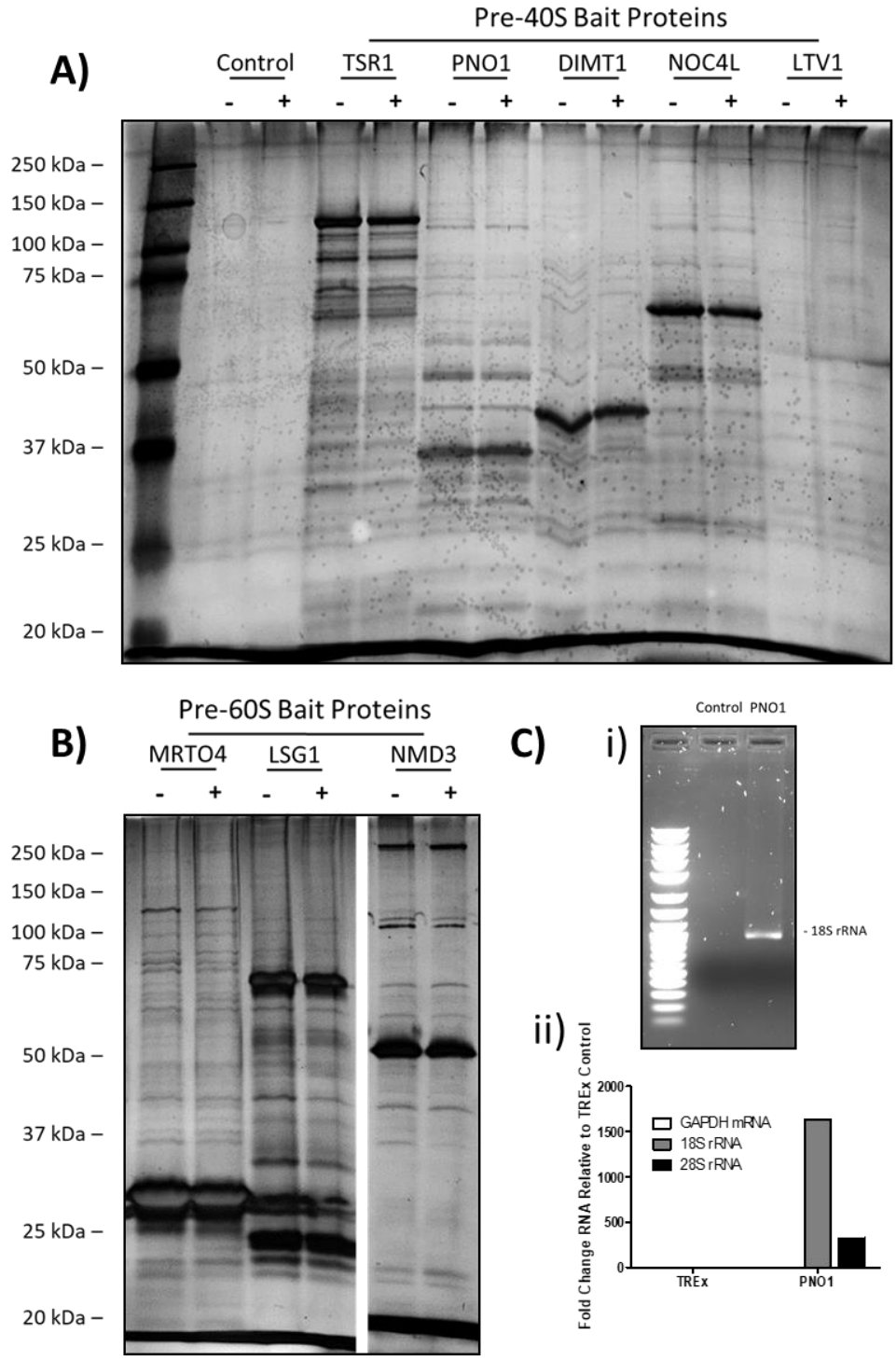

Figure 3.5 Pre-ribosomal complexes isolated from latent (-) and lytically replicating (+) infected TREx BCBL1-Rta cells. Whole cell lysates from a control cell line or cell lines stably expressing pre-ribosome biogenesis bait proteins were subject to Twin-Strep-tag® pulldowns. Silver stain gels of isolated pre-40S ribosome complexes **(A)** and pre-60S ribosome complexes **(B)**. Total nucleic acids was isolated from whole cell lysate pulldowns from control cells and PNO1 bait protein expressing cells **(C)**. Denaturing polyacrylamide gel electrophoresis **(i)** and two-step RT-qPCR, with primers specific for GAPDH mRNA, 18S rRNA and 28S rRNA **(ii)**.

Again, to further confirm the successful isolation of pre-ribosome complexes, MRTO4-pre-60S complexes were purified and their crude structure determined by single particle negative stain electron microscopy. Particles observed on electromicrograms were between 10-25 nm in size which correlated well with published pre-60S complexes, having a maximum size of 25 nm (Figure 3.6 A)[359]. The top twenty 2D class averages also looked very similar to the top twenty 2D class averages generated from low resolution back projections of a Ma et al. high resolution cryo-EM Nmd3-pre-60S ribosomal yeast complex (Figure 3.6 B and C)[294]. Furthermore, the final low resolution density map from 3D reconstruction of the MRTO4-pre-60S complexes again looked very similar to the Ma et al. 3.07 Å atomic model (Figure 3.6 D and E)[294].

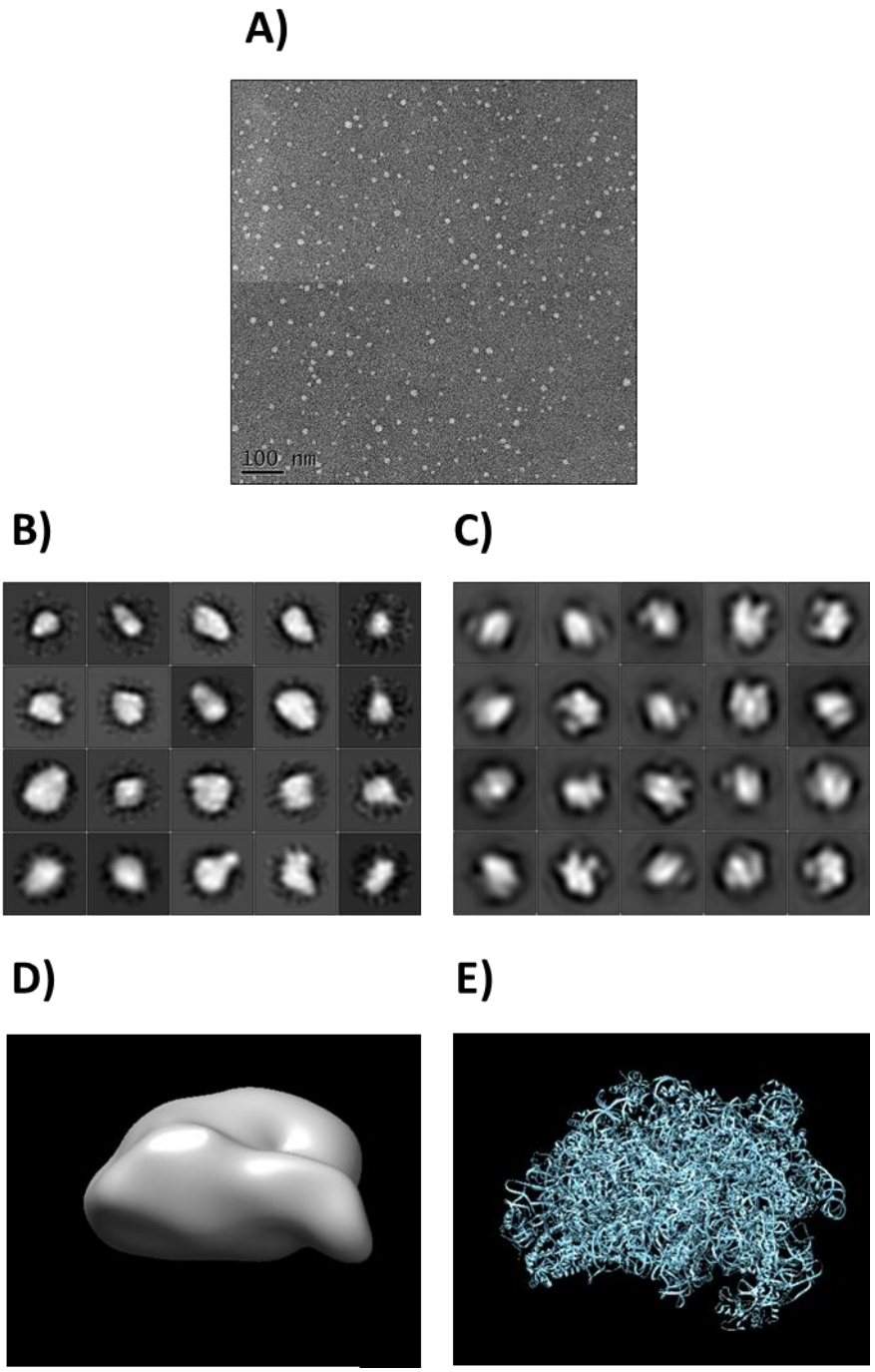

Figure 3.6 Negative stain EM reconstruction of pre-60S ribosomal complexes. Pre-60S ribosomal complexes isolated from TREx BCBL1-Rta cells stably expressing an MRTO4 bait protein and published Ma et al. cryo-EM pre-60S NMD3 ribosome complexes. Representative negative stain micrograph of isolated MRTO4-pre-60S ribosome complexes **(A)**. The top 20, 2D class averages of MRTO4-pre-60S ribosome complexes **(B)**. The top 20 low resolution, 2D class averages back projected from the Ma et al. high resolution cryo-EM NMD3-pre-60S ribosomal complex **(C)**. Density map of the 3D reconstruction for MRTO4-pre-60S ribosome complexes **(D)**. Atomic model of published Ma et al. NMD3-pre-60S ribosome complexes to 3.07 Å **(E)**.

3.4 Analysis of Changes to Pre-ribosomal complexes during KSHV infection

To determine the composition and stoichiometry of purified pre-40S and pre-60S ribosome complexes, isolated from TREx BCBL1-Rta cells latently infected with KSHV or 24 hours post lytic reactivation, pulldowns were analysed using TMT coupled to LC-MS/MS. Overall, each bait protein pulldown co-precipitated many of the core ribosomal proteins and RBFs associated with each pre-ribosomal complex (Figure 3.7 and Figure 3.8, and Appendix 1 and 2).

However, two exceptions were the LSG1 and NMD3 pulldowns which only isolated a few directly interacting ribosomal proteins and RBFs while also co-precipitating other cellular proteins (Figure 3.8 B and C, and appendix 2.2 and 2.3). There are two plausible reasons for this firstly, the bait protein tag could have interrupted the interaction of the bait protein with the pre-ribosomal complex. Secondly, the other cellular interactions observed could be due to secondary non-ribosomal functions of LSG1 and NMD3. A combination of these two outcomes is most likely as even a small disruption of the bait protein's interaction with pre-ribosomal complexes could bias towards the functional use of the native RBF instead of the bait protein during ribosome biogenesis and therefore any extra ribosomal functions of the bait protein RBF would be favoured.

Of the pre-40S bait protein pull downs the DIMT1 complexes contained the most 60S subunit ribosomal proteins. DIMT1 associates with the pre-ribosome processome at the stages before biogenesis of the 40S subunit and 60S subunit separates, which therefore explains the presence of many 60S subunit proteins (Figure 1.13 and Figure 3.7 C, and appendix 1.3). Interestingly, TSR1-pre-40S complexes also contain multiple of 60S subunit ribosomal proteins (Figure 3.7 D and appendix 1.4). The NOC4L-pre-40S complexes contained a high number of cellular non-ribosomal proteins therefore also potentially highlighting extra non-ribosomal functions of this RBF (Figure 3.7 E and appendix 1.5). Finally, the MRTO4-pre-60S complexes also contain a high number of 40S subunit ribosomal proteins potentially indicating that MRTO4 interacts during early stages and not just at later stages of nucleolar ribosome biogenesis (Figure 3.1 and Figure 3.8 A, and appendix 2.1).

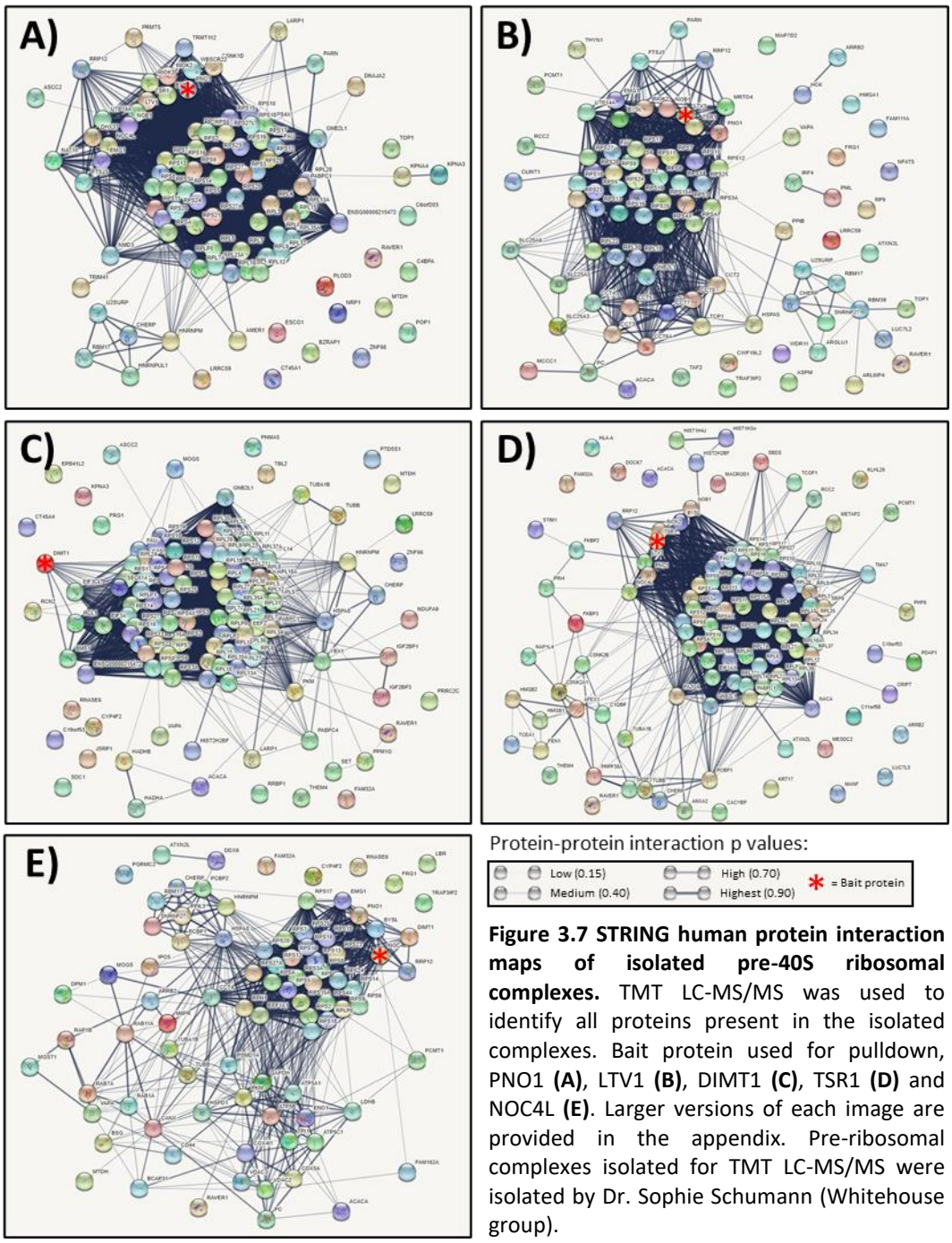

Figure 3.7 STRING human protein interaction maps of isolated pre-40S ribosomal complexes. TMT LC-MS/MS was used to identify all proteins present in the isolated complexes. Bait protein used for pulldown, PNO1 **(A)**, LTV1 **(B)**, DIMT1 **(C)**, TSR1 **(D)** and NOC4L **(E)**. Larger versions of each image are provided in the appendix. Pre-ribosomal complexes isolated for TMT LC-MS/MS were isolated by Dr. Sophie Schumann (Whitehouse group).

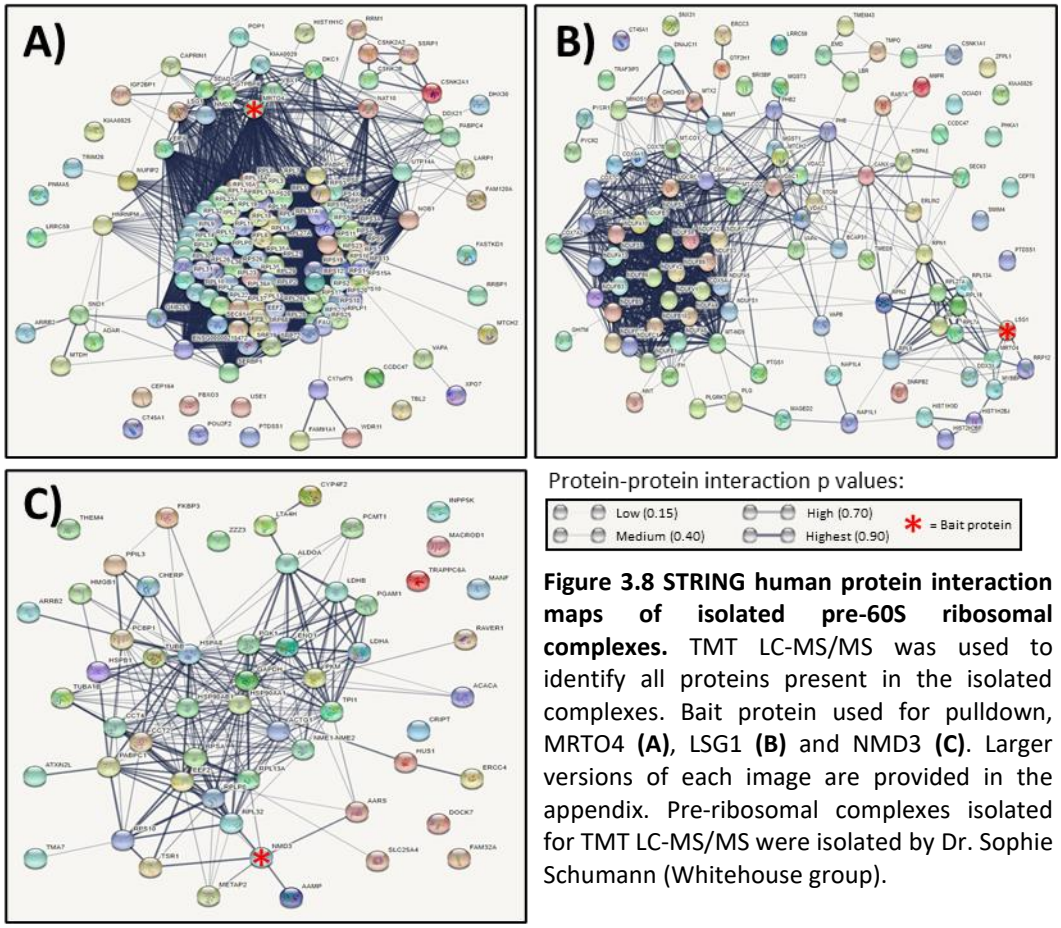

Figure 3.8 STRING human protein interaction maps of isolated pre-60S ribosomal complexes. TMT LC-MS/MS was used to identify all proteins present in the isolated complexes. Bait protein used for pulldown, MRTO4 **(A)**, LSG1 **(B)** and NMD3 **(C)**. Larger versions of each image are provided in the appendix. Pre-ribosomal complexes isolated for TMT LC-MS/MS were isolated by Dr. Sophie Schumann (Whitehouse group).

Pulldowns using 40S subunit RBF bait proteins overall isolated complexes most representative of pre-ribosome complexes. In addition, most of the dynamic changes were also observed in pre-40S pulldowns when comparing complexes isolated from cells with lytically replicating KSHV compared to latently infected cells (Figure 3.9 A-E, appendix 1 and 2). Therefore, the pre-40S complexes were focused on for the remainder of this thesis.

The majority of proteins present in pre-40S complexes, including all core ribosomal proteins, did not change in association when isolated from cells infected with latent or lytically replicating KSHV (Figure 3.9). However, interesting two groups of RBFs were identified to have increased association with pre-40S ribosomal subunits during lytic KSHV infection compared to latent KSHV infection, these groups are BUD23-TRMT112 and NOC4L-NOP14-EMG1. The RBF BUD23 is an RNA methyltransferase that mediates the N^7-methylation of G1639 in the 18S rRNA, and TRMT112 is a co-factor of BUD23[281]. The RBF EMG1 is also an RNA modifying enzyme which catalyses N^1-methylation of the hypermodified U1191 base of the 18S rRNA[286]. EMG1 is recruited to the nucleolus, where it associates with pre-40S complexes, via the NOC4L-NOP14-UTP14A complex[286].

The BUD23-TRMT112 complex was only detected and enriched in PNO1 and LTV1 pulldowns, likely due to the temporal association of the other RBF bait proteins with pre-40S complexes (Figure 3.9 F and Figure 3.1). BUD23-TRMT112 only associates with pre-40S complexes at later stages of 40S subunit biogenesis as they exit the nucleus[191]. Although the bait protein TSR1 also associates with pre-40S complexes at this stage of ribosome biogenesis its spatial localisation on pre-40S complexes is potentially more distal to BUD23 than LTV1 and PNO1[191].

Furthermore, the NOC4L-NOP14-EMG1 complex was detected in all but the DIMT1 pulldown (Figure 3.9 F). DIMT1 associates very early in ribosome biogenesis with the SSU processome prior to the association of the NOC4L-NOP14-UTP14A-EMG1 complex, again demonstrating a temporal difference of the five bait protein purified pre-40S complexes (Figure 3.1). Unsurprisingly, no enrichment of the NOC4L-NOP14-EMG1 group was observed in the NOC4L bait protein pull down from lytic KSHV cells compared to latent. This is probably due to the overwhelming expression of exogenous strep tag NOC4L masking any biological effects on NOC4L and its association with pre-40S ribosome subunits. Additionally, as a result of using NOC4L as a bait protein, only pre-40S complexes containing this bait protein are purified which in turn mask the ability to observe any biological changes of its association with pre-40S complexes.

A small number of proteins also had a decreased association with pre-40S complexes isolated from lytically replicating KSHV cells compared to latent cells (Figure 3.9 A-E). However, these proteins were not consistent across any of the different bait protein pulldowns possibly because most have more casual links to ribosome biogenesis and therefore probably only very transiently associate with pre-40S ribosome subunits. In addition, this initial quantitative mass spectrometry investigation was just a screen and therefore was not repeated which could contribute to these potential variations.

Notably, a viral protein, ORF11, was detected in all purified pre-40S complexes apart from complexes isolated by the TSR1 RBF bait protein. As the TSR1 pre-ribosome complexes failed to co-precipitate BUD23 or ORF11, in contrast to PNO1- and LTV1-pre-40S complexes, this strongly suggested the spatial location of TSR1's interaction with pre-40S ribosomal subunits is not in direct or close interaction with these proteins.

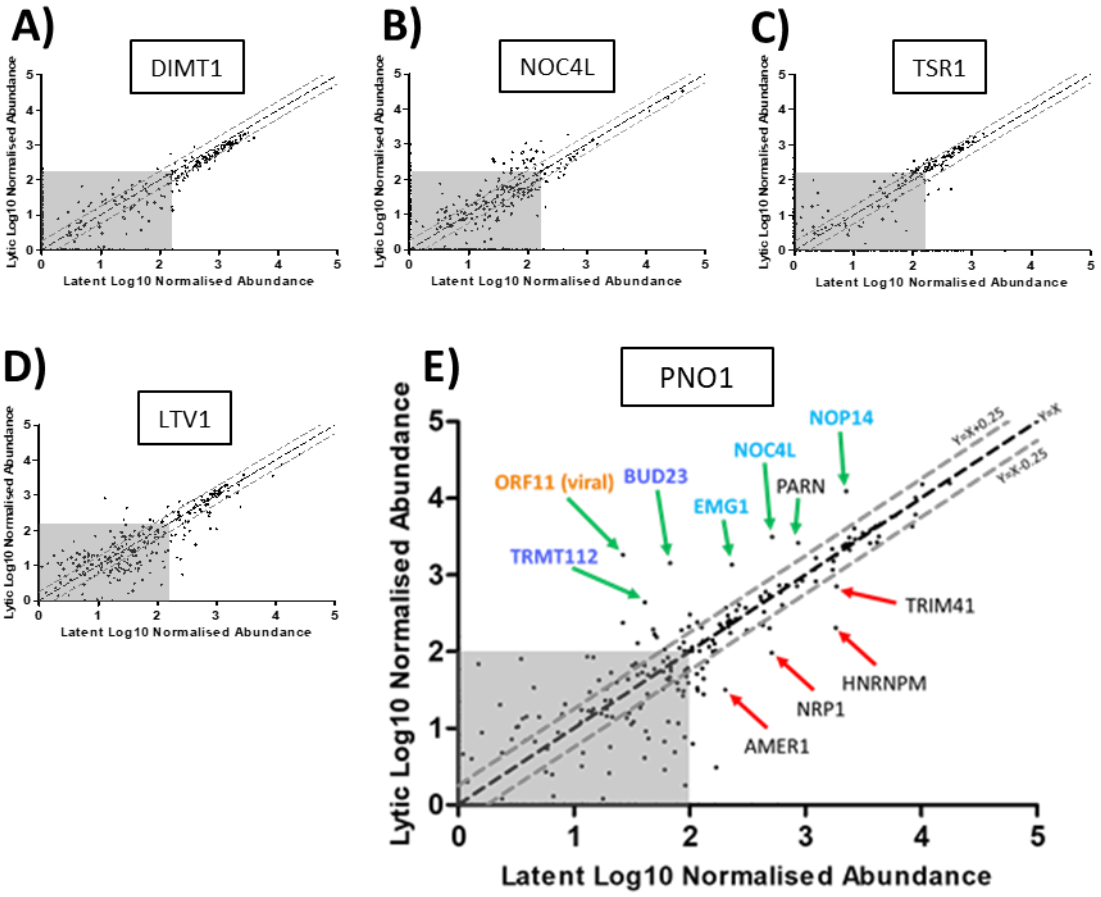

F)

Ribosome Biogenesis Proteins	Pre-40S Bait Proteins: PNO1	LTV1	TSR1	NOC4L	DIMT1
BUD23	21.21	2.63*	-	-	-
TRMT112	10.73	∞*	-	-	-
NOC4L	6.09	4.90	1.37	N/A	-
NOP14	5.53	1.85	∞	0.98	-
EMG1	5.92	1.44	∞*	0.97	-
Viral Protein					
ORF11	✓	✓	-	✓	✓

Figure 3.9 Changes to pre-40S ribosomal complexes during KSHV infection determined by quantitative mass spectrometry. Incorporation of each protein into the pre-40S ribosomal complexes isolated from cells infected with latent KSHV (X-axis) compared to cells infected with KSHV 24 hours post lytic reactivation (Y-axis) **(A-E)**. A minimum cut-off for incorporation was set to 150 abundance indicated by the grey boxes. A minimum threshold for increase and decrease incorporation of proteins into complexes isolated from lytic KSHV cells was set using the equations Y=X+0.25 and Y=X-0.25 respectively. Ratio increases in incorporation of two select groups of ribosome biogenesis associated proteins in pre-40S ribosomal complexes isolated from cells infected with lytic KSHV compared to latent KSHV **(F)**. ∞ = only detected in lytic pre-40S complexes. * = bellow 150 abundance.

3.5 Discussion

Overall, this chapter outlines the successful development of a system for purifying pre-40S and pre-60S ribosomal subunits from TREx BCBL1-Rta cell lines that are latently or undergoing lytic KSHV replication. Furthermore, the composition and stoichiometry of purified pre-40S and pre-60S complexes was analysed by TMT coupled to LC-MS/MS. Two complexes of RBFs, BUD23-TRMT112 and NOC4L-NOP14-EMG1, were identified to have increased association with pre-40S ribosomal subunits during lytic KSHV replication compared to latent KSHV infection. In addition, the viral protein ORF11 was identified to associate with pre-40S complexes during lytic KSHV replication.

Together these data suggest that KSHV, through ORF11 may regulate ribosome biogenesis during lytic replication to generate modified ribosomes. Interestingly, both BUD23 and EMG1 are two of only a few specific RNA modifying enzymes that function during ribosome biogenesis. The rRNA base G1639 that BUD23 methylates is located at a ridge forming a steric block between the tRNA E- and P-site sites of the ribosome and accompanies the ratcheting of tRNAs from the P-site to the E-site[364]. The functional relevance of the m^7G1639 site during translation is not fully understood. However, due to its location and movement with the mRNA and tRNAs it has been suggested to be involved in 40S subunit scanning and translocation[365]. The 18S rRNA base U1240 is hypermodified by SNORA14-dyskerin, EMG1 and TSR3 and is located in the decoding centre of the tRNA P-site[349]. Again, the functional relevance of the U1240 modifications have not been fully investigated, however, obviously due to its location, the modification has been hypothesised to be involved in decoding of the mRNA[349]. The functional relevance during translation of the BUD23 and EMG1 modified 18S rRNA bases demonstrates the relevance of the increased association of these RBFs with pre-40S complexes during lytic KSHV replication.

The remainder of this thesis focuses on the role of BUD32 during lytic KSHV replication. The increased association of EMG1 with pre-40S ribosome complexes during lytic infection and the role of the KSHV protein ORF11 as a regulator of ribosome biogenesis are ongoing areas of research in the Whitehouse laboratory.

Chapter Four

~

BUD23 is Required for Efficient Lytic KSHV Infection

4 BUD23 is Required for Efficient Lytic KSHV Infection

4.1 Introduction

Chapter three highlighted that BUD23 has increased association with pre-40S ribosomes during KSHV lytic replication. BUD23 methylation of the 18S rRNA base G1639 would be an ideal aspect of ribosome biogenesis that KSHV could manipulate to generate specialised ribosomes that efficiently translate viral mRNAs during lytic replication.

Although the function of the BUD23 m^7G1639 modification is not fully understood, BUD23 and its 18S rRNA modification have been implicated in heart disease, breast cancer and myeloma[327,366,367]. Furthermore, the BUD23 gene is deleted in the sporadic multigene deletion disease Williams-Beuren syndrome[326]. The role of BUD23 in other diseases of specific tissues and phenotypes adds to the hypothesis that BUD23 can specialise ribosomes for the translation of specific populations of mRNAs. As viruses co-opt mechanisms of cellular regulation, a hypothesis was developed whereby KSHV co-opts BUD23 during lytic infection to produce virus-specific specialised ribosomes.

In this results chapter, the increased association of BUD23 with pre-40S ribosomal complexes was validated. Furthermore, to understand the impact of BUD23's increased association with pre-40S ribosomal subunits during the KSHV lytic life cycle, BUD23 depletion studies were performed. Stable BUD23 knockdown TREx BCBL1-Rta cell lines were produced and extensively validated. Finally, the effect on KSHV lytic replication was comprehensively analysed in the presence of BUD23 knockdown.

4.2 BUD23 has Significantly Higher Incorporation into Pre-40S Ribosome Complexes During KSHV Lytic Replication

To validate the quantitative mass spectrometry screen in chapter three PNO1-pre-40S ribosomal complexes were again purified from cells latently infected with KSHV or 24 hours post lytic reactivation (Figure 4.1). Densitometric analysis of Immunoblots performed on the purified complexes showed an average 4.3 and 3.1 fold increase of BUD23 and NOC4L respectively in complexes isolated from cells undergoing KSHV lytic replication compared to latent KSHV cells. Whereas no change was observed for a core ribosomal protein RPS19. This confirms the specific increased association of BUD23 and NOC4L with pre-40S ribosomal complexes during KSHV lytic replication.

Additional controls included a FLAG western blot which showed the same amount of PNO1-pre-40S complexes were purified and loaded in each experiment. In addition, western blots of whole cell lysates probing for GAPDH showed that an equal number of cells were used and probing for ORF57 confirmed KSHV was successfully reactivated in relevant samples.

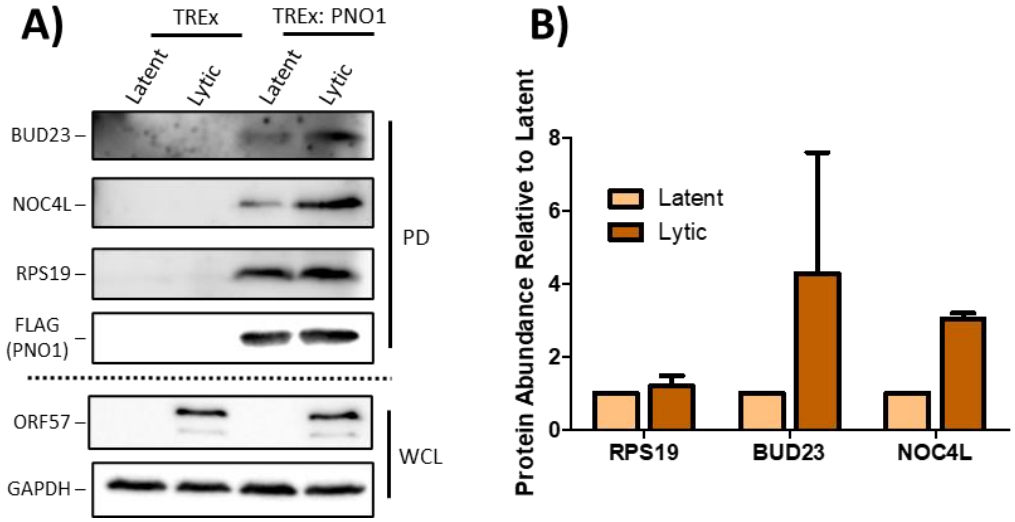

Figure 4.1 Western Blot Validation of PNO1 pre-40S ribosome complexes. Latent and 24 hours post lytic reactivation whole cell lysates from a control cell line or a cell line stably expressing a PNO1 bait protein were subject to Twin-Strep-tag® pulldowns. Representative western blots from pulldowns (PD) and whole cell lysate (WCL) inputs **(A)**. Densitometric analysis of pulldown western blots normalised to bait protein PNO1, presented as mean ± standard deviation (SD) (N=3) **(B)**.

4.3 Development of Stable BUD23 Knockdown TREx BCBL1-Rta Cell Lines

To investigate the effects of BUD23 depletion on KSHV lytic replication, stable BUD23 TREx BCBL1-Rta cell lines were produced using a lentivirus expression system expressing BUD23 targeted shRNAs. TREx BCBL1-Rta cell lines were transduced with a non-targeting scrambled (Scr) shRNA or two different shRNAs targeting BUD23 (shRNA 1 and 2). As determined by immunoblotting and qPCR, BUD23 protein and mRNA levels were reduced in knockdown cells by 70-80% compared to the Scr control (Figure 4.2).

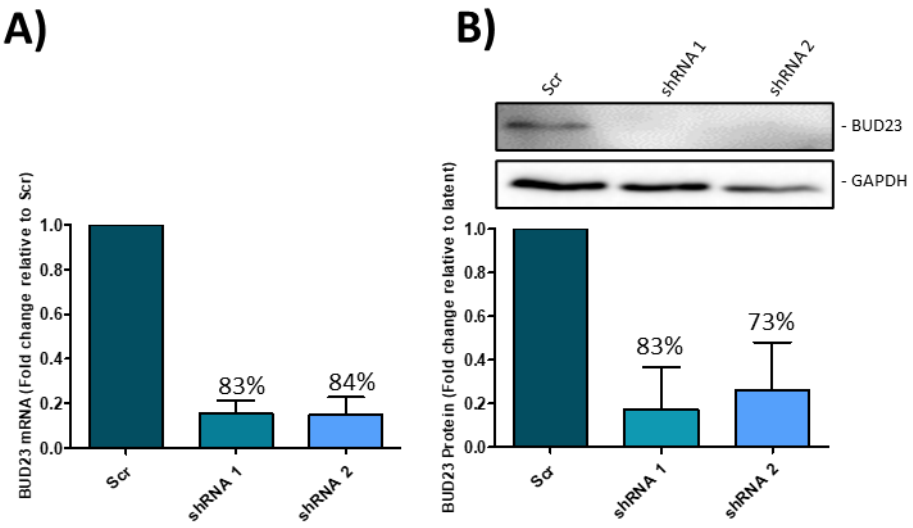

Figure 4.2 BUD23 stable knockdown in TREx BCBL1-Rta cells. A Lentivirus expression system was used to stably transduced TREx BCBL1-Rta cells with a non-targeting scrambled shRNA (Scr) or two different shRNAs targeting BUD23 (shRNA 1 and 2). Data are presented as mean ± SD. BUD23 mRNA production was assayed by two step RT-qPCR and analysed by comparison to the Scr control using a ΔΔCT method (N=7) **(A)**. Whole cell lysates were collected and analysed by western blot, GAPDH was included as a reference gene **(B)**, representative western blots and densitometric analysis relative to the Scr control (N=7).

To confirm depletion of BUD23 had no overall deleterious effects, the cell lines were monitored and analysed to assess any changes in cell proliferation, the global cell ribosome population or global translation (Figure 4.3 A-C). To monitor cell proliferation, BUD23 knockdown cells lines and a Scr control were counted twice over a 48 hour period, the rate of growth for each cell line remained consistent (Figure 4.3 A).

Polysome profiles of each cell line were performed to analyse any changes in the global ribosome populations of the cell lines (Figure 4.3 B). In brief, whole cell lysates were ultracentrifuged over sucrose gradients to isolate total cellular ribosome populations. The gradients were then cut and the rRNA analysed by absorbance at 254 nm. Neither the population of 40S or 60S ribosomal subunits or the actively translating polysomes or singularly translating 80S ribosomes were affected by knockdown of BUD23 compared to the Scr control.

The high turnover cell cycle regulator CDK1 was used as a proxy for global protein translation[368]. Western blot analysis of whole cell lysates probing for CDK1 showed constant amounts from BUD23 knockdown cell lines compared with Scr cells (Figure 4.3 C).

These results suggest that the depletion of BUD23 does not affect overall cell biology. Therefore, BUD23 stably depleted cell lines can be used to specifically investigate the effects of BUD23 knockdown on KSHV lytic replication.

However, as BUD23 is implicated in the methylation of the 18S rRNA base G1639, the level of m7G1639 modification was analysed by qPCR in the BUD23 knockdown cell lines compared to the Scr control cell line. In the Scr control cell line about 80% of the 18S rRNA contained the m7G1639 modification, however BUD23 depletion resulted in a reduction of 50-60% of m7G1639 in both knockdown cell lines (Figure 4.3 D). All though BUD23 depletion is not deleterious to the cell these data reinforce its role in methylation of the 18S rRNA base G1639.

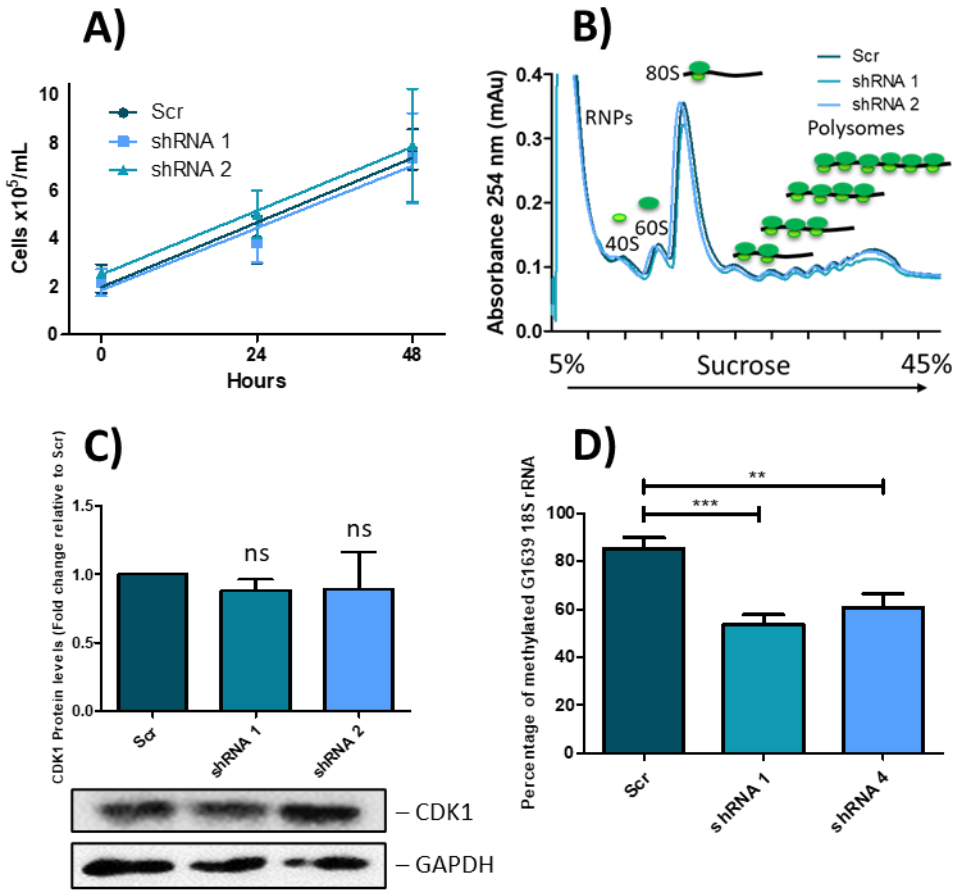

Figure 4.3 Knockdown of BUD23 does not affect gross cell functions but significantly reduces the 18S rRNA m7G1639 methylation. TREx BCBL1-Rta cells expressing a Scr shRNA or two different shRNAs targeting BUD23 were counted over 48 hours to measure cell proliferation (n=3) **(A)**, the gross ribosome population in the cells was determined by polysome profiling **(B)**, and protein turnover was determined by whole cell lysate western blots for CDK1 with GAPDH included as a loading control and representative western blots and densitometric analysis relative to the Scr control (n=3) **(C)**. Total RNA was isolated and chemical cleaved at m7G sites. The proportion of cleaved to uncleaved rRNA at 18S G1639 was determined by qPCR with primers flanking the cleave site and analysed using a ΔΔCT method (n=3) **(D)**. Data are presented as mean ± SD. Significance was calculated by one-way analysis of variance (ANOVA) with a Dunnett's multiple comparison post-test. Asterisks denote a significant difference between the specified groups (* p≤ 0.05, ** p<0.01 and *** p<0.001).

4.4 The level of BUD23 is not affected during KSHV Lytic Replication, however G1639 Methylation is Increased

To gain a greater understanding of the relationship between BUD23 and its increased association with pre-40S complexes during KSHV lytic replication, BUD23 mRNA and protein levels were analysed over a time course of lytic replication. Furthermore, levels of the BUD23 catalysed m^7G1639 modification of the 18S rRNA were also measured over the same time course.

No significant change to either BUD23's mRNA or protein levels were detected over the 48 hour time course (Figure 4.4 A and B). However, the percentage of methylated G1639 of the 18S rRNA increased from about 83% to 92% (Figure 4.4 C).

These data suggests that during lytic replication KSHV specifically increases the association of BUD23 with pre-40S ribosomal complexes instead of just increasing the levels of freely available BUD23 which can bind pre-40S complexes. Furthermore, the increased association of BUD23 with pre-40S ribosomal complexes leads to an increase in methylation of the 18S rRNA base G1639.

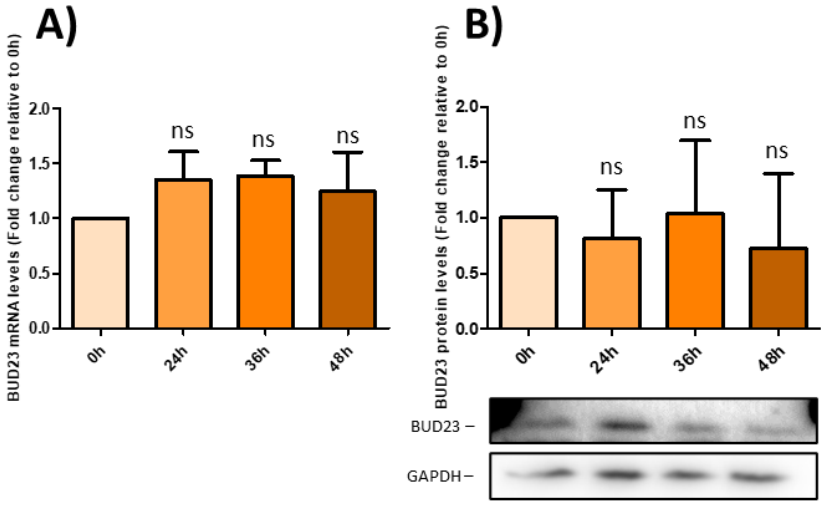

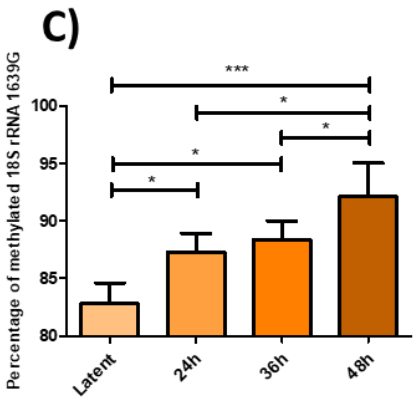

Figure 4.4 The levels of BUD23 and its m^7G1639 18S rRNA modification during a time course of KSHV lytic replication. KSHV was reactivated in TREx BCBL1-Rta cells with samples taken at 0 (latent), 24, 36 and 48 hours post reactivation. Total RNA was isolated from cells and quantified by two-step RT-qPCR, with primers specific for BUD23 and GAPDH as a reference gene (n=3) **(A)**. Data was analysed by comparison to GAPDH and the latent timepoint using a ΔΔCT method. Whole cell lysates were collected and analysed by western blot probing for BUD23 with GAPDH included as a loading control. Representative western blots and densitometric analysis are shown (n=3) **(B)**. Total RNA was isolated and chemical cleaved at m^7G sites. The proportion of cleaved to uncleaved rRNA at 18S G1639 was determined by qPCR with primers flanking the cleave site (n=3-4) **(C)**. Data was analysed by comparison to GAPDH and the 48h Scr control using a ΔΔCT method. Data are presented as mean ± SD. Significance was calculated by one-way ANOVA with a Dunnett's multiple comparison post test. Asterisks denote a significant difference between the specified groups (* $p \leq 0.05$, ** $p<0.01$ and *** $p<0.001$).

4.5 BUD23 is required for the efficient expression of late lytic KSHV genes

To start to assess the effect of BUBD23 knockdown on the lytic replication cycle of KSHV, the expression of the early lytic KSHV genes ORF57 and ORF59 were analysed over a 48 hour time course of lytic KSHV reactivation. Overall, little change to either the protein or mRNA levels of ORF57 or ORF59 were observed in BUD23 knockdown cells compared to the Scr control (Figure 4.5). However, a slight but significant drop of ORF57 and ORF59 mRNA occurred in the BUD23 knockdown shRNA 2 cell line at 48 hours post lytic reactivation compared to the Scr cells (Figure 4.5 D and E).

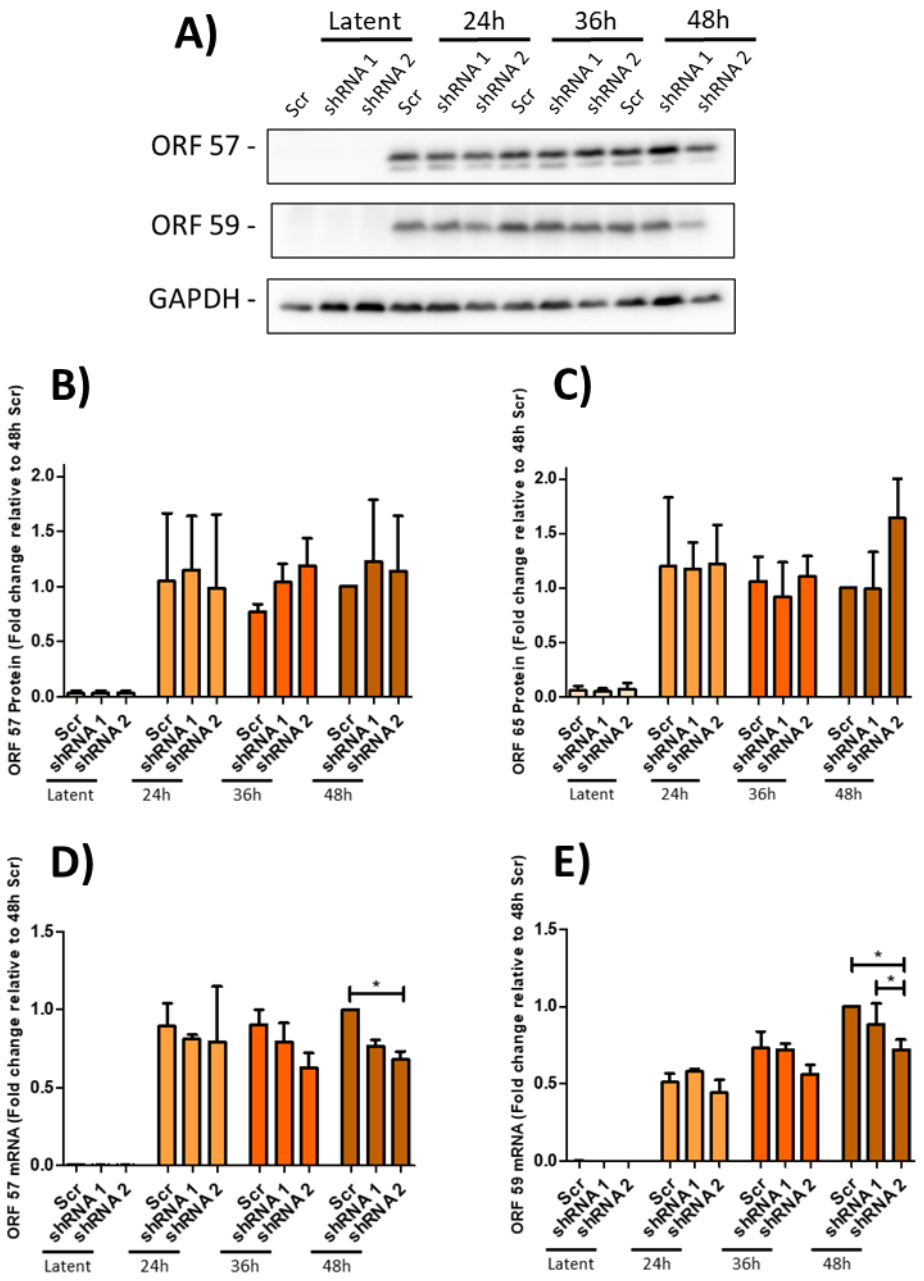

Figure 4.5 Knockdown of BUD23 does not effect the expression of early lytic KSHV genes. TREx BCBL1-Rta cells expressing a Scr shRNA or two different shRNAs targeting BUD23 were used for a time course of KSHV lytic reactivation over 48 hours, with samples collected at 0 (latent), 24, 36 and 48 hours (n=3). Whole cell lysates were collected and analysed by western blot probing for early lytic KSHV proteins ORF57 and ORF59, GAPDH was included as a loading control. Representative western blots **(A)**, and densitometric analysis of ORF57 **(B)** and ORF59 **(C)** relative to GAPDH are shown. Total RNA was isolated from cells and quantified by two-step RT-qPCR, with primers specific for ORF57 **(D)**, ORF59 **(E)**, and GAPDH as a quantity control. Data was analysed by comparison to GAPDH and the 48h Scr control using a ΔΔCT method. Data are presented as mean ± SD. Significance was calculated by one-way ANOVA with a Dunnett's multiple comparison post test. Asterisks denote a significant difference between the specified groups (* p≤ 0.05, ** p<0.01 and *** p<0.001).

The effect of BUD23 knockdown was then assessed on the expression of the late lytic viral genes K8.1 and ORF65. Overall, the protein expression of K8.1 and ORF65 was dramatically reduced in the BUD23 knockdown cells compared to Scr cells (Figure 4.6). At 48 hours post lytic reactivation, western blot densitometric analysis showed that K8.1 protein expression was reduced by about 50% in BUD23 knockdown cells compared to Scr cells and ORF65 protein expression was reduced by over 70% (Figure 4.6 B and C). Again, a slight but significant reduction of both K8.1 and ORF65 mRNA is observed. At 48 hours post lytic reactivation qPCR analysis of K8.1 and ORF65 mRNA showed a reduction of about 30% (Figure 4.6 D and E).

Overall, these results suggest BUD23 greatly impacts the translation of KSHV late lytic genes but not early lytic genes. However, at late timepoints of KSHV lytic replication the depletion of BUD23 also starts to impact the transcription of KSHV genes. Although, as proteins of the KSHV lytic cascade fail to be efficiently translated this results in a breakdown of the lytic cascade which can feedback to lytic gene transcription resulting in the deceased levels of mRNA observed. Furthermore, the drop in mRNA levels of K8.1 and ORF65 are considerably less than the drop in protein levels. Together this suggests that the driving force behind the reduction in KSHV late lytic gene protein expression is a reduction in translation.

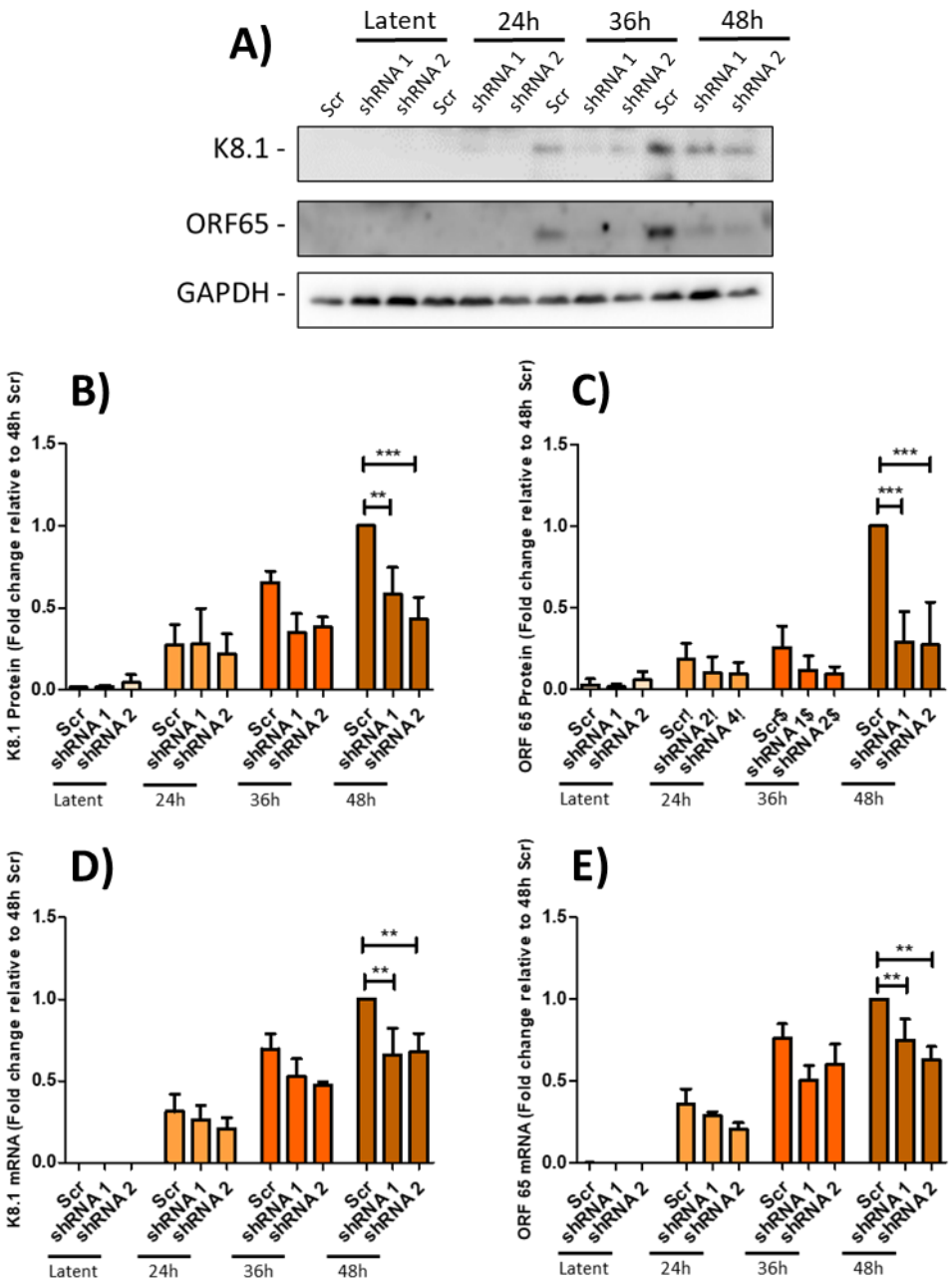

Figure 4.6 Knockdown of BUD23 significantly reduces the translation of late lytic KSHV genes. TREx BCBL1-Rta cells expressing a Scr shRNA or two different shRNAs targeting BUD23 were used for a time course of KSHV lytic reactivation over 48 hours, with samples collected at 0 (latent), 24, 36 and 48 hours (n=3). Whole cell lysates were collected and analysed by western blot probing for late lytic KSHV proteins K8.1 and ORF65, GAPDH was included as a loading control. Representative western blots **(A)**, and densitometric analysis of K8.1 **(B)** and ORF65 **(C)** relative to GAPDH are shown. Total RNA was isolated from cells and quantified by two-step RT-qPCR, with primers specific for K8.1 **(D)**, ORF65 **(E)**, and GAPDH as a quantity control. Data was analysed by comparison to GAPDH and the 48h Scr control using a ΔΔCT method. Data are presented as mean ± SD. Significance was calculated by one-way ANOVA with a Dunnett's multiple comparison post test. Asterisks denote a significant difference between the specified groups (* p≤ 0.05, ** p<0.01 and *** p<0.001).

4.6 BUD23 is required for the efficient production of infectious virions

Following the observed reduction in KSHV late protein production upon BUD23 depletion, it was next determined what effect this had upon viral genome replication and infectious virion production. KSHV genome levels were determined by the level of genomic ORF57 present in the cells analysed by qPCR. Results showed the knockdown of BUD23 in TREx BCBL1-Rta cells reduced the number of KSHV genome copies 72 hours after lytic reactivation by 60% compared to Scr cells (Figure 4.7 A).

Furthermore, the number of infectious virus particles produced by Scr and BUD23 depleted cells at 72 hours post lytic reactivation was determined by a virus reinfection assay of naive 293T cells. Results showed a dramatic reduction of up to 90% of infections virus particles produced by BUD23 knockdown cells compared to Scr cells (Figure 4.7 B).

These data suggest that as the KSHV lytic cascade collapses due to a reduction in late protein translation the final processes of virion production are even more affected resulting in almost a total loss of infectious virion production. Furthermore, a significant reduction in KSHV lytic genome replication is observed at 72 hours most likely again due to the breakdown of the lytic gene cascade and overall reduction of late lytic processes.

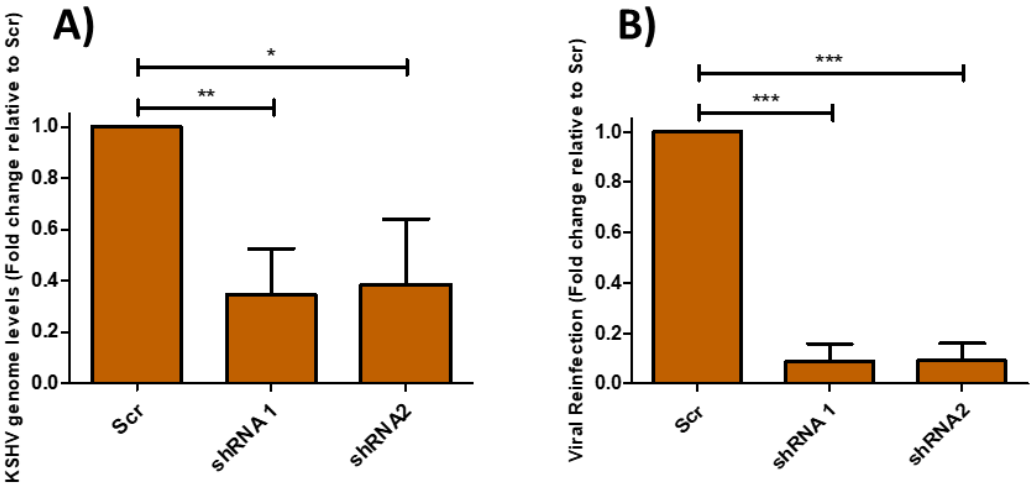

Figure 4.7 BUD23 knockdown reduces the production of viral genome copies and virus reinfection of 293T cells. Lytic reactivation of KSHV was induced in TREx BCBL1-Rta cells expressing a Scr shRNA or two different shRNAs targeting BUD23 for 72 hours. Genome production was analysed by purifying total gDNA from cells and quantifying by qPCR, with primers specific for ORF57 (n=3) **(A)**. Virus released from TREx BCBL1-Rta cell lines was collected and 293T cells reinfect with the virus for 48 hours. Total RNA was RNA was isolated from cells and quantified by two-step RT-qPCR, with primers specific for the early viral gene ORF57 (n=3) **(B)**. Data was analysed by comparison to GAPDH and the Scr control using a ΔΔCT method. Data are presented as mean ± SD. Significance was calculated by one-way ANOVA with a Dunnett's multiple comparison post test. Asterisks denote a significant difference between the specified groups (* p≤ 0.05, ** p<0.01 and *** p<0.001). The final version of both experiments presented were completed by Ms. Elena Harrington (Whitehouse group).

4.7 Discussion

In this chapter the increased association of BUD23 with pre-40S ribosomal subunits during KSHV lytic replication was validated by western blotting, confirming the quantitative mass spectrometry in chapter one (Figure 4.1). Interestingly however, the expression of BUD23 does not significantly change during KSHV reactivation (Figure 4.4 A and B). Taken together this suggest that KSHV specifically increases the association of BUD23 with pre-40S ribosomal complexes and does not just increasing its expression and there the freely available amount of BUD23 that can bind. These results also agree with the hypothesis that the viral protein ORF11, shown to bind to pre-40S ribosomal subunits, is responsible for driving the changes seen in these complexes during KSHV lytic replication (Figure 3.9).

Stable TREx BCBL1-Rta cell lines with BUD23 knockdown were produced and shown not to have any change to overall cell behaviour compared to a non-targeting scrambled knockdown cell line (Figure 4.2 andFigure 4.3). Therefore, any effect on the KSHV lytic replication cycle is most likely directly due to BUD23 knockdown and not due to changes in the cell environment.

The knockdown of BUD23 drastically impacts the translation of the late lytic KSHV proteins K8.1 and ORF65 but not early lytic proteins ORF57 and ORF59 (Figure 4.5 and Figure 4.6). Furthermore, knockdown of BUD23 results in almost a total loss in overall production of infectious virus particles (Figure 4.7 B). The significant but slight reduction of viral mRNA expression observed at 48 hours post lytic reactivation is probably due to the collapse in the viral gene lytic cascade. Effective continuation of the KSHV lytic life cycle requires the correct expression of all genes at each step of the way towards ultimately the production of new virions and their final egress out of the cell[369,370]. Therefore, by 48 hours post lytic reactivation in BUD23 knockdown cells the translation of viral genes has been greatly affected this intern leads to a drop in transcription of viral genes. However, due to the drop in translation observed been by as much as 70% for ORF65 at 48 hours and the reduction of mRNA only been by 30% it would seem very plausible that the main driving factor of BUD23 knockdown on disrupting the KSHV lytic cascade is the drastic drop in translation.

The level of m^7G modification of the 18S rRNA base G1639 was shown to be reduced from 80% in Scr cells to 50-60% in BUD23 knockdown cells (Figure 4.3 D). Other studies have reported the levels of m^7G1639 to be between 70-100%[205,371]. Even with the 80% reduction

of BUD23 protein expression in BUD23 knockdown cells the residual 20% must be enough to still methylate G1639 of the 18S rRNA by up to 60%. Furthermore, the total methylation of G1639 during KSHV lytic replication increases from about 80% during latency to above 90% 48 hours post lytic reactivation (Figure 4.4 C). Overall, these results suggest that the methylation of G1639 by BUD23 is at least in part responsible for the reduction in translation of late lytic KSHV genes.

We therefore hypothesised that KSHV starts to manipulate ribosome biogenesis early during its lytic life cycle through the increased association of BUD23 and other RBFs with pre-40S ribosome complexes. This results in changes to the newly made ribosome population such as the increased m^7G methylation of the 18S rRNA base G1639. Changes to the newly made ribosomes represent KSHV specific specialised ribosomes that go on to efficiently translate viral late lytic genes leading to the effective production and egress of new virions.

Chapter Five

~

Ribosome Profiling Reveals BUD23 Knockdown Dysregulates KSHV uORF Expression

5 Ribosome Profiling Reveals BUD23 Knockdown Dysregulates KSHV uORF Expression

5.1 Introduction

Chapter four demonstrated the potential impact that BUD23 specialised 40S subunits have on the translation of lytic KSHV mRNAs. This chapter aims to determine a possible mechanism behind the effects of BUD23 specialised 40S subunits on KSHV mRNA translation.

Ribosome profiling was first developed in 2009 by Ingolia et al. and is a very powerful technique for investigating the codon specific relationship of ribosomes with translatable RNAs[372]. Briefly, translating ribosomes are purified though polysome profiling and the translated RNA is digested with RNase. However, the approximate 30 nucleotide fragment of RNA protected by the ribosome, termed the 'ribosome footprint' (FP), remains intact. Ribosome footprints, along with an input mRNA sample, are then purified and processed for next generation sequencing. Both the ribosome footprint and mRNA reads are processed and aligned back to a reference genome. Data analysis can then identify novel translation events and show translational efficiencies for all translation events on an RNA.

In this chapter ribosome profiling was used to identify changes in the association of ribosomes with KSHV mRNAs due to BUD23 ribosome specialisation. Two independent repeats of ribosome profiling were performed.

5.2 Ribosome footprinting and library preparation for next generation sequencing

A time point of 36 hours post KSHV lytic reactivation was chose to perform ribosome profiling to give sufficient time post lytic reactivation to allow for the greatest number of KSHV specific specialised ribosomes to have been synthesised. However, a further facet to consider is the effect KSHV lytic replication has upon the normal cell biology which ultimately leads to cell death through lysis. As a result, 36 hours post lytic reactivation was decided as an optimal timepoint for this experiment.

Therefore, KSHV was reactivated for 36 hours in TREx BCBL1-Rta cells Scr control cells and a BUD23 depleted cell line. Polysome profiling was performed on the cell lysates and as the gradients were cut the fractions containing the 80S peak and all the polysomes were collected, fractions 4-10 (Figure 5.1). The collected fractions were pooled and treated with

RNase to footprint the RNAs been translated. The RNase was then inactivated and polysome profiling was again performed on the samples. Finally, a singular 80S peak is observed on the polysome traces of both the Scr and BUD23 knockdown samples representing the footprinted ribosomes (Figure 5.1). Fractions four and five containing the footprinted ribosomes were collected for down-stream processing.

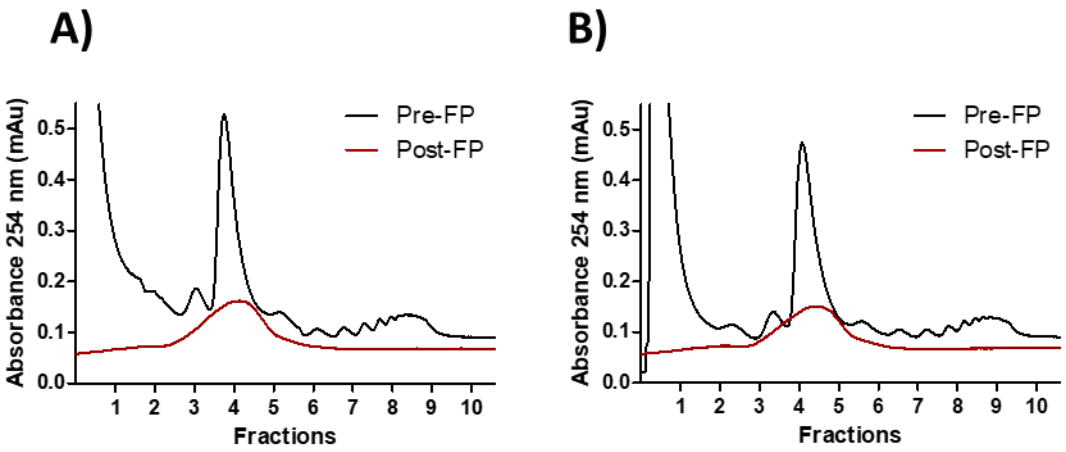

Figure 5.1 Polysome profiles of ribosome populations before and after footprinting. KSHV lytic reactivation was induced for 36 hours in TREx BCBL1-Rta cells expressing a Scr shRNA (A) or shRNA 1 targeting BUD23 (B). Polysome profiles of before and after RNase treatment. FP=footprinting

The RNA was isolated from polysome profiling ribosome FP samples and from whole cell lysate RNA reference samples and treated with DNase to remove any genomic DNA contamination. The RNA reference samples were then selected for polyadenylated (polyA) RNA, to remove all rRNA and tRNA, and then chemically fragmented. The isolated footprint samples and fragmented polyA RNA samples were purified on a denaturing RNA gel (Figure 5.2).

Bands of the desired size for each sample were cut from the gel and the RNA extracted. For the polyA RNA samples bands from 50 base pairs (bp) to 80 bp were cut from the gel and for the ribosome footprinted samples bands of 28-32 bp were cut. A bulge in the of RNA can be observed in the ribosome FP samples between the 28 and 32 bp markers which represents the FP RNA fragments. The rest of the RNA present in the footprinted samples is mainly rRNA.

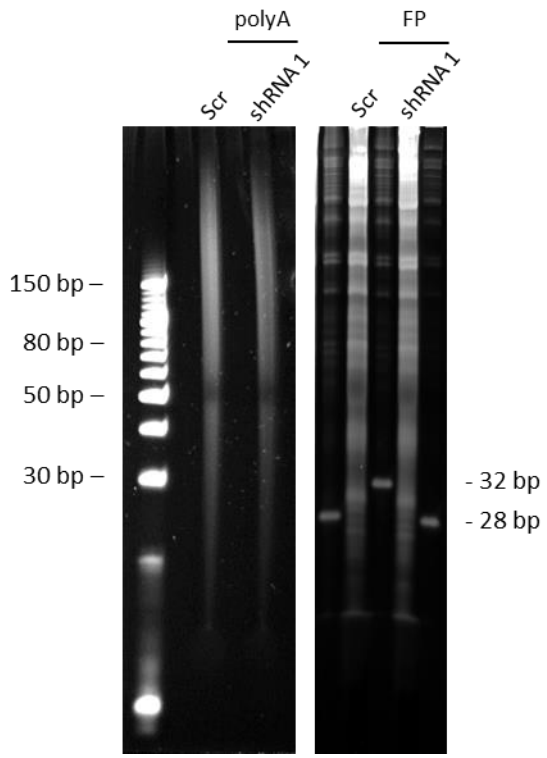

Figure 5.2 Denaturing RNA gel purification of fragmented reference polyA RNA and ribosome footprints. A 10% polyacrylamide urea gel stained with SYBR™ Gold. Samples originating from TREx BCBL1-Rta cells expressing a Scr shRNA or shRNA 1 targeting BUD23. polyA = polyadenylated RNA FP = Ribosome footprinted RNA

The 5' and 3' end of the purified fragmented polyA RNA samples and the ribosome FP samples were repaired by T4 PNK treatment. The ribosome FP samples then went through two rounds of rRNA depletion. Small fragment, multiplexable, cDNA libraries of all the samples were constructed and amplified by PCR. The final products were then purified by polyacrylamide gel electrophoresis (Figure 5.3).

Bands of specific size were cut out for the polyA cDNA libraries (170-200 bp) and FP cDNA libraries (155-165 bp). The larger size of these products compared to the last gel purification in Figure 5.2 is due to the addition of a barcode, adaptors, and primers for multiplex next generation sequencing. Other bands observed in the final gel clean up are due to PCR amplification of primer and adapter products.

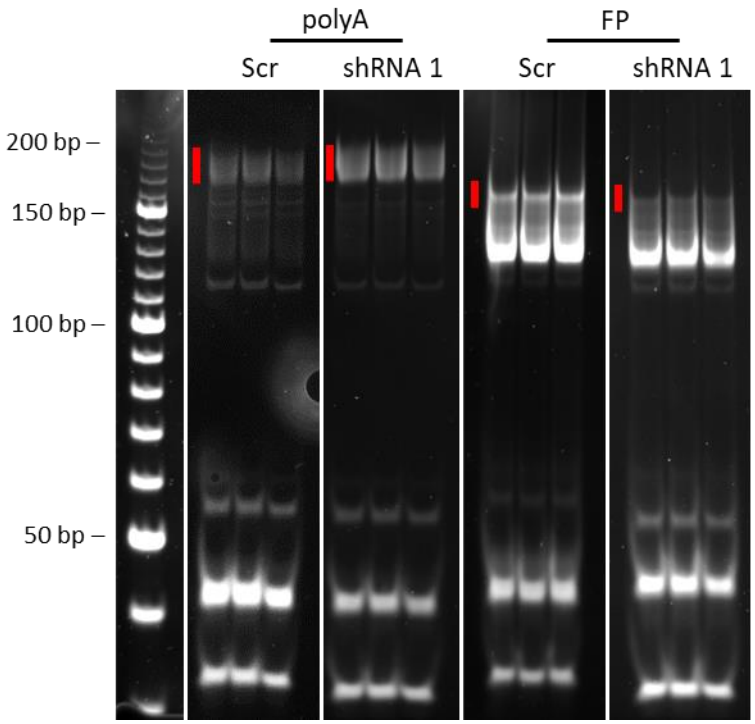

Figure 5.3 Gel clean up of cDNA libraries for next generation sequencing. An 8% polyacrylamide gel stained with SYBR™ Gold. PCR amplified samples originating from TREx BCBL1-Rta cells expressing a Scr shRNA or shRNA 1 targeting BUD23. Red markers indicate correct libraries product size, polyA 170-200 bp and FP 155-165 bp. polyA = polyadenylated cDNA samples FP = Ribosome footprinted cDNA samples.

5.3 Ribosome profiling – Data processing and quality control

The cDNA libraries were sequenced with single end, 50 bp sequencing at an average read depth of 128 million reads per library. Data processing was performed by Dr. Elton Vasconcelos (Leeds Omics, Bioinformatics Research Officer). Reads for each library were put through a quality control pipeline and then aligned to the human and KSHV genomes.

The optimal read length and triplet periodicity of the aligned FP reads was determined as a further method to increase the quality of the data. For ribosome FP libraries from both Scr and BUD23 Knockdown cells, and for human and KSHV reads the optimal read lengths were 32-34 nucleotides (nt) and the optimal triplet periodicity was frame 2 (Figure 5.4 and Figure 5.5). These read lengths and triplet periodicity contain the highest number of reads while excluding reads that less well represent ribosome footprints from TREx BCBL1-Rta cells. The read length of the library is representative of how much of the RNA is protected by the ribosome. This can vary depending on the biological species of the ribosome, the type of chemical immobilisation use to stall the ribosome, and the RNase treatment conditions[373]. The triplet periodicity of ribosome FP reads is based on the codon nature of translation and

determines reads with the same three bases present in the each tRNA site of the ribosome relative to the start codon of the mRNA. Choosing the optimal read lengths and triplet periodicity is a further form of quality control which allows the exclusion of non-ribosomal FP reads from the data sets. These non-ribosomal FP reads include imperfectly footprinted RNA fragments, rRNAs, tRNAs, snRNAs and snoRNAs.

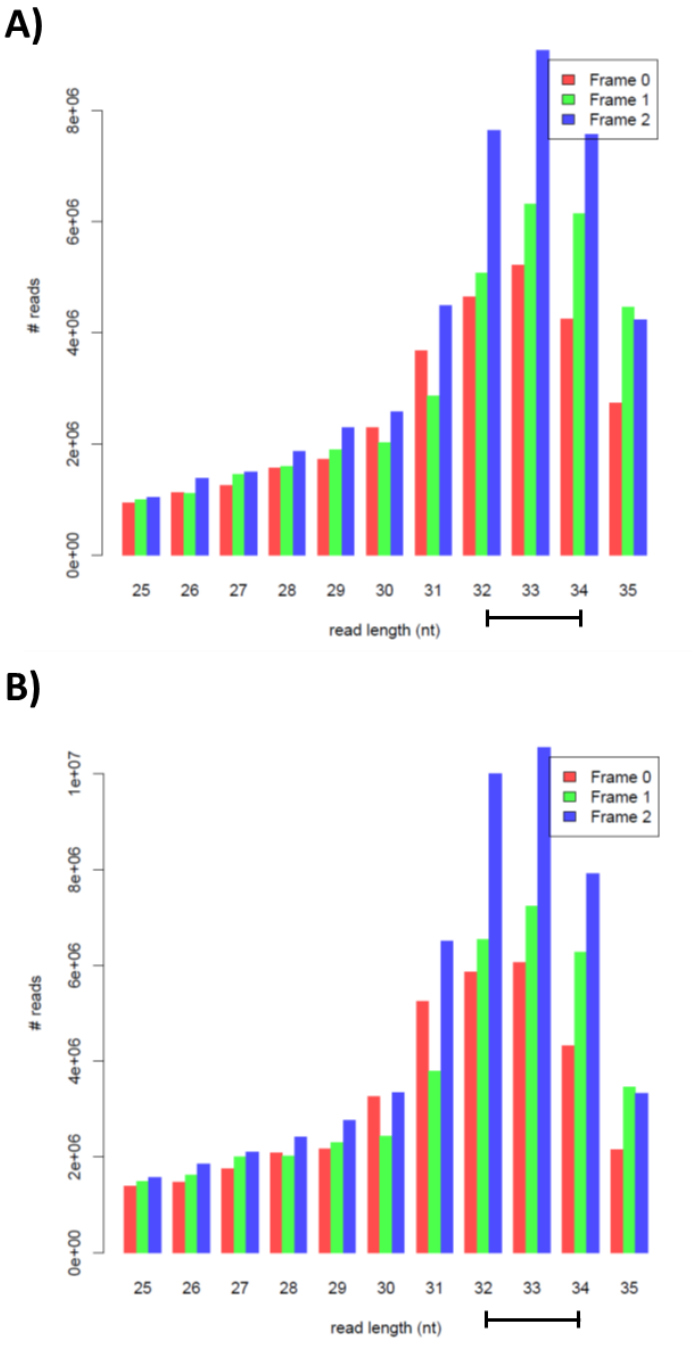

Figure 5.4 Read length and Triplet periodicity of ribosome FP libraries for human reads. Libraries originating from TREx BCBL1-Rta cells expressing a Scr shRNA **(A)** or shRNA 1 targeting BUD23 **(B)**. Data processing and figure produced by Dr. Elton Vasconcelos (Leeds Omics - Bioinformatics Research Officer).

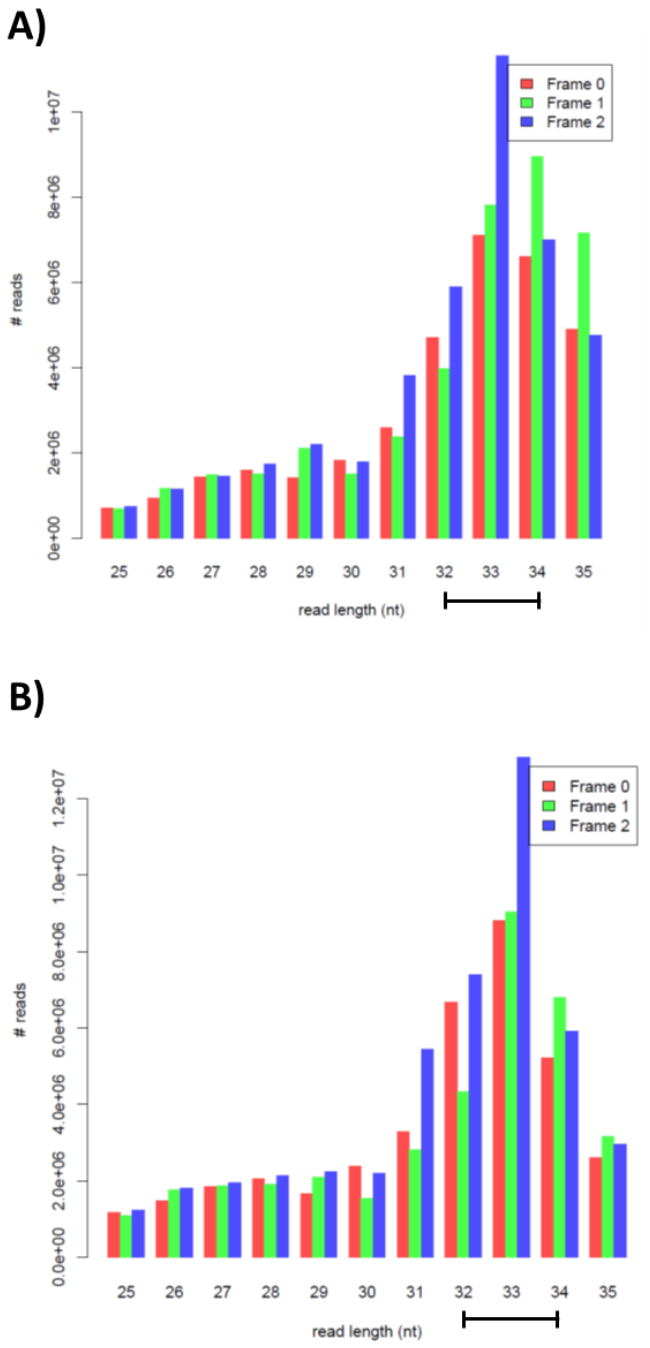

Figure 5.5 Read length and Triplet periodicity of ribosome FP libraries for KSHV reads. Libraries originating from TREx BCBL1-Rta cells expressing a Scr shRNA **(A)** or shRNA 1 targeting BUD23 **(B)**. Data processing and figure produced by Dr. Elton Vasconcelos (Leeds Omics - Bioinformatics Research Officer).

To confirm ribosome FP reads mapped as expected across an mRNA, metagene profiles showing mapped footprint read density relative to the annotated start and stop codons of all human genes were generated (Figure 5.6). As expected, most reads map to the open reading frame of a gene. Some reads map to the 5' UTR potentially due to uORF expression and unsurprisingly very few reads at all mapped to the 3' UTR due to the termination of translation at the stop codon. These data again also show frame 2 as the dominate periodicity for the reads. Unfortunately, due to complications with KSHV gene annotations because of overlapping open reading frames, metagene profiles could not be generated for footprint reads mapping to the KSHV genome.

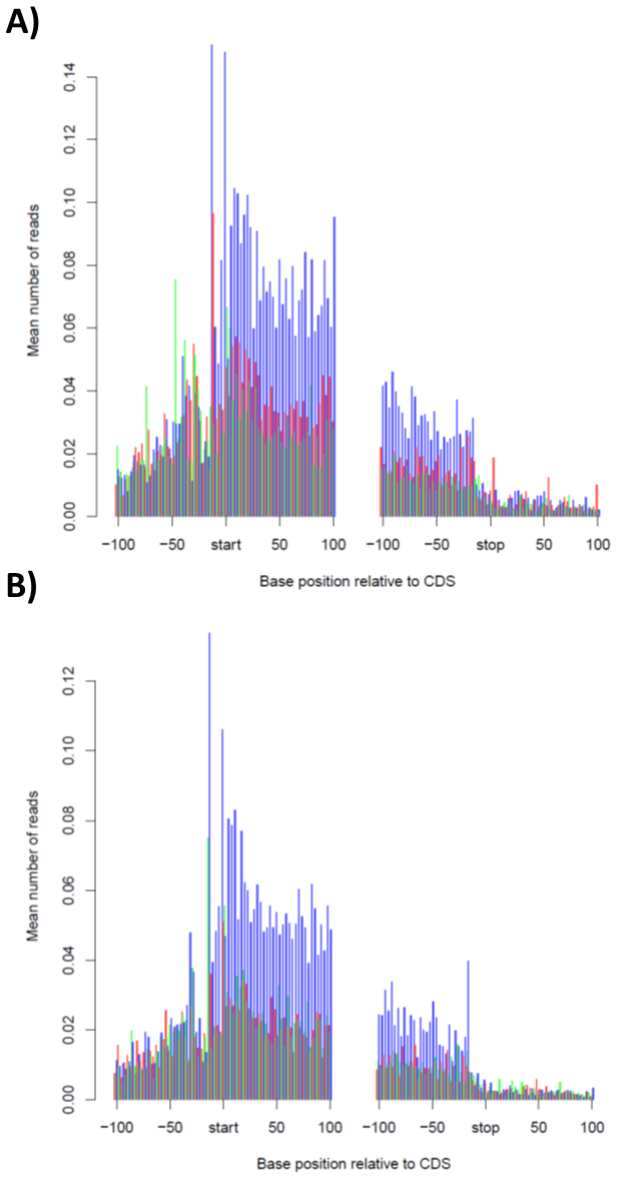

Figure 5.6 Metagene profiles of human ribosome footprint reads. Ribosome FP read libraries mapped relative to start and stop codons of all human genes. Libraries originating from TREx BCBL1-Rta cells expressing a Scr shRNA **(A)** or shRNA 1 targeting BUD23 **(B)**. Data processing and figure produced by Dr. Elton Vasconcelos (Leeds Omics - Bioinformatics Research Officer).

5.4 Ribosome profiling – Translational Efficiencies

To determine how the depletion of BUD23 effects the translation of mRNAs, translational efficiencies were calculated. Translation efficiency considers the number of ribosome FP and polyA RNA reference reads mapping to an ORF and the length of the ORF itself. This results in a value representative of the amount of translation of a gene at that specific moment in time.

Translational efficiencies of human genes were calculated for libraries originating from TREx BCBL1-Rta cells expressing a Scr shRNA compared to shRNA 1 targeting BUD23. Notably, only one human gene, nerve growth factor inducible (VGF), was calculated to have a significant change in translational efficiency in BUD23 knockdown cells compared to Scr cells (Figure 5.7).

With just one gene significantly dysregulated this could be a true representation of the biology in BUD23 knockdown cells and that no human genes are changed in their translation. However, translational efficiency software packages struggle to calculate significance with only two experimental repeats, which is the case for this experiment. Therefore, other genes that have changes to their translational efficiencies may have been missed due to the low confidence in their changes.

The one dysregulated human gene, VGF, is down regulated with a fold change of 0.005. VGF is not known to be expressed in B cells which were used in this experiment. Therefore, very low expression of the gene could amplify small changes in translational efficiency.

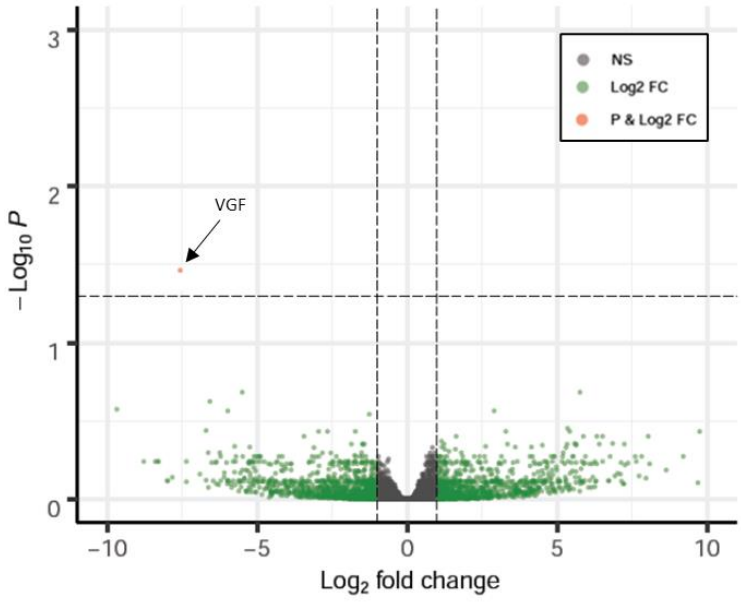

Figure 5.7 Volcano plot for human gene translational efficiency changes. Translational efficiencies calculated for libraries originating from TREx BCBL1-Rta cells expressing a Scr shRNA compared to shRNA 1 targeting BUD23. A false discovery rate was set at < 0.05 and fold change threshold set at ± 1 (Log2). NS = Not significant; FC = Fold change. Data processing and figure produced by Dr. Elton Vasconcelos (Leeds Omics - Bioinformatics Research Officer).

Translational efficiencies of KSHV genes revealed a number of changes which mainly occured in KSHV gene uORFs (Figure 5.8). Eight uORFs had an increased translational efficiency and one uORF had a decreased efficiency (Figure 5.8 B). Only three main CDSs had a significant change to their translational efficiencies, ORF62 and ORF27, which were up-regulated and ORF28 which was down-regulated (Figure 5.8 B).

The greater number of statistically significant changes in translational efficiency for KSHV genes compared to human genes is most likely down to the fact that KSHV read counts of polyA RNA and ribosome FP libraries accounted for 90% and 70% of the reads, respectively. In addition to KSHV having considerably less genes than the human genome, KSHV genes have a vastly greater read depth than human genes enabling greater confidence when analysing changes.

A)

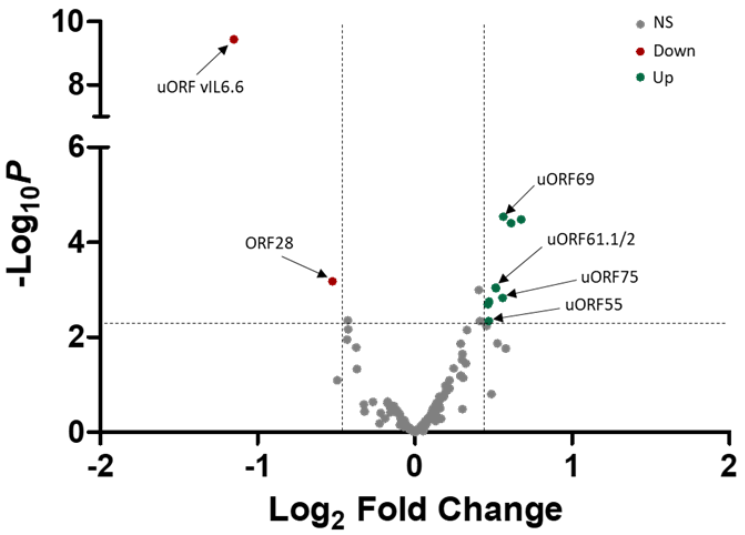

B)

Translation Product	Fold change
uORF62A	1.381
uORF62B	1.384
uORF55	1.385
ORF62	1.387
uORF61.1	1.428
uORF61.2	1.431
uORF75.1	1.474
uORF69	1.478
ORF27	1.528
uORF vIL6.5	1.600
ORF28	0.682
uORF vIL6.6	0.450

Figure 5.8 Translational efficiencies of KSHV genes. Changes in translational efficiency calculated for libraries originating from TREx BCBL1-Rta cells expressing a Scr shRNA compared to shRNA 1 targeting BUD23. A false discovery rate was set at < 0.005 and fold change threshold set at ± 0.45 (log2). Volcano plot representation of all KSHV gene translational efficiency changes **(A)**. Table of all KSHV genes with significantly changed translational efficiencies greater than ± 0.45 (log2) **(B)**. NS = Not significant

5.5 Ribosome profiling – BUD23 knockdown dysregulates the control of KSHV gene uORFs

To understand how depletion of BUD23 effects the translation of KSHV uORFs, ribosome occupancy across genes was visualised in bed graphs displaying ribosome footprint reads. As detected by changes in translational efficiencies, increased ribosome occupancy of the ORF69, ORF61 and ORF75 uORFs can be visibly seen in ribosome footprint bed graphs (Figure 5.9). The maximal ribosome occupancy of uORF69 increases by 30% from $2.0x10^5$ reads in Scr cells to $2.6x10^5$ reads in BUD23 depleted cells and uORF61.1/2 increased by 50% from $1.1x10^6$ reads to $1.7x10^6$ reads (Figure 5.9 A and B). The ribosome occupancy of uORF75.1 and .2 increases by 8% and 4% respectively with the depletion of BUD23, the ribosome occupancy further down-stream in the CDS is visually decreases in multiple regions with the largest decrease of 17% shortly after the start codon (Figure 5.9 C). This possibly highlights a potential biological mechanism behind the increased uORF occupancy.

Interestingly, much of the ribosome occupancy on the transcripts is located in the uORFs for both Scr and shRNA1 BUD23 knockdown conditions. However, at smaller scales ribosome occupancy is observable across the CDS as well.

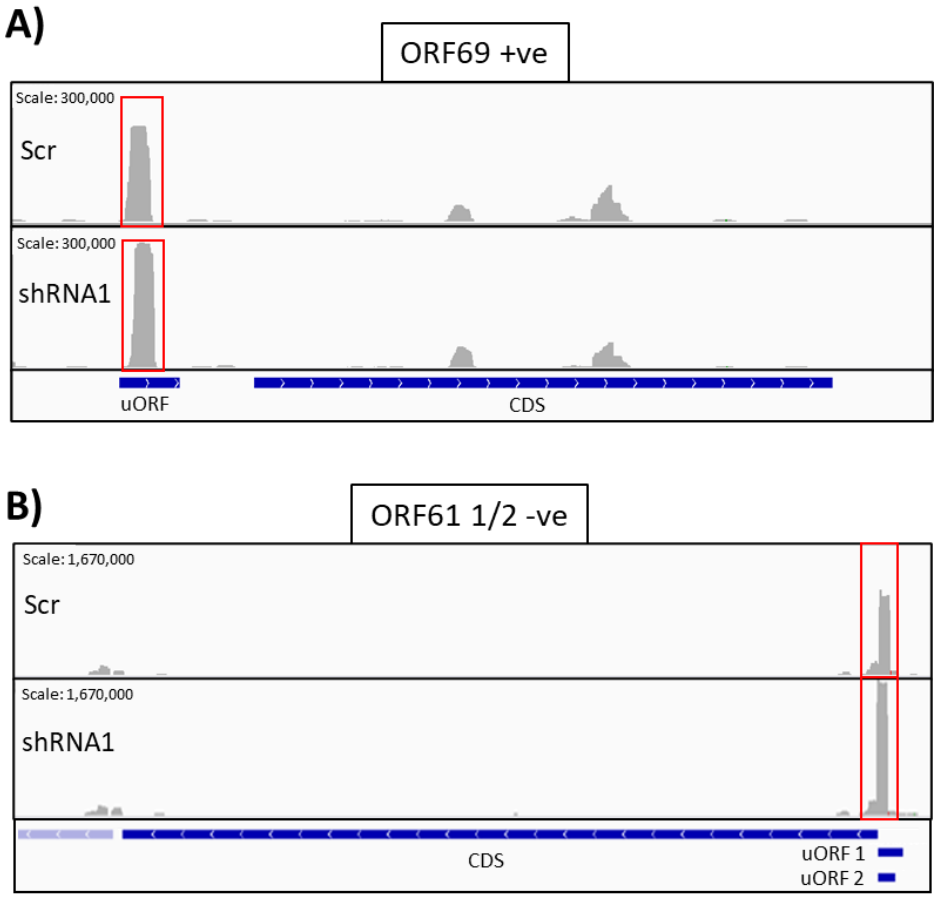

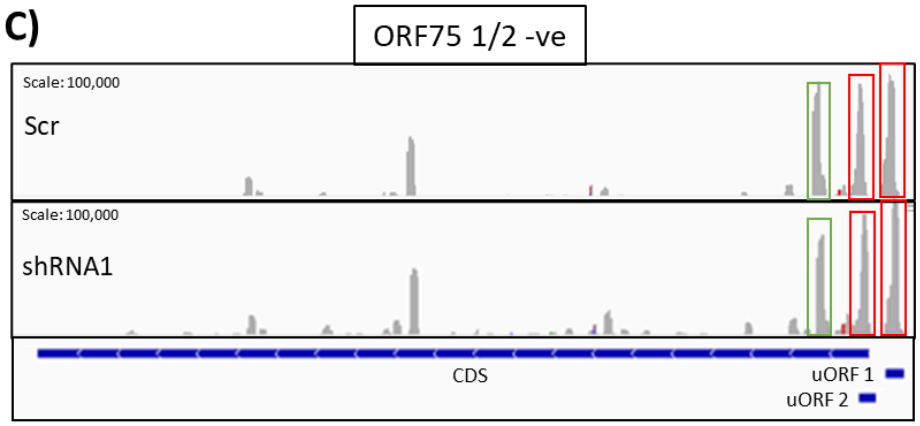

Figure 5.9 Ribosome profiles of upregulated KSHV gene uORFs. Bed graph displays of ribosome foot reads mapping to KSHV genes for libraries originating from TREx BCBL1-Rta cells expressing a Scr shRNA or shRNA 1 targeting BUD23. KSHV genes shown include ORF69 **(A)**, ORF61 **(B)**, and ORF75 **(C)**.

The KSHV gene ORF28 had a 0.682 fold decrease in translational efficiency of its CDS when BUD23 was depleted (Figure 5.8 B). Furthermore, the reduction in ribosome occupancy of the CDS of ORF28 can be observed in ribosome footprint read bed graphs (Figure 5.10 A). ORF28 also contains a uORF, however this was not detected as having a significant increase in translation during BUD23 knockdown. Changes to the ribosome occupancy of uORF28 are also unclear, however as ORF28 contains a uORF and its CDS is down regulated upon BUD23 depletion this again potentially highlights a mechanism by which CDS expression could be regulated by the presences of a uORF.

Changes in translational efficiencies of ORF65 from Scr libraries compared to BUD23 knockdown libraries were not determined to be statistically significant. However, a small increase in the maximal ribosomal occupancy can be observed in ribosome footprint bed graphs of uORF65, from $5.2x10^5$ reads in Scr cells to $6.0x10^5$ reads in BUD23 depleted cells (Figure 5.10 Bi). Furthermore, the CDS of ORF65 also appears to have decreased ribosome occupancy at multiple sites across ribosome footprint bed graphs when BUD23 is depleted compared to Scr cells (Figure 5.10 Bii). Again, this further adds to the hypothesis that the depletion of BUD23 results in the increased expression of uORFs and subsequent downregulation of the CDS.

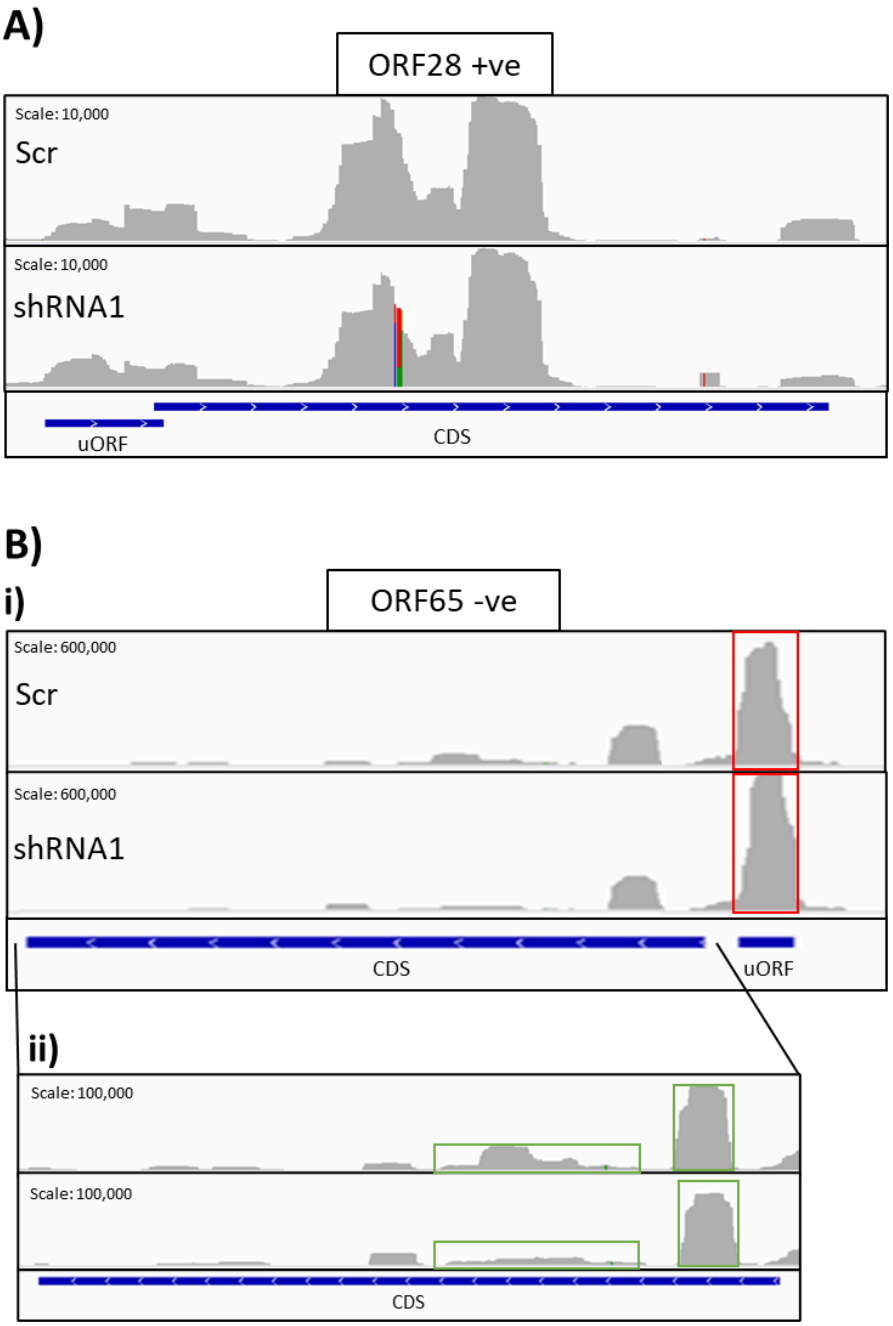

Figure 5.10 Ribosome profiles of KSHV genes with uORFs and reduced CDS occupancy. Bed graph displays of ribosome foot reads mapping to KSHV genes for libraries originating from TREx BCBL1-Rta cells expressing a Scr shRNA or shRNA 1 targeting BUD23. KSHV genes shown include ORF28 **(A)** and ORF65 **(B)**.

5.6 Discussion

Ribosome profiling is powerful technique giving a snapshot of where ribosomes are bound to mRNAs at a certain timepoint. Overall, in this chapter ribosome profiling of cells expressing a Scr shRNA or shRNA 1 targeting BUD23 has demonstrated that BUD23 is required for the corrected expression of lytic KSHV uORFs.

Five KSHV genes containing uORFs were calculated to have increased translation efficiencies of their uORFs during BUD23 depletion (Figure 5.8). Furthermore, the CDS of ORF28, ORF65, and ORF75, all of which contain uORFs, have regions with visibly less ribosome occupancy during BUD23 depletion, shown by ribosome footprint bed graphs (Figure 5.9 and Figure 5.10). Typically, if the translation of a gene's uORF is increased then the translation of its downstream CDS is decreased (Figure 1.11). These results therefore suggest that BUD23 is involved in the correct translation of KSHV uORFs which may lead to the efficient expression of the downstream CDS.

It was hypothesised that only a small number of human genes would have changes to their translation efficiency with the depletion of BUD23 as no global changes to polysome profiles, protein turnover or cell proliferation were observed during BUD23 knockdown in chapter four (Figure 4.3). In this chapter, ribosome profiling identified only one human gene with a 0.005 fold decrease in translational efficiency when BUD23 was depleted, agreeing with the original hypothesis. However, BUD23 and the m^7G modification of the 18S rRNA base 1639 must have a biological relevance for the translation of a population of cellular genes. Baxter et al. hypothesised that BUD23 is involved in the translation of mRNAs with low 5' UTR GC contents[327]. The authors sequenced 'light' (2-4 ribosomes bound) and 'heavy' (>4 ribosome bound) polysomes from Scr and BUD23 knockdown cells. They found that mRNAs with a lower 5' UTR GC content shifted from heavy polysomes in Scr cells to light polysomes in BUD23 knockdown cells, indicating a reduction in translation of these mRNAs.

However, in light of BUD23's relevance for the correct translation of KSHV uORFs it would seem reasonable to hypothesis that BUD23 could also be important for the correct translation of some cellular uORFs. As discussed previously, only the one human gene, VGF, had a significant change to its translational efficiency in BUD23 knockdown cells compared to Scr cells. However, due to a combination of only having two ribosome profiling repeats and the low read depth of human genes, other human genes with dysregulated translational

efficiencies may not have been recognised due to low statistical confidence, especially short translatable elements such as uORFs. Therefore, more targeted and in depth analysis of the ribosome profiling data specifically looking at human uORFs would be an interesting line of research in the future to investigate this potential mechanism in human genes.

Chapter Six

~

Discussion

6 Discussion

The rapidly developing concept of specialised ribosomes, in many aspects of biology poses an intriguing question as to whether viruses co-opt this cellular mechanism to enhance the translation of their own mRNAs. Viruses do not encode translational machinery and therefore rely on host ribosomes to synthesise their proteins. Furthermore, the translational demand of viruses on the cell during infection is very large, in order to create enough structural proteins to produce large amounts of new infectious virions. As viruses co-opt and manipulate most other biological processes it would seem highly likely that some viruses also utilise the concept of specialised ribosomes to efficiently produce new virions.

Many viruses regulate and manipulate translation in a variety of ways. For example mechanisms include: viral IRESs (translation initiation), eIF2α kinase inhibition (ternary complex formation), polyA-binding protein inhibition, and cap dependent translation initiation factor regulation which is inhibited by IRES containing viruses and enhancement by cap-dependent translation initiation viruses[374–379].

Emerging evidence has also demonstrated that viruses can alter the ribosome itself to enhance the translation of viral mRNAs. VSV specifically requires the large ribosomal subunit protein RPL40 for cap-dependent translation initiation of its mRNAs but bulk cellular translation does not require RPL40[350]. A poxvirus kinase phosphorylates serine/threonine residues in the human small ribosomal subunit protein RACK1 that are not phosphorylated in uninfected cells or cells infected by other viruses[309]. The phosphorylation of RACK1 dictates ribosome selectivity towards viral RNAs with 5' UTR polyA-leaders[309]. Metagenome studies of viruses have revealed that some viruses, mainly bacteriophages, encode core ribosomal proteins. These proteins are homologues of host cell ribosomal proteins which are generally solvent exposed suggesting they can be easily exchanged to produced virus-specific ribosomes[380].

Previously, the Whitehouse lab identified changes to the ratio of nucleolar/nuclear/cytoplasmic localisation of some ribosomal and RBF proteins during lytic KSHV replication (data unpublished). This led to the hypothesis that KSHV may alter ribosomes during their biogenesis.

Although ribosomes are synthesised at a phenomenally fast rate, it would still take time to accumulate virus specific specialised ribosomes generated during ribosome biogenesis[381].

Fast acting viruses with short life cycles, such as picornaviruses with replication cycles as short as 6 hours, would most likely lack the time to substantially change the ribosome population of the cell[382]. Herpesviruses on the other hand have long life cycles of up to 72 hours, as is the case for KSHV. KSHV is therefore an ideal candidate to pose the question of whether it manipulates ribosome biogenesis during the course of lytic infection to generate ribosomes that promote the efficient translation of viral mRNAs.

6.1 KSHV increases the association of specific RBFs with pre-40S ribosomal subunits during lytic infection

To investigate changes to ribosomes during KSHV lytic infection, pre-ribosome complexes were focused on. This was firstly because of the long half-life of ribosomes and focusing on pre-ribosome complexes allowed the distinction between newly formed ribosomes during KSHV lytic replication and pre-existing ones in the cell. Secondly, ribosome biogenesis was hypothesised to be the point at which KSHV would most likely alter ribosome composition.

A system was developed using cell lines expressing tagged RBFs for the purification of pre-ribosomal complexes from cells during latent and lytic KSHV replication cycles. The composition and stoichiometry of purified pre-40S and pre-60S ribosomal complexes was analysed by quantitative mass spectrometry. Previous studies have used similar methods of purification of pre-ribosomal complexes[191,269,357–359]. However, quantitative mass spectrometry has only been used to determine the composition and stoichiometry of mature ribosomes to identify changes for specialisation, making this a novel approach for pre-ribosome complexes[348,360,361].

Pre-ribosome complex pulldown buffer ion composition and strengths were optimised along with centrifugation speeds and wash techniques. Both silver stain gels, and negative stain EM 3D reconstruction closely resembled previously published data of purified pre-ribosomal complexes[294,357].

Quantitative mass spectrometry of isolated pre-ribosomal complexes also confirmed the successful purification of these particles. Each RBF bait protein pulled-down pre-ribosomal complexes from different timepoints in ribosome biogenesis and from spatially different locations on pre-ribosomal complexes. Therefore, both the ribosomal and RBF composition of complexes isolated by different bait proteins varied. However, the majority of proteins isolated from complexes of the same bait protein did not change between those isolated

from cells latently infected with KSHV compared to complexes isolated from cells 24 hours after KSHV lytic reactivation. A timepoint of 24 hours post lytic reactivation was chosen to allow enough time for KSHV to have expressed all its early lytic genes and therefore have an impact on ribosome biogenesis. Later timepoints were not chosen mainly because any changes to ribosome biogenesis need to occur early enough in the KSHV lytic replication cycle to have an impact on the translation of lytically expressed genes.

Most interestingly, two groups of RBFs change in their association with pre-40S ribosomal complexes during lytic KSHV replication compared to latent infection, these were BUD23-TRMT112 and NOC4L-NOP14-EMG1. Both complexes contain RBFs with enzymatic functions for rRNA modifications. The RBF BUD23 catalyses the N^7-methylguanosine modification on 18S rRNA base G1639[281]. The RBF EMG1 catalyses the N^1-methylation of the hypermodified 18S rRNA base U1240, which can also contain a pseudouridylation and N^3-aminocarboxypropylation[278]. The functions of the other RBFs in the complexes include, TRMT112 acts as a co-factor of BUD23, and NOC4L and NOP14 are responsible for recruiting EMG1 to pre-40S subunits in the nucleolus along with structural roles in ribosome biogenesis. The increased association of these two RBF complexes with pre-40S ribosomal subunits, during ribosome biogenesis, suggests that KSHV specifically requires their activity and therefore most likely the enzymatic activity of BUD23 and EMG1.

Quantitative mass spectrometry showed that the viral ORF11 protein also associates with pre-40S ribosomal subunits during lytic replication. The TSR1 bait protein pulldown failed to co-precipitate either the BUD23 complex or ORF11, and its association with the EMG1 complex was also a lot weaker. This suggests that TSR1 binds at a more distant site on pre-ribosome subunits from the RBF complexes and ORF11. Taken together, all the different pre-40S ribosome complex pulldowns suggests that ORF11 binds closely or directly to the BUD23 and EMG1 complexes. Overall, this suggests that ORF11 maybe the viral factor involved in manipulating the increased association of the BUD23 and EMG1 complexes with pre-40S ribosome complexes during lytic replication.

The function of ORF11 during KSHV lytic replication is unknown. However, research by Dr. Sophie Schumann in the Whitehouse laboratory has revealed two potential temporal roles of ORF11 during KSHV lytic replication, firstly during ribosome biogenesis and then later during lytic replication at the cell membrane potentially for viral egress. Further work supporting a role of ORF11 in specialised ribosome formation involved pulldowns of

exogenously tagged ORF11 which co-precipitates many core ribosomal proteins and RBFs including RPS3, RPS19, BUD23 and NOC4L. Furthermore, during KSHV lytic replication ORF11 co-precipitates increased amounts of BUD23 but the level of core ribosomal proteins, such as RPS3 and RPS19, remains the same. These data confirm and validate the quantitative mass spectrometry and further biochemical analysis of BUD23.

Immunofluorescent microscopy of exogenously tagged ORF11 demonstrated subcellular localisation in both the nucleolus and nucleoplasm as well as at the cell membrane, suggesting ORF11 has more than one function. Notably, two transcripts for ORF11 are transcribed during KSHV lytic replication. The first is a single transcript which is expressed from eight hours post lytic reactivation, the second transcript is polycistronic containing ORFs 8, 9, 10 and 11, which is expressed from 24 hours post lytic reactivation[52]. This further suggests ORF11 may have more than one temporal role during KSHV lytic reactivation, one during immediate early stages and one at late stages. The early expression of ORF11 on its singular transcript is an ideal timepoint for the expression of a viral protein that would manipulate ribosome biogenesis. This therefore adds to the evidence making ORF11 a strong candidate as the viral protein responsible for the development of KSHV specific specialised ribosomes.

To gain a greater understanding of ORF11's relationship with pre-40S ribosome complexes we wanted to observe exactly where on these complexes ORF11 binds and which proteins it directly binds. We determined the best approach for this would be to use crosslinking-coupled with mass spectrometry to then build the identified interactions back onto published pre-40S subunit structures[383]. This approach is currently being optimised by Ms. Elena Harrington in the Whitehouse laboratory. Overall, this experiment will hopefully provide mechanistic proof that ORF11, through a direct interaction, enhances the association of BUD23 and EMG1 with pre-40S ribosomal subunits.

6.2 BUD23 and ribosome specialisation

Over 100 bases of the rRNAs are modified, the main modifications are pseudouridylation and 2'-*O*-ribose methylation which are guided and catalysed by two families of small nucleolar RNPs called H/ACA box (pseudouridylation) and C/D box snoRNPs (2'-O-ribose methylation)[273]. There are nine other enzymes known to carry out specific modifications of rRNAs, including BUD23 and EMG1 (Table 1.6).

The functional role of most modifications remains unknown, however modifications cluster in functionally important regions including the decoding centre, tRNA binding sites, the peptidyltransferase centre and the intersubunit interface[384]. The modification m^7G1639 of the 18S rRNA, which is catalysed by BUD23, is located at a ridge forming a steric block between the tRNA E- and P-site sites of the ribosome and accompanies the ratcheting of tRNAs from the P-site to the E-site[364]. Due to the location of m^7G1639 and movement with the mRNA and tRNAs it has been suggested to be involved in 40S subunit scanning and/or translocation[365].

It is agreed that the catalytic function of BUD23 is not required for ribosome biogenesis, which has been demonstrated with catalytically inactive mutants of BUD23[190]. However, some authors have demonstrated that the presences of BUD23 is required for efficient progression of pre-40S subunit ribosome biogenesis[190]. In contrast, Yan et al. did not observe any effect on cell proliferation upon BUD23 knockdown, indicating that ribosome biogenesis must also function effectively[385]. Results in chapter four agree with Yan et al. showing that BUD23 knockdown in TREx BCBL1-Rta cells does not affect cell proliferation, the total ribosome population or protein turnover.

As BUD23 is not required for overall cellular functioning it would suggest that its modification of G1639 in the 18S rRNA is not required for general translation but a more subtle and specific role in translation of particular types of mRNAs which could also be cell type specific. Furthermore, the BUD23 gene is lost in the sporadic multigene deletion disease Williams-Beuren syndrome[326]. As patients can still live with this disease, albeit with significant morbidity, this again suggests that the role of BUD23 and m^7G1639 is not essential but more specialised to cellular biology and translation. Furthermore, one of the main disease pathologies of Williams-Beuren syndrome is cardiovascular abnormalities again suggesting that m^7G1639 is important for the translation of specific mRNAs that are more required by cardiac cells.

During lytic KSHV replication, methylation of the 18S rRNA base G1639 increases from a basal level of about 80% during latency to above 90%. Latent levels of about 80% G1639 methylation agree with the literature where studies have reported methylation at this site to be between 70% and 100%[205,371]. While modest, the increase of G1639 methylation during KSHV lytic replication shows the importance of this rRNA modification to its lytic

replication. This suggests that the significance of BUD23 enhanced association with pre-40S ribosomal complexes during lytic replication is related to its enzymatic function.

6.3 BUD23 is essential for KSHV late lytic gene expression

Results in chapter four demonstrate that the knockdown of BUD23 greatly impacts the lytic replication cycle of KSHV. However, early lytic gene expression is not affected although this would be expected as KSHV would need time to build up a specialised ribosome population that specifically aids the translation of viral lytic genes.

Notably, the translation of late lytic genes was greatly reduced during BUD23 knockdown, suggesting that BUD23-mediated methylation of G1639 of the 18S rRNA is required for the efficient translation of these mRNAs. However, the greatest impact of BUD23 knockdown on KSHV lytic replication was at the stage of infectious virion production with a loss of up to 90%. This again would be expected as virion production is the endpoint of the lytic replication cycle and therefore the lack of translation of late lytic structural genes would be exaggerated at this stage.

Due to the impact on translation of late genes by the knockdown of BUD23, knock-on effects were seen to the lytic cascade. A slight but significant reduction in transcription of both early and late lytic genes was observed, in addition to a 60% reduction of KSHV genome copies at 72 hours post lytic reactivation. As specific parts of the KSHV lytic cascade become affected the overall progression from gene transcription to DNA replication are also impacted[386,387]. Therefore, due to BUD23-mediated methylation of the 18S rRNA base G1639 it was hypothesised that the driving force behind the collapse of the KSHV lytic cascade is the reduction in translation of late lytic mRNAs.

Interestingly, further research in the Whitehouse group by Ms. Elena Harrington with EMG1 depleted cell lines has also demonstrated a reduction in the translation of KSHV late lytic genes and further reduction of infectious virion production. Together with BUD23 this suggests a concerted effort by the virus to regulate 40S ribosome subunit biogenesis to create specialised ribosomes that efficiently translate late lytic genes.

6.4 BUD23 regulates KSHV lytic uORF expression

Ribosome profiling data identified the increased expression of KSHV lytic gene uORFs during BUD23 knockdown. This suggests a potential mechanism for how methylation of G1639

impacts the translation of KSHV mRNAs as typically the expression of uORFs leads to a reduction in translation of the CDS of an mRNA. Furthermore, ribosome occupancies of the ORF28, ORF65 and ORF75 CDS were visibly reduced in ribosome footprint bed graphs from BUD23 depleted cells.

Of the 25 KSHV lytic genes with known timepoints of expression and function, 17 genes expressed late or involved in late lytic gene expression contain uORFs (Table 6.1). Many of the late genes that contain uORFs encode structural proteins which would further explain why such a drastic drop in infectious virion production occurs in BUD23 knockdown cells (Table 6.1). Most interestingly though two key viral proteins, ORF30 and ORF34, of the late gene transcription preinitiation complex contain uORFs (Table 6.1). This could explain why the lytic cascade collapses after the expression of the early lytic genes as this complex is fundamental to the expression of late lytic genes[170].

Gene	Translation	Function
ORFK15	Internal	Glycoprotein
ORF10	uORF	Regulator of interferon function
ORF21	uORF	Thymidine Kinase
ORF28	uORF	BDLF3 EBV homolog
ORF30	uORF	Late gene regulation
ORF32	Internal	Capsid associated tegument complex
ORF34	uORF	Late gene expression
ORF38	uORF	Viral maturation and egress/Tegument
ORF45	uORF	Tegument protein and RSK activator
ORF47	uORF	Envelope glycoprotein L
ORF54	Alt. Start	dUTPase/Immunmodulator
ORF55	uORF	Tegument protein
ORF62	Alt. Start	Capsid protein Tri1
ORF65	uORF	Smallest capsid protein
ORF68	Internal	Viral DNA replication
ORF69	uORF	BRLF2 Nuclear egress
ORF75	uORF	FGARAT enzyme

Table 6.1 KSHV late Lytic genes that contain uORFs. Translation events: alternative start site (Alt. Start); internal CDS ORF (Internal).

Of the few early genes that contain uORFs none of them are known to be integral to expression or regulation of the early lytic cascade. This further suggests why BUD23 knockdown does not impact the early lytic replication cycle of KSHV. Furthermore, the presence of uORFs in some early lytic genes could be to regulate their expression at later timepoints in KSHV lytic replication cycle.

The most important future experiment is to firstly investigate and validate the regulation of BUD23 on KSHV late lytic gene uORFs. To achieve this a dual-luciferase reporter assay system could be used in 293T cell lines with stable knockdown of BUD23 or a control cell line (Figure 6.1)[388,389]. Briefly, the 5' UTR of KSHV late genes which contain uORFs will be cloned upstream of a luciferase reporter CDS or as a reference control the uORF could be mutated. If the hypothesis is correct, then a reduction in luciferase activity would be observed for BUD23 knockdown cells compared to control cells with the uORF containing luciferase reporter construct.

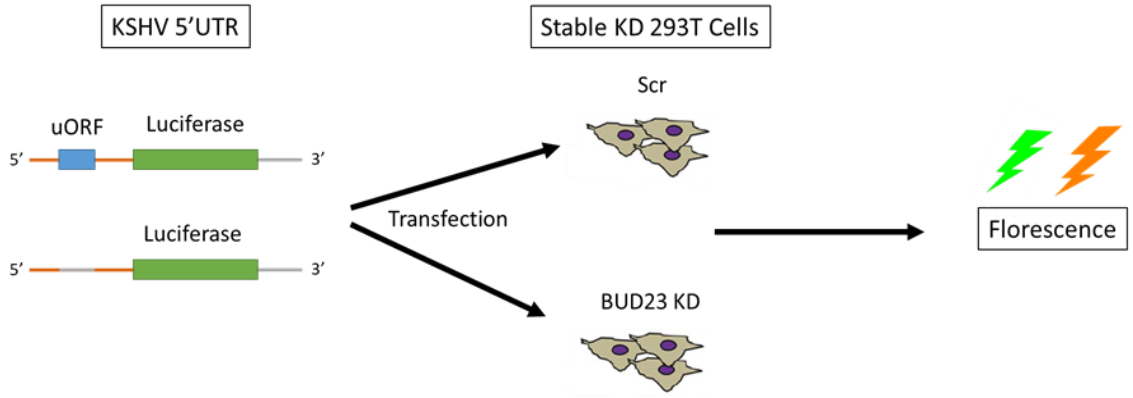

Figure 6.1 KSHV late lytic gene uORF dual luciferase assay. Dual luciferase constructs with 5'UTRs of KSHV uORF containing late lytic genes or with mutated uORFs will be cloned up streams of a luciferase reported. 293T cells stalely depleted of BUD23 or control cells will be transfected with the constructs. Luciferase activity will be measured to analyse the effects of BUD23 depletion on KSHV late lytic gene uORFs.

It has been reported that up to 50% of cellular genes contain uORFs[389]. As described in chapter one specific uORFs and groups of uORFs are regulated by a variety of different mechanism. As such the context of each uORF or group of uORFs varies greatly enabling certain genes or gene groups containing uORFs to be specifically regulated[390,391]. Factors effecting the context of uORFs include: the distance of a uORF from the start site to the mRNA cap, the start codon usage of the uORF, the Kozak sequence consensus of the start codon, the number of uORFs present in the 5' UTR and the distance of the uORF stop codon to the CDS[257]. It is therefore hypothesised that uORFs of KSHV late lytic genes have a specific context which is highly sensitive to BUD23-mediated methylation of the ribosomal rRNA base G1639. To start to address this hypothesis, bioinformatic analysis investigating the context of late lytic gene uORF's may be able to identify a consensus around the context of these uORFs in late lytic genes.

The methylation of G1639 by BUD23 has been hypothesised to be involved in the translocation and/or scanning of the 40S subunit. If methylation at this site positively regulates the scanning of 40S subunits along the 5' UTR of mRNAs then BUD23 knockdown could impact the speed at which this process occurs. Slower scanning of 40S pre-initiation complexes along mRNA 5' UTRs has been reported to increase the translation of uORFs[392,393]. This is due to the complex having more time to recognise less favourable translation initiation sites, which uORFs typically contain, such as near-cognate start codons and suboptimal Kozak sequences. This could be a potential mechanism by which the methylation of G1639 regulates uORF and subsequent downstream CDS expression.

To investigate the hypothesis that m^7G1639 modification of the 18S rRNA regulates the scanning rate of pre-initiation complexes. Ribosomes from BUD23 knockout cells and control cells would be isolated and used in an *in vitro* translation assay described by Vassilenko et al. which uses a real-time luciferase activity monitoring system with varying lengths of mRNA 5' UTRs to determine scanning rates of ribosomes[394].

Interestingly, EMG1-mediated N^1-methylation of the 18S rRNA base U1240 has been hypothesised to be involved in decoding of the mRNA[349]. A reason for the lytic KSHV induced increase of EMG1's association with pre-ribosomal complexes could be that absence of EMG1 and its rRNA modification may promote the decoding of less favourable translation initiation sites such as uORFs. This role could link the increased association of BUD23 and EMG1 with pre-40S ribosomal complexes to the regulation of uORF and subsequent downstream CDS expression. This link would again demonstrate a concerted effort by KSHV to regulate ribosome biogenesis to create specialised ribosomes for the enhanced translation of late lytic proteins.

The role of BUD23 and its m^7G1639 modification of the 18S rRNA in the translation of cellular mRNAs has been proposed by Baxter et al. to regulate the translation of mRNAs with low 5' UTR GC content[327]. However, results demonstrating the regulation of KSHV uORF translation by BUD23 suggest that the m^7G1639 modification of the 18S rRNA could also be a mechanism by which the cell can control uORF expression of its own cellular mRNAs.

6.5 Overall conclusions and future directions

KSHV tailors the biogenesis of 40S ribosomal subunits during lytic reactivation through the increased association of RBF complexes BUD23-TRMT112 and NOC4L-NOP14-EMG1. The previously uncharacterised KSHV protein ORF11 most likely acts as the viral agent responsible for these changes. BUD23 is essential for the effective and efficient lytic life cycle of KSHV through the correct expression of uORFs in late genes or genes involved in late gene expression. This thesis provides evidence that KSHV manipulates ribosome biogenesis during lytic reactivation to create ribosomes that are specialised for the effective translation of its late lytic mRNAs (Figure 6.2).

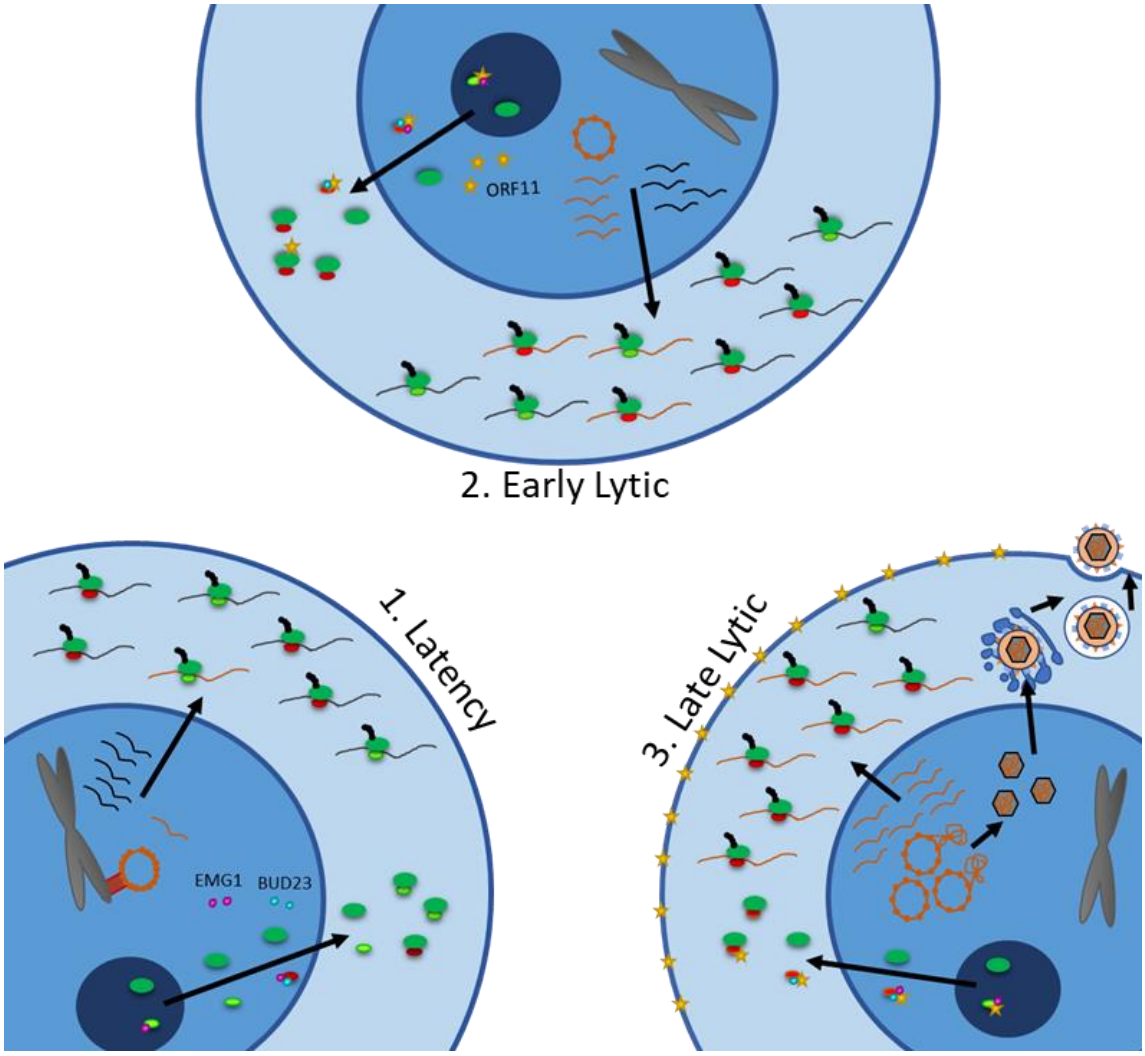

Figure 6.2 KSHV co-opts ribosome biogenesis during lytic replication to produce KSHV specific specialised ribosomes. ORF11 increases the association of BUD23 and EMG1 with pre-40S ribosome complexes during early KSHV lytic replication. Ribosomes with the 18S rRNA modifications m7G1639 and m1ΨU1240 then efficiently translate KSHV late lytic genes or genes involved in late gene expression. ORF11 associates with the cell membrane during late lytic KSHV replication, potentially adding viral egress.

An exciting future direction for this research to take would be to investigate whether this mechanism of virus-induced specialised ribosomes is conserved amongst other *Gammaherpesviruses* or even across the *Herpesviridae*. The ORF11 protein is conserved across almost all gamma-herpesviruses[395]. It would therefore be ideal to firstly investigate the human gamma-herpesvirus EBV, which is most closely resalted to KSHV, to identify if BUD23 has an increased association with pre-40S ribosomal complexes during EBV lytic replication. Further experiments could then investigate the impact of BUD23 depletion on EBV lytic replication and whether EBV ORF11 co-precipitates pre-40S ribosomal complexes.

Finally, another very exciting future direction this project could take would be to explore the possible translational impact this research could have in the clinic. The discovery that specialised ribosomes have a role in the development of some diseases such as cancers has led to the idea that they could be targets for therapeutic intervention[349,396]. Due to the number of different ways in which ribosomes can be modified the treatment options could vary greatly. However, this opens the idea that KSHV specific specialised ribosomes could also act as targets for the development of antiviral therapies. Due to the role of the viral protein ORF11 in targeting ribosome biogenesis, though binding pre-40S ribosome complexes, this would seem to have the greatest opportunity as a target for therapeutic intervention. A number of therapeutic options could be explored to disrupt the binding of ORF11 to pre-40S ribosomal complexes from small molecule inhibitors to larger protein-protein interaction inhibitors such as stabled peptides or affimers[397–399].

References

1. McGeoch, D. J., Davison, A. J., Dolan, A., Gatherer, D. & Sevilla-Reyes, E. E. Molecular Evolution of the Herpesvirales. *Orig. Evol. Viruses* 447–475 (2008). doi:10.1016/B978-0-12-374153-0.00020-5

2. Walker, P. J. *et al.* Changes to virus taxonomy and the International Code of Virus Classification and Nomenclature ratified by the International Committee on Taxonomy of Viruses (2019). *Arch. Virol.* **164**, 2417–2429 (2019).

3. Davison, A. J. *Comparative analysis of the genomes*. *Human Herpesviruses: Biology, Therapy, and Immunoprophylaxis* (2007). doi:10.1017/CBO9780511545313.003

4. Andrade-Martínez, J. S., Moreno-Gallego, J. L. & Reyes, A. Defining a Core Genome for the Herpesvirales and Exploring their Evolutionary Relationship with the Caudovirales. *Sci. Rep.* **9**, 1–13 (2019).

5. Simmonds, P. *et al.* Consensus statement: Virus taxonomy in the age of metagenomics. *Nat. Rev. Microbiol.* **15**, 161–168 (2017).

6. Matthews, R. E. F. Classification and Nomenclature of Viruses. *Intervirology* **12**, 129–136 (1979).

7. Louten, J. Chapter 13 – Herpesviruses. in *Essential Human Virology* (ed. Louten, J. B. T.-E. H. V.) 235–256 (Academic Press, 2016). doi:10.1016/B978-0-12-800947-5.00013-2

8. Smith, T. T. & Whitley, R. J. Section 8 Clinical Microbiology: Viruses. in *Infectious Diseases* (eds. Cohen, J., Powderly, W. G. & Opal, S. M. B. T.-I. D. (Fourth E.) 1426-1438.e1 (Elsevier, 2017). doi:10.1016/B978-0-7020-6285-8.00166-0

9. Wu, S.-E. & Miller, W. E. The human cytomegalovirus lytic cycle is induced by 1,25-dihydroxyvitamin D3 in peripheral blood monocytes and in the THP-1 monocytic cell line. *Virology* **483**, 83–95 (2015).

10. Grefte, A., Giessen, M. van der, Son, W. van & The, T. H. Circulating Cytomegalovirus (CMV)-Infected Endothelial Cells in Patients with an Active CMV Infection. *J. Infect. Dis.* **167**, 270–277 (1993).

11. Hong, Y. K. *et al.* Lymphatic reprogramming of blood vascular endothelium by Kaposi sarcoma-associated herpesvirus. *Nat. Genet.* **36**, 683–685 (2004).

12. Chen, L. & Lagunoff, M. Establishment and Maintenance of Kaposi's Sarcoma-Associated Herpesvirus Latency in B Cells. *J. Virol.* **79**, 14383–14391 (2005).

13. Chang, Y. *et al.* Identification of herpesvirus-like DNA sequences in AIDS-associated Kaposi's sarcoma. *Science (80-.).* **266**, 1865–1869 (1994).

14. Boshoff, C. *et al.* Kaposi's-sarcoma-associated herpesvirus in HIV-negative Kaposi's sarcoma. *Lancet (London, England)* **345**, 1043–1044 (1995).

15. Schalling, M., Ekman, M., Kaaya, E. E., Linde, A. & Biberfeld, P. A role for a new herpes virus (KSHV) in different forms of Kaposi's sarcoma. *Nat. Med.* **1**, 707–708 (1995).

16. Cesarman, E., Chang, Y., Moore, P. S., Said, J. W. & Knowles, D. M. Kaposi's Sarcoma–Associated Herpesvirus-Like DNA Sequences in AIDS-Related Body-Cavity–Based Lymphomas. *N. Engl. J. Med.* **332**, 1186–1191 (1995).

17. Soulier, J. *et al.* Kaposi's sarcoma-associated herpesvirus-like DNA sequences in multicentric Castleman's disease. *Blood* **86**, 1276–1280 (1995).

18. Rohner, E. *et al.* HHV-8 seroprevalence: A global view. *Syst. Rev.* **3**, 1–7 (2014).

19. Guttman-Yassky, E. *et al.* Infection with Kaposi's sarcoma-associated herpesvirus among families of patients with Classic Kaposi's sarcoma. *Arch. Dermatol.* **141**, 1429–1434 (2005).

20. Melbye, M. *et al.* Risk factors for Kaposi's-sarcoma-associated herpesvirus (KSHV/HHV-8) seropositivity in a cohort of homosexual men, 1981-1996. *Int. J. cancer* **77**, 543–8 (1998).

21. Cannon, M. J. *et al.* Blood-borne and sexual transmission of human herpesvirus 8 in women with or at risk for human immunodeficiency virus infection. *N. Engl. J. Med.* **344**, 637–43 (2001).

22. Boldogh, I. *et al.* Kaposi's sarcoma herpesvirus-like DNA sequences in the saliva of individuals infected with human immunodeficiency virus. *Clin. Infect. Dis.* **23**, 406–7 (1996).

23. Hladik, W. *et al.* Transmission of human herpesvirus 8 by blood transfusion. *N. Engl. J. Med.* **355**, 1331–8 (2006).

24. Minhas, V. & Wood, C. Epidemiology and transmission of kaposi's sarcoma-associated herpesvirus. *Viruses* **6**, 4178–4194 (2014).

25. Manners, O., Murphy, J. C., Coleman, A., Hughes, D. J. & Whitehouse, A. Contribution of the KSHV and EBV lytic cycles to tumourigenesis. *Curr. Opin. Virol.* **32**, 60–70 (2018).

26. An, J., Sun, Y., Sun, R. & Rettig, M. B. Kaposi's sarcoma-associated herpesvirus encoded vFLIP induces cellular IL-6 expression: The role of the NF-κB and JNK/AP1 pathways. *Oncogene* **22**, 3371–3385 (2003).

27. Sin, S.-H., Kim, Y. B. & Dittmer, D. P. Latency Locus Complements MicroRNA 155 Deficiency In Vivo. *J. Virol.* **87**, 11908–11911 (2013).

28. Friborg, J., Kong, W. P., Hottlger, M. O. & Nabel, G. J. p53 Inhibition by the LANA protein of KSHV protects against cell death. *Nature* **402**, 889–894 (1999).

29. Monini, P. *et al.* Reactivation and persistence of human herpesvirus-8 infection in B cells and monocytes by Th-1 cytokines increased in Kaposi's sarcoma. *Blood* **93**, 4044–4058 (1999).

30. Staskus, K. A. *et al.* Kaposi's sarcoma-associated herpesvirus gene expression in endothelial (spindle) tumor cells. *J. Virol.* **71**, 715–719 (1997).

31. Jenner, R. G., Albà, M. M., Boshoff, C. & Kellam, P. Kaposi's Sarcoma-Associated Herpesvirus Latent and Lytic Gene Expression as Revealed by DNA Arrays. *J. Virol.* **75**, 891–902 (2001).

32. Kaposi, M. Idiopathisches multiples Pigmentsarkom der Haut. *Arch. Dermatol. Syph.* **4**, 265–273 (1872).

33. Oettle, A. G. Geographical and racial differences in the frequency of Kaposi's sarcoma as evidence of environmental or genetic causes. *Acta Unio Int. Contra Cancrum* **18**, 330–363 (1962).

34. Penn, I. Development of cancer in transplantation patients. *Adv. Surg.* **12**, 155–191

(1978).

35. Beral, V., Peterman, T. A., Berkelman, R. L. & Jaffe, H. W. Kaposi's sarcoma among persons with AIDS: a sexually transmitted infection? *Lancet* **335**, 123–128 (1990).

36. Radu, O. & Pantanowitz, L. Kaposi Sarcoma. *Arch. Pathol. Lab. Med.* **137**, 289–294 (2013).

37. Uldrick, T. S. & Whitby, D. Update on KSHV epidemiology, Kaposi Sarcoma pathogenesis, and treatment of Kaposi Sarcoma. *Cancer Lett.* **305**, 150–162 (2011).

38. Szajerka, T. & Jablecki, J. Kaposi's sarcoma revisited. *AIDS Rev.* **9**, 230–6 (2004).

39. Coen, N., Duraffour, S., Snoeck, R. & Andrei, G. KSHV targeted therapy: An update on inhibitors of viral lytic replication. *Viruses* **6**, 4731–4759 (2014).

40. Narkhede, M., Arora, S. & Ujjani, C. Primary effusion lymphoma: Current perspectives. *Onco. Targets. Ther.* **11**, 3747–3754 (2018).

41. Lurain, K. *et al.* Viral, immunologic, and clinical features of primary effusion lymphoma. *Blood* **133**, 1753–1761 (2019).

42. Guillet, S. *et al.* Classic and extracavitary primary effusion lymphoma in 51 HIV-infected patients from a single institution. *Am. J. Hematol.* **91**, 233–237 (2016).

43. Van Rhee, F. *et al.* International, evidence-based consensus treatment guidelines for idiopathic multicentric castleman disease. *Blood* **132**, 2115–2124 (2018).

44. Dossier, A. *et al.* Human herpesvirus 8-related Castleman disease in the absence of HIV infection. *Clin. Infect. Dis.* **56**, 833–842 (2013).

45. Leroy, S. *et al.* Multicentric Castleman disease in an HHV-8-infected child born to consanguineous parents. *Pediatrics* **129**, 199–203 (2012).

46. Uldrick, T. S., Polizzotto, M. N. & Yarchoan, R. Recent advances in Kaposi sarcoma herpesvirus-associated multicentric Castleman disease. *Curr. Opin. Oncol.* **24**, 495–505 (2012).

47. Song, S. N. J. *et al.* Down-regulation of hepcidin resulting from long-term treatment

with an anti-IL-6 receptor antibody (tocilizumab) improves anemia of inflammation in multicentric Castleman disease. *Blood* **116**, 3627–3634 (2010).

48. Williams, S. C. P. First IL-6–blocking drug nears approval for rare blood disorder. *Nat. Med.* **19**, 1193 (2013).

49. Uldrick, T. S. *et al.* Rituximab plus liposomal doxorubicin in HIV-infected patients with KSHV-associated multicentric Castleman disease. *Blood* **124**, 3544–3552 (2014).

50. Tagawa, T. *et al.* Discovery of Kaposi's sarcoma herpesvirus-encoded circular RNAs and a human antiviral circular RNA. *Proc. Natl. Acad. Sci. U. S. A.* **115**, 12805–12810 (2018).

51. Toptan, T. *et al.* Circular DNA tumor viruses make circular RNAs. *Proc. Natl. Acad. Sci. U. S. A.* **115**, E8737–E8745 (2018).

52. Arias, C. *et al.* KSHV 2.0: a comprehensive annotation of the Kaposi's sarcoma-associated herpesvirus genome using next-generation sequencing reveals novel genomic and functional features. *PLoS Pathog.* **10**, e1003847 (2014).

53. Cai, X. *et al.* Kaposi's sarcoma-associated herpesvirus expresses an array of viral microRNAs in latently infected cells. *Proc. Natl. Acad. Sci. U. S. A.* **102**, 5570–5575 (2005).

54. Marshall, V. *et al.* Kaposi sarcoma (KS)-associated herpesvirus microRNA sequence analysis and KS risk in a European AIDS-KS case control study. *J. Infect. Dis.* **202**, 1126–35 (2010).

55. Juillard, F., Tan, M., Li, S. & Kaye, K. M. Kaposi's sarcoma herpesvirus genome persistence. *Front. Microbiol.* **7**, 1–15 (2016).

56. Mesri, E. A., Cesarman, E. & Boshoff, C. Kaposi's sarcoma herpesvirus/ Human herpesvirus-8 (KSHV/HHV8), and the oncogenesis of Kaposi's sarcoma. *Nat. Rev. Cancer* **10**, 707–719 (2010).

57. Gong, D. *et al.* Virus-Like Vesicles of Kaposi's Sarcoma-Associated Herpesvirus Activate Lytic Replication by Triggering Differentiation Signaling. *J. Virol.* **91**, 1–18 (2017).

58. Dai, X. *et al.* Structure and mutagenesis reveal essential capsid protein interactions for KSHV replication. *Nature* **553**, 521–525 (2018).

59. Gong, D. *et al.* DNA-Packing Portal and Capsid-Associated Tegument Complexes in the Tumor Herpesvirus KSHV. *Cell* **178**, 1329-1343.e12 (2019).

60. Sathish, N., Wang, X. & Yuan, Y. Tegument proteins of kaposi's sarcoma-associated herpesvirus and related gamma-herpesviruses. *Front. Microbiol.* **3**, 1–13 (2012).

61. Sathish, N., Zhu, F. X. & Yuan, Y. Kaposi's sarcoma-associated herpesvirus ORF45 Interacts with kinesin-2 transporting viral capsid-tegument complexes along microtubules. *PLoS Pathog.* **5**, (2009).

62. Liang, Q. *et al.* ORF45 of Kaposi's Sarcoma-Associated Herpesvirus Inhibits Phosphorylation of Interferon Regulatory Factor 7 by IKKε and TBK1 as an Alternative Substrate. *J. Virol.* **86**, 10162–10172 (2012).

63. Bechtel, J. T., Winant, R. C. & Ganem, D. Host and Viral Proteins in the Virion of Kaposi's Sarcoma-Associated Herpesvirus. *J. Virol.* **79**, 4952–4964 (2005).

64. Chen, W., Sin, S. H., Wen, K. W., Damania, B. & Dittmer, D. P. Hsp90 Inhibitors Are Efficacious against Kaposi Sarcoma by Enhancing the Degradation of the Essential Viral Gene LANA, of the Viral Co-Receptor EphA2 as well as Other Client Proteins. *PLoS Pathog.* **8**, (2012).

65. Baquero-Pérez, B. & Whitehouse, A. Hsp70 Isoforms Are Essential for the Formation of Kaposi's Sarcoma-Associated Herpesvirus Replication and Transcription Compartments. *PLOS Pathog.* **11**, e1005274 (2015).

66. Nanbo, A., Noda, T. & Ohba, Y. Epstein-barr virus acquires its final envelope on intracellular compartments with Golgi markers. *Front. Microbiol.* **9**, 1–13 (2018).

67. Koyano, S., Mar, E. C., Stamey, F. R. & Inoue, N. Glycoproteins M and N of human herpesvirus 8 form a complex and inhibit cell fusion. *J. Gen. Virol.* **84**, 1485–1491 (2003).

68. Baghian, A. *et al.* Glycoprotein B of human herpesvirus 8 is a component of the virion in a cleaved form composed of amino- and carboxyl-terminal fragments. *Virology*

269, 18–25 (2000).

69. Naranatt, P. P., Akula, S. M. & Chandran, B. Characterization of γ2-human herpesvirus-8 glycoproteins gH and gL. *Arch. Virol.* **147**, 1349–1370 (2002).

70. Spiller, O. B. *et al.* Dissecting the Regions of Virion-Associated Kaposi's Sarcoma-Associated Herpesvirus Complement Control Protein Required for Complement Regulation and Cell Binding. *J. Virol.* **80**, 4068–4078 (2006).

71. Akula, S. M., Wang, F. Z., Vieira, J. & Chandran, B. Human herpesvirus 8 interaction with target cells involves heparan sulfate. *Virology* **282**, 245–255 (2001).

72. Dollery, S. J. Towards understanding KSHV fusion and entry. *Viruses* **11**, 1–17 (2019).

73. Mercader, M. *et al.* Induction of HHV-8 lytic cycle replication by inflammatory cytokines produced by HIV-1-infected T cells. *Am. J. Pathol.* **156**, 1961–1971 (2000).

74. Merat, R. *et al.* HIV-1 infection of primary effusion lymphoma cell line triggers Kaposi's sarcoma-associated herpesvirus (KSHV) reactivation. *Int. J. Cancer* **97**, 791–795 (2002).

75. Cohen, A., Brodie, C. & Sarid, R. An essential role of ERK signalling in TPA-induced reactivation of Kaposi's sarcoma-associated herpesvirus. *J. Gen. Virol.* **87**, 795–802 (2006).

76. Davis, D. A. *et al.* Hypoxia induces lytic replication of Kaposi sarcoma-associated herpesvirus. *Blood* **97**, 3244–3250 (2001).

77. Veettil, M. V. *et al.* Kaposi's Sarcoma-Associated Herpesvirus Forms a Multimolecular Complex of Integrins (αVβ5, αVβ3, and α3β1) and CD98-xCT during Infection of Human Dermal Microvascular Endothelial Cells, and CD98-xCT Is Essential for the Postentry Stage of Infection. *J. Virol.* **82**, 12126–12144 (2008).

78. Rappocciolo, G. *et al.* DC-SIGN Is a Receptor for Human Herpesvirus 8 on Dendritic Cells and Macrophages. *J. Immunol.* **176**, 1741–1749 (2006).

79. Rappocciolo, G. *et al.* Human Herpesvirus 8 Infects and Replicates in Primary Cultures of Activated B Lymphocytes through DC-SIGN. *J. Virol.* **82**, 4793–4806

(2008).

80. Kerur, N. *et al.* Characterization of entry and infection of monocytic THP-1 cells by Kaposi's sarcoma associated herpesvirus (KSHV): Role of heparan sulfate, DC-SIGN, integrins and signaling. *Virology* **406**, 103–116 (2010).

81. Kumar, B. & Chandran, B. KSHV entry and trafficking in target cells—Hijacking of cell signal pathways, actin and membrane dynamics. *Viruses* **8**, (2016).

82. Akula, S. M. *et al.* Kaposi's Sarcoma-Associated Herpesvirus (Human Herpesvirus 8) Infection of Human Fibroblast Cells Occurs through Endocytosis. *J. Virol.* **77**, 7978–7990 (2003).

83. Inoue, N., Winter, J., Lal, R. B., Offermann, M. K. & Koyano, S. Characterization of Entry Mechanisms of Human Herpesvirus 8 by Using an Rta-Dependent Reporter Cell Line. *J. Virol.* **77**, 8147–8152 (2003).

84. Stampfer, S. D., Lou, H., Cohen, G. H., Eisenberg, R. J. & Heldwein, E. E. Structural Basis of Local, pH-Dependent Conformational Changes in Glycoprotein B from Herpes Simplex Virus Type 1. *J. Virol.* **84**, 12924–12933 (2010).

85. Sathiyamoorthy, K. *et al.* Assembly and Architecture of the EBV B Cell Entry Triggering Complex. *PLoS Pathog.* **10**, (2014).

86. Naranatt, P. P., Krishnan, H. H., Smith, M. S. & Chandran, B. Kaposi's Sarcoma-Associated Herpesvirus Modulates Microtubule Dynamics via RhoA-GTP-Diaphanous 2 Signaling and Utilizes the Dynein Motors To Deliver Its DNA to the Nucleus. *J. Virol.* **79**, 1191–1206 (2005).

87. Lieberman, P. M. Keeping it quiet: chromatin control of gammaherpesvirus latency. *Nat. Rev. Microbiol.* **11**, 863–75 (2013).

88. Kintner, C. R. & Sugden, B. The structure of the termini of the DNA of Epstein-Barr virus. *Cell* **17**, 661–671 (1979).

89. Zimmermann, J. & Hammerschmidt, W. Structure and role of the terminal repeats of Epstein-Barr virus in processing and packaging of virion DNA. *J. Virol.* **69**, 3147–3155 (1995).

90. Ballestas, M. E., Chatis, P. A. & Kaye, K. M. Efficient persistence of extrachromosomal KSHV DNA mediated by latency- associated nuclear antigen. *Science (80-.).* **284**, 641–644 (1999).

91. Tavalai, N. & Stamminger, T. Interplay between herpesvirus infection and host defense by PML nuclear bodies. *Viruses* **1**, 1240–1264 (2009).

92. Uppal, T., Banerjee, S., Sun, Z., Verma, S. C. & Robertson, E. S. KSHV LANA--the master regulator of KSHV latency. *Viruses* **6**, 4961–4998 (2014).

93. Si, H., Verma, S. C., Lampson, M. A., Cai, Q. & Robertson, E. S. Kaposi's Sarcoma-Associated Herpesvirus-Encoded LANA Can Interact with the Nuclear Mitotic Apparatus Protein To Regulate Genome Maintenance and Segregation. *J. Virol.* **82**, 6734–6746 (2008).

94. Hu, J. & Renne, R. Characterization of the Minimal Replicator of Kaposi's Sarcoma-Associated Herpesvirus Latent Origin. *J. Virol.* **79**, 2637–2642 (2005).

95. Lu, F. *et al.* Identification of Host-Chromosome Binding Sites and Candidate Gene Targets for Kaposi's Sarcoma-Associated Herpesvirus LANA. *J. Virol.* **86**, 5752–5762 (2012).

96. Sun, R., Liang, D., Gao, Y. & Lan, K. Kaposi's Sarcoma-Associated Herpesvirus-Encoded LANA Interacts with Host KAP1 To Facilitate Establishment of Viral Latency. *J. Virol.* **88**, 7331–7344 (2014).

97. Lan, K., Kuppers, D. A., Verma, S. C. & Robertson, E. S. Kaposi's Sarcoma-Associated Herpesvirus-Encoded Latency-Associated Nuclear Antigen Inhibits Lytic Replication by Targeting Rta: a Potential Mechanism for Virus-Mediated Control of Latency. *J. Virol.* **78**, 6585–6594 (2004).

98. Muromoto, R. *et al.* Physical and functional interactions between STAT3 and Kaposi's sarcoma-associated herpesvirus-encoded LANA. *FEBS Lett.* **580**, 93–98 (2006).

99. Roupelieva, M. *et al.* Kaposi's sarcoma-associated herpesvirus Lana-1 is a major activator of the serum response element and mitogen-activated protein kinase pathways via interactions with the Mediator complex. *J. Gen. Virol.* **91**, 1138–

1149 (2010).

100. Fejér, G. *et al.* The latency-associated nuclear antigen of Kaposi's sarcoma-associated herpesvirus interacts preferentially with the terminal repeats of the genome in vivo and this complex is sufficient for episomal DNA replication. *J. Gen. Virol.* **84**, 1451–1462 (2003).

101. Cotter, M. a & Robertson, E. S. The latency-associated nuclear antigen tethers the Kaposi's sarcoma-associated herpesvirus genome to host chromosomes in body cavity-based lymphoma cells. *Virology* **264**, 254–64 (1999).

102. Barbera, A. J. *et al.* The nucleosomal surface as a docking station for Kaposi's sarcoma herpesvirus LANA. *Science (80-.).* **311**, 856–861 (2006).

103. Tetsuka, T. *et al.* Visualization of a functional KSHV episome-maintenance protein LANA in living cells. *Virus Genes* **29**, 175–182 (2004).

104. Ohsaki, E. & Ueda, K. Kaposi's sarcoma-associated herpesvirus genome replication, partitioning, and maintenance in latency. *Front. Microbiol.* **3**, 1–12 (2012).

105. Verma, S. C. *et al.* Single molecule analysis of replicated DNA reveals the usage of multiple KSHV genome regions for latent replication. *PLoS Pathog.* **7**, (2011).

106. Ponnusamy, R. *et al.* KSHV but not MHV-68 LANA induces a strong bend upon binding to terminal repeat viral DNA. *Nucleic Acids Res.* **43**, 10039–10054 (2015).

107. Stedman, W., Deng, Z., Lu, F. & Lieberman, P. M. ORC, MCM, and Histone Hyperacetylation at the Kaposi's Sarcoma-Associated Herpesvirus Latent Replication Origin. *J. Virol.* **78**, 12566–12575 (2004).

108. Verma, S. C., Choudhuri, T., Kaul, R. & Robertson, E. S. Latency-Associated Nuclear Antigen (LANA) of Kaposi's Sarcoma-Associated Herpesvirus Interacts with Origin Recognition Complexes at the LANA Binding Sequence within the Terminal Repeats. *J. Virol.* **80**, 2243–2256 (2006).

109. Purushothaman, P. *et al.* Kaposi's Sarcoma-Associated Herpesvirus-Encoded LANA Recruits Topoisomerase IIβ for Latent DNA Replication of the Terminal

Repeats. *J. Virol.* **86**, 9983–9994 (2012).

110. Sun, Q. *et al.* Kaposi's sarcoma-associated herpesvirus LANA recruits the DNA polymerase clamp loader to mediate efficient replication and virus persistence. *Proc. Natl. Acad. Sci. U. S. A.* **111**, 11816–11821 (2014).

111. Lu, F., Day, L., Gao, S.-J. & Lieberman, P. M. Acetylation of the Latency-Associated Nuclear Antigen Regulates Repression of Kaposi's Sarcoma-Associated Herpesvirus Lytic Transcription. *J. Virol.* **80**, 5273–5282 (2006).

112. Lu, J., Verma, S. C., Cai, Q. & Robertson, E. S. The Single RBP-J Site within the LANA Promoter Is Crucial for Establishing Kaposi's Sarcoma-Associated Herpesvirus Latency during Primary Infection. *J. Virol.* **85**, 6148–6161 (2011).

113. Chang, P. C. & Kung, H. J. Sumo and kshv replication. *Cancers (Basel).* **6**, 1905–1924 (2014).

114. Wang, X. *et al.* Latency-associated nuclear antigen of kaposi sarcoma-associated herpesvirus promotes angiogenesis through targeting notch signaling effector hey. *Cancer Res.* **74**, 2026–2037 (2014).

115. Cai, Q. *et al.* Kaposi's Sarcoma-Associated Herpesvirus Latent Protein LANA Interacts with HIF-1α To Upregulate RTA Expression during Hypoxia: Latency Control under Low Oxygen Conditions. *J. Virol.* **80**, 7965–7975 (2006).

116. Kusano, S. & Eizuru, Y. Human I-mfa domain proteins specifically interact with KSHV LANA and affect its regulation of Wnt signaling-dependent transcription. *Biochem. Biophys. Res. Commun.* **396**, 608–613 (2010).

117. Chung, Y.-H., Means, R. E., Choi, J.-K., Lee, B.-S. & Jung, J. U. Kaposi's Sarcoma-Associated Herpesvirus OX2 Glycoprotein Activates Myeloid-Lineage Cells To Induce Inflammatory Cytokine Production. *J. Virol.* **76**, 4688–4698 (2002).

118. Osborne, J., Moore, P. S. & Chang, Y. KSHV-encoded viral IL-6 activates multiple human IL-6 signaling pathways. *Hum. Immunol.* **60**, 921–927 (1999).

119. Montaner, S., Sodhi, A., Pece, S., Mesri, E. A. & Gutkind, J. S. The Kaposi's sarcoma-associated herpesvirus G protein-coupled receptor promotes endothelial cell

survival through the activation of Akt/protein kinase B. *Cancer Res.* **61**, 2641–2648 (2001).

120. Lagunoff, M., Majeti, R., Weiss, A. & Ganem, D. Deregulated signal transduction by the K1 gene product of Kaposi's sarcoma-associated herpesvirus. *Proc. Natl. Acad. Sci. U. S. A.* **96**, 5704–5709 (1999).

121. Havemeier, A. *et al.* Activation of NF- B by the Kaposi's Sarcoma-Associated Herpesvirus K15 Protein Involves Recruitment of the NF- B-Inducing Kinase, I B Kinases, and Phosphorylation of p65. *J. Virol.* **88**, 13161–13172 (2014).

122. Israël, A. The IKK complex, a central regulator of NF-kappaB activation. *Cold Spring Harb. Perspect. Biol.* **2**, 1–15 (2010).

123. Van Dross, R. *et al.* Constitutively active K-cyclin/cdk6 kinase in kaposi sarcoma-associated herpesvirus-infected cells. *J. Natl. Cancer Inst.* **97**, 656–666 (2005).

124. McCormick, C. & Ganem, D. The kaposin B protein of KSHV activates the p38/MK2 pathway and stabilizes cytokine mRNAs. *Science (80-.).* **307**, 739–741 (2005).

125. Nachmani, D., Stern-Ginossar, N., Sarid, R. & Mandelboim, O. Diverse Herpesvirus MicroRNAs Target the Stress-Induced Immune Ligand MICB to Escape Recognition by Natural Killer Cells. *Cell Host Microbe* **5**, 376–385 (2009).

126. Lu, F., Stedman, W., Yousef, M., Renne, R. & Lieberman, P. M. Epigenetic Regulation of Kaposi's Sarcoma-Associated Herpesvirus Latency by Virus-Encoded MicroRNAs That Target Rta and the Cellular Rbl2-DNMT Pathway. *J. Virol.* **84**, 2697–2706 (2010).

127. Suffert, G. *et al.* Kaposi's sarcoma herpesvirus microRNAs target caspase 3 and regulate apoptosis. *PLoS Pathog.* **7**, (2011).

128. Giffin, L. & Damania, B. KSHV: pathways to tumorigenesis and persistent infection. *Adv. Virus Res.* **88**, 111–59 (2014).

129. Ye, F. *et al.* Reactive oxygen species hydrogen peroxide mediates Kaposi's sarcoma-associated herpesvirus reactivation from latency. *PLoS Pathog.* **7**, (2011).

130. Blackbourn, D. J. ., Fujimura, S., Kutzkey, T. & Levy, J. A. Induction of human herpesvirus-8 gene expression by recombinant interferon gamma. *Aids* **14**, 98–99 (2000).

131. Zeng, Y. *et al.* Intracellular Tat of Human Immunodeficiency Virus Type 1 Activates Lytic Cycle Replication of Kaposi's Sarcoma-Associated Herpesvirus: Role of JAK/STAT Signaling. *J. Virol.* **81**, 2401–2417 (2007).

132. Chen, J., Ye, F., Xie, J., Kuhne, K. & Gao, S. J. Genome-wide identification of binding sites for Kaposi's sarcoma-associated herpesvirus lytic switch protein, RTA. *Virology* **386**, 290–302 (2009).

133. Wang, S. E. *et al.* Role of CCAAT/Enhancer-Binding Protein Alpha (C/EBPα) in Activation of the Kaposi's Sarcoma-Associated Herpesvirus (KSHV) Lytic-Cycle Replication-Associated Protein (RAP) Promoter in Cooperation with the KSHV Replication and Transcription Activator (RTA) . *J. Virol.* **77**, 600–623 (2003).

134. Wang, S. E. *et al.* Early Activation of the Kaposi's Sarcoma-Associated Herpesvirus RTA, RAP, and MTA Promoters by the Tetradecanoyl Phorbol Acetate-Induced AP1 Pathway. *J. Virol.* **78**, 4248–4267 (2004).

135. Lukac, D. M., Kirshner, J. R. & Ganem, D. Transcriptional Activation by the Product of Open Reading Frame 50 of Kaposi's Sarcoma-Associated Herpesvirus Is Required for Lytic Viral Reactivation in B Cells. *J. Virol.* **73**, 9348–9361 (1999).

136. Song, M. J., Brown, H. J., Wu, T.-T. & Sun, R. Transcription Activation of Polyadenylated Nuclear RNA by Rta in Human Herpesvirus 8/Kaposi's Sarcoma-Associated Herpesvirus. *J. Virol.* **75**, 3129–3140 (2001).

137. Liang, Y., Chang, J., Lynch, S. J., Lukac, D. M. & Ganem, D. The lytic switch protein of KSHV activates gene expression via functional interaction with RBP-Jκ (CSL), the target of the Notch signaling pathway. *Genes Dev.* **16**, 1977–1989 (2002).

138. Deng, H., Young, A. & Sun, R. Auto-activation of the rta gene of human herpesvirus-8/Kaposi's sarcoma-associated herpesvirus. *J. Gen. Virol.* **81**, 3043–3048 (2000).

139. Yu, Y., Wang, S. E. & Hayward, G. S. The KSHV immediate-early transcription factor RTA encodes ubiquitin E3 ligase activity that targets IRF7 for proteosome-mediated degradation. *Immunity* **22**, 59–70 (2005).

140. Gould, F., Harrison, S. M., Hewitt, E. W. & Whitehouse, A. Kaposi's Sarcoma-Associated Herpesvirus RTA Promotes Degradation of the Hey1 Repressor Protein through the Ubiquitin Proteasome Pathway. *J. Virol.* **83**, 6727–6738 (2009).

141. Han, Z. & Swaminathan, S. Kaposi's Sarcoma-Associated Herpesvirus Lytic Gene ORF57 Is Essential for Infectious Virion Production. *J. Virol.* **80**, 5251–5260 (2006).

142. Majerciak, V. *et al.* Kaposi's Sarcoma-Associated Herpesvirus ORF57 Functions as a Viral Splicing Factor and Promotes Expression of Intron-Containing Viral Lytic Genes in Spliceosome-Mediated RNA Splicing. *J. Virol.* **82**, 2792–2801 (2008).

143. Majerciak, V. *et al.* Kaposi's Sarcoma-Associated Herpesvirus ORF57 Interacts with Cellular RNA Export Cofactors RBM15 and OTT3 To Promote Expression of Viral ORF59. *J. Virol.* **85**, 1528–1540 (2011).

144. Massimelli, M. J. *et al.* Stability of a long noncoding viral RNA depends on a 9-nt core element at the RNA 5' end to interact with viral ORF57 and cellular PABPC1. *Int. J. Biol. Sci.* **7**, 1145–1160 (2011).

145. Sei, E. & Conrad, N. K. Delineation of a core RNA element requires for KSHV ORF57 binding and activity. *Virology* **419**, 107–116 (2011).

146. Malik, P., Blackbourn, D. J. & Clements, J. B. The evolutionarily conserved Kaposi's sarcoma-associated herpesvirus ORF57 protein interacts with REF protein and acts as an RNA export factor. *J. Biol. Chem.* **279**, 33001–33011 (2004).

147. Boyne, J. R., Colgan, K. J. & Whitehouse, A. Recruitment of the complete hTREX complex is required for Kaposi's sarcoma-associated herpesvirus intronless mRNA nuclear export and virus replication. *PLoS Pathog.* **4**, e1000194 (2008).

148. Bujnicki, J. M. & Rychlewski, L. The Herpesvirus alkaline exonuclease belongs to the restriction endonuclease PD-(D/E)XK superfamily: Insight from molecular modeling and phylogenetic analysis. *Virus Genes* **22**, 219–230 (2001).

149. Glaunsinger, B. & Ganem, D. Lytic KSHV Infection Inhibits Host Gene Expression by Accelerating Global mRNA Turnover. *Mol. Cell* **13**, 713–723 (2004).

150. Gaglia, M. M., Rycroft, C. H. & Glaunsinger, B. A. Transcriptome-Wide Cleavage Site Mapping on Cellular mRNAs Reveals Features Underlying Sequence-Specific Cleavage by the Viral Ribonuclease SOX. *PLoS Pathog.* **11**, 1–25 (2015).

151. Hiura, K. *et al.* KSHV ORf59 and pan RNA recruit histone demethylases to the viral chromatin during lytic reactivation. *Viruses* **12**, (2020).

152. Campbell, M. & Izumiya, Y. PAN RNA: Transcriptional exhaust from a viral engine. *J. Biomed. Sci.* **27**, 1–10 (2020).

153. Cheng, F. *et al.* KSHV reactivation from latency requires pim-1 and pim-3 kinases to inactivate the latency-associated nuclear antigen LANA. *PLoS Pathog.* **5**, (2009).

154. Zoeteweij, J. P. *et al.* Targeted inhibition of calcineurin signaling blocks calcium-dependent reactivation of Kaposi sarcoma-associated herpesvirus. *Blood* **97**, 2374–2380 (2001).

155. Lang, S. M., Bynoe, M. O. F., Karki, R., Tartell, M. A. & Means, R. E. Kaposi's Sarcoma-Associated Herpesvirus K3 and K5 Proteins Down Regulate Both DC-SIGN and DC-SIGNR. *PLoS One* **8**, (2013).

156. Weber, K. S. C. *et al.* Selective recruitment of Th2-type cells and evasion from a cytotoxic immune response mediated by viral macrophage inhibitory protein-II. *Eur. J. Immunol.* **31**, 2458–2466 (2001).

157. Wang, H. W., Sharp, T. V., Koumi, A., Koentges, G. & Boshoff, C. Characterization of an anti-apoptotic glycoprotein encoded by Kaposi's sarcoma-associated herpesvirus which resembles a spliced variant of human survivin. *EMBO J.* **21**, 2602–2615 (2002).

158. Spiller, O. B. *et al.* Complement Regulation by Kaposi's Sarcoma-Associated Herpesvirus ORF4 Protein. *J. Virol.* **77**, 592–599 (2003).

159. Sathish, N., Zhu, F. X., Golub, E. E., Liang, Q. & Yuan, Y. Mechanisms of autoinhibition of IRF-7 and a probable model for inactivation of IRF-7 by Kaposi's

Sarcoma-associated herpesvirus protein ORF45. *J. Biol. Chem.* **286**, 746–756 (2011).

160. Gregory, S. M. & Damania, B. Inhibition of the inflammasome response by a viral protein that interacts with NLRs. *Commun. Integr. Biol.* **4**, 416–418 (2011).

161. Inn, K.-S. *et al.* Inhibition of RIG-I-Mediated Signaling by Kaposi's Sarcoma-Associated Herpesvirus-Encoded Deubiquitinase ORF64. *J. Virol.* **85**, 10899–10904 (2011).

162. Full, F. *et al.* Kaposi's Sarcoma Associated Herpesvirus Tegument Protein ORF75 Is Essential for Viral Lytic Replication and Plays a Critical Role in the Antagonization of ND10-Instituted Intrinsic Immunity. *PLoS Pathog.* **10**, (2014).

163. AuCoin, D. P., Colletti, K. S., Xu, Y., Cei, S. A. & Pari, G. S. Kaposi's Sarcoma-Associated Herpesvirus (Human Herpesvirus 8) Contains Two Functional Lytic Origins of DNA Replication. *J. Virol.* **76**, 7890–7896 (2002).

164. Aneja, K. K. & Yuan, Y. Reactivation and lytic replication of Kaposi's sarcoma-associated herpesvirus: An update. *Front. Microbiol.* **8**, 1–23 (2017).

165. Wang, Y., Tang, Q., Maul, G. G. & Yuan, Y. Kaposi's Sarcoma-Associated Herpesvirus ori-Lyt-Dependent DNA Replication: DualRole of Replication and Transcription Activator. *J. Virol.* **80**, 12171–12186 (2006).

166. AuCoin, D. P. *et al.* Amplification of the Kaposi's sarcoma-associated herpesvirus/human herpesvirus 8 lytic origin of DNA replication is dependent upon a cis-acting AT-rich region and an ORF50 response element and the trans-acting factors ORF50 (K-Rta) and K8 (K-bZIP). *Virology* **318**, 542–555 (2004).

167. Wang, Y., Li, H., Tang, Q., Maul, G. G. & Yuan, Y. Kaposi's Sarcoma-Associated Herpesvirus ori-Lyt-Dependent DNA Replication: Involvement of Host Cellular Factors. *J. Virol.* **82**, 2867–2882 (2008).

168. González-Molleda, L., Wang, Y. & Yuan, Y. Potent antiviral activity of topoisomerase I and II inhibitors against Kaposi's sarcoma-associated herpesvirus. *Antimicrob. Agents Chemother.* **56**, 893–902 (2012).

169. Tang, S., Yamanegi, K. & Zheng, Z.-M. Requirement of a 12-Base-Pair TATT-Containing Sequence and Viral Lytic DNA Replication in Activation of the Kaposi's Sarcoma-Associated Herpesvirus K8.1 Late Promoter. *J. Virol.* **78**, 2609–2614 (2004).

170. Nishimura, M., Watanabe, T., Yagi, S., Yamanaka, T. & Fujimuro, M. Kaposi's sarcoma-associated herpesvirus ORF34 is essential for late gene expression and virus production. *Sci. Rep.* **7**, 1–12 (2017).

171. Wyrwicz, L. S. & Rychlewski, L. Identification of Herpes TATT-binding protein. *Antiviral Res.* **75**, 167–172 (2007).

172. Brulois, K. *et al.* Association of Kaposi's Sarcoma-Associated Herpesvirus ORF31 with ORF34 and ORF24 Is Critical for Late Gene Expression. *J. Virol.* **89**, 6148–6154 (2015).

173. Deng, B., O'Connor, C. M., Kedes, D. H. & Zhou, Z. H. Cryo-electron tomography of Kaposi's sarcoma-associated herpesvirus capsids reveals dynamic scaffolding structures essential to capsid assembly and maturation. *J. Struct. Biol.* **161**, 419–427 (2008).

174. Mettenleiter, T. C., Klupp, B. G. & Granzow, H. Herpesvirus assembly: An update. *Virus Res.* **143**, 222–234 (2009).

175. Aksyuk, A. A. *et al.* Subassemblies and asymmetry in assembly of herpes simplex virus procapsid. *MBio* **6**, 1–11 (2015).

176. Dünn-Kittenplon, D. (Dana), Kalt, I., Lellouche, J. P. (Moshe) & Sarid, R. The KSHV portal protein ORF43 is essential for the production of infectious viral particles. *Virology* **529**, 205–215 (2019).

177. Heming, J. D., Huffman, J. B., Jones, L. M. & Homa, F. L. Isolation and Characterization of the Herpes Simplex Virus 1 Terminase Complex. *J. Virol.* **88**, 225–236 (2014).

178. Gardner, M. R. & Glaunsinger, B. A. Kaposi's Sarcoma-Associated Herpesvirus ORF68 Is a DNA Binding Protein Required for Viral Genome Cleavage and

Packaging. *J. Virol.* **92**, 1–13 (2018).

179. Klupp, B. G. *et al.* Vesicle formation from the nuclear membrane is induced by coexpression of two conserved herpesvirus proteins. *Proc. Natl. Acad. Sci. U. S. A.* **104**, 7241–7246 (2007).

180. Rozen, R., Sathish, N., Li, Y. & Yuan, Y. Virion-Wide Protein Interactions of Kaposi's Sarcoma-Associated Herpesvirus. *J. Virol.* **82**, 4742–4750 (2008).

181. Leege, T., Granzow, H., Fuchs, W., Klupp, B. G. & Mettenleiter, T. C. Phenotypic similarities and differences between UL37-deleted pseudorabies virus and herpes simplex virus type 1. *J. Gen. Virol.* **90**, 1560–1568 (2009).

182. de Oliveira, A. P. *et al.* Live Visualization of Herpes Simplex Virus Type 1 Compartment Dynamics. *J. Virol.* **82**, 4974–4990 (2008).

183. Sugimoto, K. *et al.* Simultaneous Tracking of Capsid, Tegument, and Envelope Protein Localization in Living Cells Infected with Triply Fluorescent Herpes Simplex Virus 1. *J. Virol.* **82**, 5198–5211 (2008).

184. Klupp, B. G., Nixdorf, R. & Mettenleiter, T. C. Pseudorabies Virus Glycoprotein M Inhibits Membrane Fusion. *J. Virol.* **74**, 6760–6768 (2000).

185. Crump, C. M. *et al.* Alphaherpesvirus glycoprotein M causes the relocalization of plasma membrane proteins. *J. Gen. Virol.* **85**, 3517–3527 (2004).

186. Wang, X. *et al.* Mono-ubiquitylated ORF45 Mediates Association of KSHV Particles with Internal Lipid Rafts for Viral Assembly and Egress. *PLoS Pathog.* **11**, 1–26 (2015).

187. Khatter, H., Myasnikov, A. G., Natchiar, S. K. & Klaholz, B. P. Structure of the human 80S ribosome. *Nature* **520**, 640–645 (2015).

188. Klinge, S. & Woolford, J. L. Ribosome assembly coming into focus. *Nat. Rev. Mol. Cell Biol.* **20**, 116–131 (2019).

189. Natchiar, S. K., Myasnikov, A. G., Kratzat, H., Hazemann, I. & Klaholz, B. P. Visualization of chemical modifications in the human 80S ribosome structure. *Nature* **551**, 472–477 (2017).

190. Zorbas, C. *et al.* The human 18S rRNA base methyltransferases DIMT1L and WBSCR22-TRMT112 but not rRNA modification are required for ribosome biogenesis. *Mol. Biol. Cell* **26**, 2080–2095 (2015).

191. Ameismeier, M., Cheng, J., Berninghausen, O. & Beckmann, R. Visualizing late states of human 40S ribosomal subunit maturation. *Nature* **558**, 249–253 (2018).

192. Greber, B. J. & Ban, N. Structure and Function of the Mitochondrial Ribosome. *Annu. Rev. Biochem.* **85**, 103–132 (2016).

193. Schmeing, T. M. & Ramakrishnan, V. What recent ribosome structures have revealed about the mechanism of translation. *Nature* **461**, 1234–1242 (2009).

194. DiMauro, S. & Davidzon, G. Mitochondrial DNA and disease. *Ann. Med.* **37**, 222–232 (2005).

195. Ott, M. & Herrmann, J. M. Co-translational membrane insertion of mitochondrially encoded proteins. *Biochim. Biophys. Acta - Mol. Cell Res.* **1803**, 767–775 (2010).

196. Stegeman, W. J., Cooper, C. S. & Avers, C. J. Physical characterization of ribosomes from purified mitochondria of yeast. *Biochem. Biophys. Res. Commun.* **39**, 69–76 (1970).

197. Koc, E. C. *et al.* The large subunit of the mammalian mitochondrial ribosome: Analysis of the complement of ribosomal proteins present. *J. Biol. Chem.* **276**, 43958–43969 (2001).

198. Koc, E. C., Burkhart, W., Blackburn, K., Moseley, A. & Spremulli, L. L. The small subunit of the mammalian mitochondrial ribosome: Identification of the full complement of ribosomal proteins present. *J. Biol. Chem.* **276**, 19363–19374 (2001).

199. Brown, A. *et al.* Structure of the large ribosomal subunit from human mitochondria. *Science* **346**, 718–722 (2014).

200. Ott, M. *et al.* Mba1, a membrane-associated ribosome receptor in mitochondria. *EMBO J.* **25**, 1603–1610 (2006).

201. Gaur, R. *et al.* A Single Mammalian Mitochondrial Translation Initiation Factor Functionally Replaces Two Bacterial Factors. *Mol. Cell* **29**, 180–190 (2008).

202. Dever, T. E. & Green, R. The elongation, termination, and recycling phases of translation in eukaryotes. *Cold Spring Harb. Perspect. Biol.* **4**, a013706 (2012).

203. Frank, J. & Agrawal, R. K. A ratchet-like inter-subunit reorganization of the ribosome during translocation. *Nature* **406**, 318–322 (2000).

204. Budkevich, T. V *et al.* Regulation of the mammalian elongation cycle by subunit rolling: a eukaryotic-specific ribosome rearrangement. *Cell* **158**, 121–31 (2014).

205. Taoka, M. *et al.* Landscape of the complete RNA chemical modifications in the human 80S ribosome. *Nucleic Acids Res.* **46**, 9289–9298 (2018).

206. Simsek, D. & Barna, M. An emerging role for the ribosome as a nexus for post-translational modifications. *Curr. Opin. Cell Biol.* **45**, 92–101 (2017).

207. Lareau, L. F., Hite, D. H., Hogan, G. J. & Brown, P. O. Distinct stages of the translation elongation cycle revealed by sequencing ribosome-protected mRNA fragments. *Elife* **2014**, 1–16 (2014).

208. Yang, Y. & Wang, Z. IRES-mediated cap-independent translation, a path leading to hidden proteome. *J. Mol. Cell Biol.* **11**, 911–919 (2019).

209. Truitt, M. L. & Ruggero, D. New frontiers in translational control of the cancer genome. *Nat. Rev. Cancer* **16**, 288–304 (2016).

210. Schuller, A. P. & Green, R. Roadblocks and resolutions in eukaryotic translation. *Nat. Rev. Mol. Cell Biol.* **19**, 526–541 (2018).

211. Kieft, J. S. Viral IRES RNA structures and ribosome interactions. *Trends Biochem. Sci.* **33**, 274–83 (2008).

212. Leppek, K., Das, R. & Barna, M. Functional 5′ UTR mRNA structures in eukaryotic translation regulation and how to find them. *Nat. Rev. Mol. Cell Biol.* **19**, 158–174 (2018).

213. Volpon, L., Osborne, M. J., Topisirovic, I., Siddiqui, N. & Borden, K. L. B. Cap-free

structure of eIF4E suggests a basis for conformational regulation by its ligands. *EMBO J.* **25**, 5138–5149 (2006).

214. Von Der Haar, T., Gross, J. D., Wagner, G. & McCarthy, J. E. G. The mRNA cap-binding protein eIF4E in post-transcriptional gene expression. *Nat. Struct. Mol. Biol.* **11**, 503–511 (2004).

215. Gross, J. D. *et al.* Ribosome loading onto the mRNA cap is driven by conformational coupling between eIF4G and eIF4E. *Cell* **115**, 739–50 (2003).

216. Marintchev, A. *et al.* Topology and Regulation of the Human eIF4A/4G/4H Helicase Complex in Translation Initiation. *Cell* **136**, 447–460 (2009).

217. LeFebvre, A. K. *et al.* Translation Initiation Factor eIF4G-1 Binds to eIF3 through the eIF3e Subunit. *J. Biol. Chem.* **281**, 22917–22932 (2006).

218. Jackson, R. J., Hellen, C. U. T. & Pestova, T. V. The mechanism of eukaryotic translation initiation and principles of its regulation. *Nat. Rev. Mol. Cell Biol.* **11**, 113–27 (2010).

219. Pestova, T. V. & Kolupaeva, V. G. The roles of individual eukaryotic translation initiation factors in ribosomal scanning and initiation codon selection. *Genes Dev.* **16**, 2906–2922 (2002).

220. Kozak, M. Structural features in eukaryotic mRNAs that modulate the initiation of translation. *J. Biol. Chem.* **266**, 19867–19870 (1991).

221. Kapp, L. D. & Lorsch, J. R. GTP-dependent Recognition of the Methionine Moiety on Initiator tRNA by Translation Factor eIF2. *J. Mol. Biol.* **335**, 923–936 (2004).

222. Unbehaun, A., Borukhov, S. I., Hellen, C. U. T. & Pestova, T. V. The 40S subunit in 48S complexes formed at the initiation codon of mRNA is bound to eukaryotic initiation factor (eIF) 3, eIF1, eIF1A, and an eIF2/GTP/Met-tRNA. *Genes Dev.* 3078–3093 (2004). doi:10.1101/gad.1255704.eIF1

223. Pestova, T. V. *et al.* The joining of ribosomal subunits in eukaryotes requires eIF5B. *Nature* **403**, 332–335 (2000).

224. Acker, M. G. *et al.* Kinetic Analysis of Late Steps of Eukaryotic Translation

Initiation. *J. Mol. Biol.* **385**, 491–506 (2009).

225. Jang, S. K. *et al.* A segment of the 5’ nontranslated region of encephalomyocarditis virus RNA directs internal entry of ribosomes during in vitro translation. *J. Virol.* **62**, 2636–2643 (1988).

226. Pelletier, J. & Sonenberg, N. Internal initiation of translation of eukaryotic mRNA directed by a sequence derived from poliovirus RNA. *Nature* **334**, 320–325 (1988).

227. Lomakin, I. B., Hellen, C. U. & Pestova, T. V. Physical association of eukaryotic initiation factor 4G (eIF4G) with eIF4A strongly enhances binding of eIF4G to the internal ribosomal entry site of encephalomyocarditis virus and is required for internal initiation of translation. *Mol. Cell. Biol.* **20**, 6019–29 (2000).

228. Kanamori, Y. & Nakashima, N. A tertiary structure model of the internal ribosome entry site (IRES) for methionine-independent initiation of translation. *RNA* **7**, 266–74 (2001).

229. Buck, C. B. *et al.* The human immunodeficiency virus type 1 gag gene encodes an internal ribosome entry site. *J. Virol.* **75**, 181–91 (2001).

230. Belsham, G. J. & Brangwyn, J. K. A region of the 5’ noncoding region of foot-and-mouth disease virus RNA directs efficient internal initiation of protein synthesis within cells: involvement with the role of L protease in translational control. *J. Virol.* **64**, 5389–5395 (1990).

231. Tsukiyama-Kohara, K., Iizuka, N., Kohara, M. & Nomoto, A. Internal ribosome entry site within hepatitis C virus RNA. *J. Virol.* **66**, 1476–1483 (1992).

232. Othman, Z. *et al.* Functional analysis of Kaposi’s sarcoma-associated herpesvirus vFLIP expression reveals a new mode of IRES-mediated translation. *Rna* **20**, 1803–1814 (2014).

233. Komar, A. A. & Hatzoglou, M. Cellular IRES-mediated translation: The war of ITAFs in pathophysiological states. *Cell Cycle* **10**, 229–240 (2011).

234. Meyer, K. D. *et al.* 5’ UTR m6A Promotes Cap-Independent Translation. *Cell* **163**, 999–1010 (2015).

235. Yang, Y. *et al.* Extensive translation of circular RNAs driven by N6-methyladenosine. *Cell Res.* **27**, 626–641 (2017).

236. Dresios, J., Chappell, S. A., Zhou, W. & Mauro, V. P. An mRNA-rRNA base-pairing mechanism for translation initiation in eukaryotes. *Nat. Struct. Mol. Biol.* **13**, 30–34 (2006).

237. Jakobsson, M. E., Małecki, J. & Falnes, P. Regulation of eukaryotic elongation factor 1 alpha (eEF1A) by dynamic lysine methylation. *RNA Biol.* **15**, 314–319 (2018).

238. Shao, S. *et al.* Decoding Mammalian Ribosome-mRNA States by Translational GTPase Complexes. *Cell* **167**, 1229-1240.e15 (2016).

239. Munro, J. B., Altman, R. B., O'Connor, N. & Blanchard, S. C. Identification of Two Distinct Hybrid State Intermediates on the Ribosome. *Mol. Cell* **25**, 505–517 (2007).

240. Agirrezabala, X. *et al.* Visualization of the Hybrid State of tRNA Binding Promoted by Spontaneous Ratcheting of the Ribosome. *Mol. Cell* **32**, 190–197 (2008).

241. Taylor, D. J. *et al.* Structures of modified eEF2.80S ribosome complexes reveal the role of GTP hydrolysis in translocation. *EMBO J.* **26**, 2421–2431 (2007).

242. Ratje, A. H. *et al.* Head swivel on the ribosome facilitates translocation by means of intra-subunit tRNA hybrid sites. *Nature* **468**, 713–716 (2010).

243. Flis, J. *et al.* tRNA Translocation by the Eukaryotic 80S Ribosome and the Impact of GTP Hydrolysis. *Cell Rep.* **25**, 2676-2688.e7 (2018).

244. Chen, C. *et al.* Allosteric vs. spontaneous exit-site (E-site) tRNA dissociation early in protein synthesis. *Proc. Natl. Acad. Sci. U. S. A.* **108**, 16980–16985 (2011).

245. Frolova, L. Y. *et al.* Mutations in the highly conserved GGQ motif of class I polypeptide release factors abolish ability of human eRF1 to trigger peptidyl-tRNA hydrolysis. *Rna* **5**, 1014–1020 (1999).

246. Frolova, L. *et al.* Eukaryotic polypeptide chain release factor eRF3 is an eRF1- and ribosome-dependent guanosine triphosphatase. *Rna* **2**, 334–341 (1996).

247. Kong, C. *et al.* Crystal structure and functional analysis of the eukaryotic class II release factor eRF3 from S. pombe. *Mol. Cell* **14**, 233–245 (2004).

248. Alkalaeva, E. Z., Pisarev, A. V., Frolova, L. Y., Kisselev, L. L. & Pestova, T. V. In Vitro Reconstitution of Eukaryotic Translation Reveals Cooperativity between Release Factors eRF1 and eRF3. *Cell* **125**, 1125–1136 (2006).

249. Barthelme, D. *et al.* Ribosome recycling depends on a mechanistic link between the FeS cluster domain and a conformational switch of the twin-ATPase ABCE1. *Proc. Natl. Acad. Sci. U. S. A.* **108**, 3228–3233 (2011).

250. Gouridis, G. *et al.* ABCE1 Controls Ribosome Recycling by an Asymmetric Dynamic Conformational Equilibrium. *Cell Rep.* **28**, 723-734.e6 (2019).

251. Preis, A. *et al.* Cryoelectron microscopic structures of eukaryotic translation termination complexes containing eRF1-eRF3 or eRF1-ABCE1. *Cell Rep.* **8**, 59–65 (2014).

252. Nürenberg-Goloub, E., Heinemann, H., Gerovac, M. & Tampé, R. Ribosome recycling is coordinated by processive events in two asymmetric ATP sites of ABCE1. *Life Sci. Alliance* **1**, 1–12 (2018).

253. Heuer, A. *et al.* Structure of the 40S-ABCE1 post-splitting complex in ribosome recycling and translation initiation. *Nat. Struct. Mol. Biol.* **24**, 453–460 (2017).

254. Andreev, D. E. *et al.* TASEP modelling provides a parsimonious explanation for the ability of a single uorf to derepress translation during the integrated stress response. *Elife* **7**, 1–20 (2018).

255. Uchiyama-Kadokura, N. *et al.* Polyamine-responsive ribosomal arrest at the stop codon of an upstream open reading frame of the AdoMetDC1 gene triggers nonsense-mediated mRNA decay in Arabidopsis thaliana. *Plant Cell Physiol.* **55**, 1556–1567 (2014).

256. Kashiwagi, K. *et al.* Crystal structure of eukaryotic translation initiation factor 2B. *Nature* **531**, 122–125 (2016).

257. Zhang, H., Wang, Y. & Lu, J. Function and Evolution of Upstream ORFs in

Eukaryotes. *Trends Biochem. Sci.* **44**, 782–794 (2019).

258. Hinnebusch, A. G. Translational regulation of GCN4 and the general amino acid control of yeast. *Annu. Rev. Microbiol.* **59**, 407–450 (2005).

259. Ivanov, I. P., Loughran, G. & Atkins, J. F. uORFs with unusual translational start codons autoregulate expression of eukaryotic ornithine decarboxylase homologs. *Proc. Natl. Acad. Sci. U. S. A.* **105**, 10079–10084 (2008).

260. Ivanov, I. P. *et al.* Polyamine Control of Translation Elongation Regulates Start Site Selection on Antizyme Inhibitor mRNA via Ribosome Queuing. *Mol. Cell* **70**, 254-264.e6 (2018).

261. Bartkoski, M. & Roizman, B. RNA synthesis in cells infected with herpes simple virus. XIII. Differences in the methylation patterns of viral RNA during the reproductive cycle. *J. Virol.* **20**, 583–588 (1976).

262. Bohnsack, K. E. & Bohnsack, M. T. Uncovering the assembly pathway of human ribosomes and its emerging links to disease. *EMBO J.* **38**, 1–20 (2019).

263. Lewis, J. D. & Tollervey, D. Like attracts like: Getting RNA processing together in the nucleus. *Science (80-.).* **288**, 1385–1389 (2000).

264. Farley-Barnes, K. I. *et al.* Diverse Regulators of Human Ribosome Biogenesis Discovered by Changes in Nucleolar Number. *Cell Rep.* **22**, 1923–1934 (2018).

265. Badertscher, L. *et al.* Genome-wide RNAi Screening Identifies Protein Modules Required for 40S Subunit Synthesis in Human Cells. *Cell Rep.* **13**, 2879–2891 (2015).

266. Tafforeau, L. *et al.* The complexity of human ribosome biogenesis revealed by systematic nucleolar screening of pre-rRNA processing factors. *Mol. Cell* **51**, 539–551 (2013).

267. O'Donohue, M. F., Choesmel, V., Faubladier, M., Fichant, G. & Gleizes, P. E. Functional dichotomy of ribosomal proteins during the synthesis of mammalian 40S ribosomal subunits. *J. Cell Biol.* **190**, 853–866 (2010).

268. Kornprobst, M. *et al.* Architecture of the 90S Pre-ribosome: A Structural View on

the Birth of the Eukaryotic Ribosome. *Cell* **166**, 380–393 (2016).

269. Zhang, L., Wu, C., Cai, G., Chen, S. & Ye, K. Stepwise and dynamic assembly of the earliest precursors of small ribosomal subunits in yeast. *Genes Dev.* **30**, 718–32 (2016).

270. De La Cruz, J., Karbstein, K. & Woolford, J. L. Functions of ribosomal proteins in assembly of eukaryotic ribosomes in vivo. *Annu. Rev. Biochem.* **84**, 93–129 (2015).

271. Nicolas, E. *et al.* Involvement of human ribosomal proteins in nucleolar structure and p53-dependent nucleolar stress. *Nat. Commun.* **7**, (2016).

272. Watkins, N. J. & Bohnsack, M. T. The box C/D and H/ACA snoRNPs: Key players in the modification, processing and the dynamic folding of ribosomal RNA. *Wiley Interdiscip. Rev. RNA* **3**, 397–414 (2012).

273. Aubert, M., O'donohue, M. F., Lebaron, S. & Gleizes, P. E. Pre-ribosomal RNA processing in human cells: From mechanisms to congenital diseases. *Biomolecules* **8**, (2018).

274. Sloan, K. E., Bohnsack, M. T., Schneider, C. & Watkins, N. J. The roles of SSU processome components and surveillance factors in the initial processing of human ribosomal RNA. *RNA* **20**, 540–550 (2014).

275. Tomecki, R., Labno, A., Drazkowska, K., Cysewski, D. & Dziembowski, A. hUTP24 is essential for processing of the human rRNA precursor at site A1but not at site A0. *RNA Biol.* **12**, 1010–1029 (2015).

276. Wells, G. R. *et al.* The ribosome biogenesis factor yUtp23/hUTP23 coordinates key interactions in the yeast and human pre-40S particle and hUTP23 contains an essential PIN domain. *Nucleic Acids Res.* **45**, 4796–4809 (2017).

277. Sloan, K. E. *et al.* Both endonucleolytic and exonucleolytic cleavage mediate ITS1 removal during human ribosomal RNA processing. *J. Cell Biol.* **200**, 577–588 (2013).

278. Wurm, J. P. *et al.* The ribosome assembly factor Nep1 responsible for Bowen-Conradi syndrome is a pseudouridine-N1-specific methyltransferase. *Nucleic*

Acids Res. **38**, 2387–2398 (2010).

279. Meyer, B. *et al.* Ribosome biogenesis factor Tsr3 is the aminocarboxypropyl transferase responsible for 18S rRNA hypermodification in yeast and humans. *Nucleic Acids Res.* **44**, 4304–4316 (2016).

280. Ito, S. *et al.* Human NAT10 is an ATP-dependent RNA acetyltransferase responsible for N4-acetylcytidine formation in 18 S ribosomal RNA (rRNA). *J. Biol. Chem.* **289**, 35724–30 (2014).

281. Haag, S., Kretschmer, J. & Bohnsack, M. T. WBSCR22/Merm1 is required for late nuclear pre-ribosomal RNA processing and mediates N 7 -methylation of G1639 in human 18S rRNA. *RNA* **21**, 180–187 (2015).

282. Waku, T. *et al.* NML-mediated rRNA base methylation links ribosomal subunit formation to cell proliferation in a p53-dependent manner. *J. Cell Sci.* **129**, 2382–2393 (2016).

283. Schosserer, M. *et al.* Methylation of ribosomal RNA by NSUN5 is a conserved mechanism modulating organismal lifespan. *Nat. Commun.* **6**, (2015).

284. Bourgeois, G. *et al.* Eukaryotic rRNA modification by yeast 5- methylcytosine-methyltransferases and human proliferation-associated antigen p120. *PLoS One* **10**, 1–16 (2015).

285. Ma, H. *et al.* N 6-Methyladenosine methyltransferase ZCCHC4 mediates ribosomal RNA methylation. *Nat. Chem. Biol.* **15**, 88–94 (2019).

286. Warda, A. S. *et al.* Effects of the Bowen-Conradi syndrome mutation in EMG1 on its nuclear import, stability and nucleolar recruitment. *Hum. Mol. Genet.* **25**, 5353–5364 (2016).

287. Montellese, C. *et al.* Poly(A)-specific ribonuclease is a nuclear ribosome biogenesis factor involved in human 18S rRNA maturation. *Nucleic Acids Res.* **45**, 6822–6836 (2017).

288. Landry-Voyer, A.-M. *et al.* Human PDCD2L Is an Export Substrate of CRM1 That Associates with 40S Ribosomal Subunit Precursors. *Mol. Cell. Biol.* **36**, 3019–3032

(2016).

289. Zemp, I. *et al.* Distinct cytoplasmic maturation steps of 40S ribosomal subunit precursors require hRio2. *J. Cell Biol.* **185**, 1167–1180 (2009).

290. Lebaron, S. *et al.* Proofreading of pre-40S ribosome maturation by a translation initiation factor and 60S subunits. *Nat. Struct. Mol. Biol.* **19**, 744–753 (2012).

291. Strunk, B. S., Novak, M. N., Young, C. L. & Karbstein, K. A translation-like cycle is a quality control checkpoint for maturing 40S ribosome subunits. *Cell* **150**, 111–21 (2012).

292. Leidig, C. *et al.* 60S ribosome biogenesis requires rotation of the 5S ribonucleoprotein particle. *Nat. Commun.* **5**, (2014).

293. Gupta, V. & Warner, J. R. Ribosome-omics of the human ribosome. *RNA* **20**, 1004–1013 (2014).

294. Ma, C. *et al.* Structural snapshot of cytoplasmic pre-60S ribosomal particles bound by Nmd3, Lsg1, Tif6 and Reh1. *Nat. Struct. Mol. Biol.* **24**, 214–220 (2017).

295. Lo, K. Y. *et al.* Defining the pathway of cytoplasmic maturation of the 60S ribosomal subunit. *Mol. Cell* **39**, 196–208 (2010).

296. Schillewaert, S., Wacheul, L., Lhomme, F. & Lafontaine, D. L. J. The Evolutionarily Conserved Protein LAS1 Is Required for Pre-rRNA Processing at Both Ends of ITS2. *Mol. Cell. Biol.* **32**, 430–444 (2012).

297. Finkbeiner, E., Haindl, M., Raman, N. & Muller, S. SUMO routes ribosome maturation. *Nucleus* **2**, 527–532 (2011).

298. Raman, N., Weir, E. & Müller, S. The AAA ATPase MDN1 Acts as a SUMO-Targeted Regulator in Mammalian Pre-ribosome Remodeling. *Mol. Cell* **64**, 607–615 (2016).

299. Schilders, G., van Dijk, E. & Pruijn, G. J. M. C1D and hMtr4p associate with the human exosome subunit PM/Scl-100 and are involved in pre-rRNA processing. *Nucleic Acids Res.* **35**, 2564–2572 (2007).

300. Couté, Y. *et al.* ISG20L2, a novel vertebrate nucleolar exoribonuclease involved in

ribosome biogenesis. *Mol. Cell. Proteomics* **7**, 546–559 (2008).

301. Wang, M. & Pestov, D. G. 5′-end surveillance by Xrn2 acts as a shared mechanism for mammalian pre-rRNA maturation and decay. *Nucleic Acids Res.* **39**, 1811–1822 (2011).

302. Malyutin, A. G., Musalgaonkar, S., Patchett, S., Frank, J. & Johnson, A. W. Nmd3 is a structural mimic of eIF5A, and activates the cpGTPase Lsg1 during 60S ribosome biogenesis. *EMBO J.* **36**, 854–868 (2017).

303. Bai, B., Moore, H. M. & Laiho, M. CRM1 and its ribosome export adaptor NMD3 localize to the nucleolus and affect rRNA synthesis. *Nucleus* **4**, (2013).

304. Ansel, K. M. *et al.* Mouse Eri1 interacts with the ribosome and catalyzes 5.8S rRNA processing. *Nat. Struct. Mol. Biol.* **15**, 523–530 (2008).

305. Kappel, L. *et al.* Rlp24 activates the AAA-ATPase Drg1 to initiate cytoplasmic pre-60S maturation. *J. Cell Biol.* **199**, 771–782 (2012).

306. Weis, F. *et al.* Mechanism of eIF6 release from the nascent 60S ribosomal subunit. *Nat. Struct. Mol. Biol.* **22**, 914–919 (2015).

307. Gartmann, M. *et al.* Mechanism of eIF6-mediated inhibition of ribosomal subunit joining. *J. Biol. Chem.* **285**, 14848–14851 (2010).

308. Finch, A. J. *et al.* Uncoupling of GTP hydrolysis from eIF6 release on the ribosome causes shwachman-diamond syndrome. *Genes Dev.* **25**, 917–929 (2011).

309. Jha, S. *et al.* Trans-kingdom mimicry underlies ribosome customization by a poxvirus kinase. *Nature* **546**, 651–655 (2017).

310. Kondrashov, N. *et al.* Ribosome-mediated specificity in Hox mRNA translation and vertebrate tissue patterning. *Cell* **145**, 383–397 (2011).

311. Ferretti, M. B., Ghalei, H., Ward, E. A., Potts, E. L. & Karbstein, K. Rps26 directs mRNA-specific translation by recognition of Kozak sequence elements. *Nat. Struct. Mol. Biol.* **24**, (2017).

312. García-Marcos, A. *et al.* Yeast ribosomal stalk heterogeneity in vivo shown by two-

photon FCS and molecular brightness analysis. *Biophys. J.* **94**, 2884–2890 (2008).

313. Hebras, J., Krogh, N., Marty, V., Nielsen, H. & Cavaillé, J. Developmental changes of rRNA ribose methylations in the mouse. *RNA Biol.* **17**, 150–164 (2020).

314. Moore, K. S. & von Lindern, M. RNA binding proteins and regulation of mRNA translation in erythropoiesis. *Front. Physiol.* **9**, 1–17 (2018).

315. Mustoe, A. M., Corley, M., Laederach, A. & Weeks, K. M. Messenger RNA Structure Regulates Translation Initiation: A Mechanism Exploited from Bacteria to Humans. *Biochemistry* **57**, 3537–3539 (2018).

316. Statello, L., Guo, C. J., Chen, L. L. & Huarte, M. Gene regulation by long non-coding RNAs and its biological functions. *Nat. Rev. Mol. Cell Biol.* **22**, 96–118 (2021).

317. Crick, F. H. Biochemical activities of nucleic acids. The present position of the coding problem. *Brookhaven Symp. Biol.* **12**, 35–9 (1959).

318. Palade, G. E. Microsomes and ribonucleoproteins. In Microsomal particles and protein synthesis. *New York Washingt. Acad. Sci.* (1958).

319. Mauro, V. P. & Edelman, G. M. The ribosome filter hypothesis. *Proc. Natl. Acad. Sci. U. S. A.* **99**, 12031–6 (2002).

320. Yewdell, J. W. & Nicchitta, C. V. The DRiP hypothesis decennial: support, controversy, refinement and extension. *Trends Immunol.* **27**, 368–373 (2006).

321. Komili, S., Farny, N. G., Roth, F. P. & Silver, P. A. Functional specificity among ribosomal proteins regulates gene expression. *Cell* **131**, 557–71 (2007).

322. Genuth, N. R. & Barna, M. The Discovery of Ribosome Heterogeneity and Its Implications for Gene Regulation and Organismal Life. *Mol. Cell* **71**, 364–374 (2018).

323. Xue, S. & Barna, M. Specialized ribosomes: a new frontier in gene regulation and organismal biology. *Nat. Rev. Mol. Cell Biol.* **13**, 355–369 (2012).

324. Norris, K., Hopes, T. & Aspden, J. L. Ribosome heterogeneity and specialization in development. *Wiley Interdiscip. Rev. RNA* 1–23 (2021). doi:10.1002/wrna.1644

325. Narla, A. & Ebert, B. L. Ribosomopathies: Human disorders of ribosome dysfunction. *Blood* **115**, 3196–3205 (2010).

326. Twite, M. D., Stenquist, S. & Ing, R. J. Williams syndrome. *Paediatr. Anaesth.* **29**, 483–490 (2019).

327. Baxter, M. *et al.* Cardiac mitochondrial function depends on BUD23 mediated ribosome programming. *Elife* **9**, 1–26 (2020).

328. Boria, I. *et al.* The ribosomal basis of Diamond-Blackfan Anemia: mutation and database update. *Hum. Mutat.* **31**, 1269–79 (2010).

329. Ebert, B. L. *et al.* Identification of RPS14 as a 5q- syndrome gene by RNA interference screen. *Nature* **451**, 335–339 (2008).

330. Bolze, A. *et al.* Haploinsufficiency in Humans with Isolated Congenital Asplenia. **340**, 976–979 (2013).

331. Paolini, N. A. *et al.* A Ribosomopathy Reveals Decoding Defective Ribosomes Driving Human Dysmorphism. *Am. J. Hum. Genet.* **100**, 506–522 (2017).

332. Selmi, C. *et al.* X chromosome gene methylation in peripheral lymphocytes from monozygotic twins discordant for scleroderma. *Clin. Exp. Immunol.* **169**, 253–262 (2012).

333. Armistead, J. *et al.* Mutation of a Gene Essential for Ribosome Biogenesis, EMG1, Causes Bowen-Conradi Syndrome. *Am. J. Hum. Genet.* **84**, 728–739 (2009).

334. Heiss, N. S. *et al.* X-linked dyskeratosis congenita is caused by mutations in a highly conserved gene with putative nucleolar functions. *Nat. Genet.* **19**, 32–8 (1998).

335. Vulliamy, T. *et al.* The RNA component of telomerase is mutated in autosomal dominant dyskeratosis congenita. *Nature* **413**, 432–435 (2001).

336. Vulliamy, T. *et al.* Mutations in the telomerase component NHP2 cause the premature ageing syndrome dyskeratosis congenita. *Proc. Natl. Acad. Sci. U. S. A.* **105**, 8073–8078 (2008).

337. M, R. *et al.* Mutations in the RNA component of RNase MRP cause a pleiotropic

human disease, cartilage-hair hypoplasia. *Cell* **104**, 195–203 (2001).

338. Freed, E. F. & Baserga, S. J. The C-terminus of Utp4, mutated in childhood cirrhosis, is essential for ribosome biogenesis. *Nucleic Acids Res.* **38**, 4798–4806 (2010).

339. Freed, E. F., Prieto, J. L., McCann, K. L., McStay, B. & Baserga, S. J. NOL11, Implicated in the Pathogenesis of North American Indian Childhood Cirrhosis, Is Required for Pre-rRNA Transcription and Processing. *PLoS Genet.* **8**, (2012).

340. Zanni, G. *et al.* A Novel Mutation in RPL10 (Ribosomal Protein L10) Causes X-Linked Intellectual Disability, Cerebellar Hypoplasia, and Spondylo-Epiphyseal Dysplasia. *Hum. Mutat.* **36**, 1155–8 (2015).

341. Barlow, J. L. *et al.* New insights into 5q- syndrome as a ribosomopathy. *Cell Cycle* **9**, 4286–4293 (2010).

342. Jones, N. C. *et al.* Prevention of the neurocristopathy Treacher Collins syndrome through inhibition of p53 function. *Nat. Med.* **14**, 125–133 (2008).

343. Khajuria, R. K. *et al.* Ribosome Levels Selectively Regulate Translation and Lineage Commitment in Human Hematopoiesis. *Cell* **173**, 90-103.e19 (2018).

344. Alexander, T., Nolte, C. & Krumlauf, R. Hox genes and segmentation of the hindbrain and axial skeleton. *Annu. Rev. Cell Dev. Biol.* **25**, 431–456 (2009).

345. Xue, S. *et al.* RNA regulons in Hox 5' UTRs confer ribosome specificity to gene regulation. *Nature* **517**, 33–8 (2015).

346. Nadano, D., Notsu, T., Matsuda, T. & Sato, T. A. A human gene encoding a protein homologous to ribosomal protein L39 is normally expressed in the testis and derepressed in multiple cancer cells. *Biochim. Biophys. Acta - Gene Struct. Expr.* **1577**, 430–436 (2002).

347. Shi, Z. & Barna, M. Translating the Genome in Time and Space: Specialized Ribosomes, RNA Regulons, and RNA-Binding Proteins. *Annu. Rev. Cell Dev. Biol.* **31**, 31–54 (2015).

348. Shi, Z. *et al.* Heterogeneous Ribosomes Preferentially Translate Distinct Subpools

of mRNAs Genome-wide. *Mol. Cell* **67**, 71-83.e7 (2017).

349. Babaian, A. *et al.* Loss of m1acp3Ψ Ribosomal RNA Modification Is a Major Feature of Cancer. *Cell Rep.* **31**, 107611 (2020).

350. Lee, A. S.-Y., Burdeinick-Kerr, R. & Whelan, S. P. J. A ribosome-specialized translation initiation pathway is required for cap-dependent translation of vesicular stomatitis virus mRNAs. *Proc. Natl. Acad. Sci. U. S. A.* **110**, 324–9 (2013).

351. Nakamura, H. *et al.* Global Changes in Kaposi's Sarcoma-Associated Virus Gene Expression Patterns following Expression of a Tetracycline-Inducible Rta Transactivator Global Changes in Kaposi ' s Sarcoma-Associated Virus Gene Expression Patterns following Expression of a Tet. *J. Virol.* **77**, 4205–4220 (2003).

352. Scheres, S. H. W. Semi-automated selection of cryo-EM particles in RELION-1.3. *J. Struct. Biol.* **189**, 114–122 (2015).

353. Bantscheff, M., Lemeer, S., Savitski, M. M. & Kuster, B. Quantitative mass spectrometry in proteomics: Critical review update from 2007 to the present. *Anal. Bioanal. Chem.* **404**, 939–965 (2012).

354. Thompson, A. *et al.* Tandem mass tags: a novel quantification strategy for comparative analysis of complex protein mixtures by MS/MS. *Anal. Chem.* **75**, 1895–904 (2003).

355. Hirsch, C. A. & Hiatt, H. H. Turnover of liver ribosomes in fed and in fasted rats. *J. Biol. Chem.* **241**, 5936–5940 (1966).

356. Nikolov, E. N., Dabeva, M. D. & Nikolov, T. K. Turnover of ribosomes in regenerating rat liver. *Int. J. Biochem.* **15**, 1255–1260 (1983).

357. Wyler, E. *et al.* Tandem affinity purification combined with inducible shRNA expression as a tool to study the maturation of macromolecular assemblies. *RNA* **17**, 189–200 (2011).

358. Sanghai, Z. A. *et al.* Modular assembly of the nucleolar pre-60S ribosomal subunit. *Nature* **556**, 126–129 (2018).

359. Liang, X. *et al.* Structural snapshots of human pre-60S ribosomal particles before

and after nuclear export. *Nat. Commun.* **11**, 1–14 (2020).

360. Slavov, N., Semrau, S., Airoldi, E., Budnik, B. & van Oudenaarden, A. Differential Stoichiometry among Core Ribosomal Proteins. *Cell Rep.* **13**, 865–873 (2015).

361. Van De Waterbeemd, M. *et al.* Dissecting ribosomal particles throughout the kingdoms of life using advanced hybrid mass spectrometry methods. *Nat. Commun.* **9**, (2018).

362. Wild, T. *et al.* A protein inventory of human ribosome biogenesis reveals an essential function of exportin 5 in 60S subunit export. *PLoS Biol.* **8**, e1000522 (2010).

363. Thul, P. J. *et al.* A subcellular map of the human proteome. *Science (80-.).* **356**, (2017).

364. Létoquart, J. *et al.* Structural and functional studies of Bud23-Trm112 reveal 18S rRNA N7-G1575 methylation occurs on late 40S precursor ribosomes. *Proc. Natl. Acad. Sci. U. S. A.* **111**, E5518–E5526 (2014).

365. Sharma, S. & Lafontaine, D. L. J. 'View From A Bridge': A New Perspective on Eukaryotic rRNA Base Modification. *Trends Biochem. Sci.* **40**, 560–575 (2015).

366. Tiedemann, R. E. *et al.* Identification of molecular vulnerabilities in human multiple myeloma cells by RNA interference lethality screening of the druggable genome. *Cancer Res.* **72**, 757–68 (2012).

367. Nakazawa, Y., Arai, H. & Fujita, N. The novel metastasis promoter Merm1/Wbscr22 enhances tumor cell survival in the vasculature by suppressing Zac1/p53-dependent apoptosis. *Cancer Res.* **71**, 1146–1155 (2011).

368. Krishnan, A. *et al.* Oncogenic Actions of SKP2 Involves Deregulation of CDK1 Turnover Mediated by FOXM1. *J. Cell. Biochem.* **118**, 797–807 (2017).

369. Sun, R. *et al.* Kinetics of Kaposi's Sarcoma-Associated Herpesvirus Gene Expression. *J. Virol.* **73**, 2232–2242 (1999).

370. Saveliev, A. K., Zhu, F. X. & Yuan, Y. Transcription mapping and expression patterns of genes in the major immediate-early region of Kaposi's sarcoma-

associated herpesvirus. *Virology* **299**, 301–314 (2002).

371. Yang, J. *et al.* Mapping of complete set of ribose and base modifications of yeast rRNA by RP-HPLC and mung bean nuclease assay. *PLoS One* **11**, 1–18 (2016).

372. Ingolia, N. T., Ghaemmaghami, S., Newman, J. R. S. & Weissman, J. S. Genome-wide analysis in vivo of translation with nucleotide resolution using ribosome profiling. *Science (80-.).* **324**, 218–223 (2009).

373. Ingolia, N. T., Hussmann, J. A. & Weissman, J. S. Ribosome profiling: Global views of translation. *Cold Spring Harb. Perspect. Biol.* **11**, 1–20 (2019).

374. Mulvey, M., Arias, C. & Mohr, I. Maintenance of Endoplasmic Reticulum (ER) Homeostasis in Herpes Simplex Virus Type 1-Infected Cells through the Association of a Viral Glycoprotein with PERK, a Cellular ER Stress Sensor. *J. Virol.* **81**, 3377–3390 (2007).

375. Harb, M. *et al.* Nuclear Localization of Cytoplasmic Poly(A)-Binding Protein upon Rotavirus Infection Involves the Interaction of NSP3 with eIF4G and RoXaN. *J. Virol.* **82**, 11283–11293 (2008).

376. Walsh, D. & Mohr, I. Viral subversion of the host protein synthesis machinery. *Nat. Rev. Microbiol.* **9**, 860–875 (2011).

377. Castelló, A. *et al.* Regulation of host translational machinery by African swine fever virus. *PLoS Pathog.* **5**, (2009).

378. Zhang, F., Moon, A., Childs, K., Goodbourn, S. & Dixon, L. K. The African Swine Fever Virus DP71L Protein Recruits the Protein Phosphatase 1 Catalytic Subunit To Dephosphorylate eIF2α and Inhibits CHOP Induction but Is Dispensable for These Activities during Virus Infection. *J. Virol.* **84**, 10681–10689 (2010).

379. Martinez-Salas, E., Francisco-Velilla, R., Fernandez-Chamorro, J. & Embarek, A. M. Insights into structural and mechanistic features of viral IRES elements. *Front. Microbiol.* **8**, 1–15 (2018).

380. Mizuno, C. M. *et al.* Numerous cultivated and uncultivated viruses encode ribosomal proteins. *Nat. Commun.* **10**, (2019).

381. Huber, A. *et al.* Sch9 regulates ribosome biogenesis via Stb3, Dot6 and Tod6 and the histone deacetylase complex RPD3L. *EMBO J.* **30**, 3052–3064 (2011).

382. Teufel, A. I., Liu, W., Draghi, J. A., Cameron, C. E. & Wilke, C. O. Modeling poliovirus replication dynamics from live time-lapse single-cell imaging data. *Sci. Rep.* **11**, 9622 (2021).

383. Mintseris, J. & Gygi, S. P. High-density chemical cross-linking for modeling protein interactions. *Proc. Natl. Acad. Sci. U. S. A.* **117**, 93–102 (2020).

384. Sloan, K. E. *et al.* Tuning the ribosome: The influence of rRNA modification on eukaryotic ribosome biogenesis and function. *RNA Biology* **14**, 1138–1152 (2017).

385. Yan, D. *et al.* Knockdown of Merm1/Wbscr22 attenuates sensitivity of H460 non-small cell lung cancer cells to SN-38 and 5-FU without alteration to p53 expression levels. *Mol. Med. Rep.* **11**, 295–302 (2015).

386. Gabaev, I., Williamson, J. C., Crozier, T. W. M., Schulz, T. F. & Lehner, P. J. Quantitative Proteomics Analysis of Lytic KSHV Infection in Human Endothelial Cells Reveals Targets of Viral Immune Modulation. *Cell Rep.* **33**, 108249 (2020).

387. Li, D. & Swaminathan, S. Human IFIT proteins inhibit lytic replication of KSHV: A new feed-forward loop in the innate immune system. *PLoS Pathog.* **15**, 1–27 (2019).

388. Schulz, J. *et al.* Loss-of-function uORF mutations in human malignancies. *Sci. Rep.* **8**, 1–10 (2018).

389. Calvo, S. E., Pagliarini, D. J. & Mootha, V. K. Upstream open reading frames cause widespread reduction of protein expression and are polymorphic among humans. *Proc. Natl. Acad. Sci. U. S. A.* **106**, 7507–7512 (2009).

390. Kulkarni, S. D. *et al.* Temperature-dependent regulation of upstream open reading frame translation in S. cerevisiae. *BMC Biol.* **17**, 1–27 (2019).

391. Moro, S. G., Hermans, C., Ruiz-Orera, J. & Albà, M. M. Impact of uORFs in mediating regulation of translation in stress conditions. *BMC Mol. Cell Biol.* **22**, 1–13 (2021).

392. Guenther, U. *et al.* The helicase Ded1p controls use of near-cognate translation initiation codons in 5' UTRs. *Nature* **559**, 130–134 (2018).

393. Murat, P. *et al.* RNA G-quadruplexes at upstream open reading frames cause DHX36- and DHX9-dependent translation of human mRNAs. *Genome Biol.* **19**, 1–24 (2018).

394. Vassilenko, K. S., Alekhina, O. M., Dmitriev, S. E., Shatsky, I. N. & Spirin, A. S. Unidirectional constant rate motion of the ribosomal scanning particle during eukaryotic translation initiation. *Nucleic Acids Res.* **39**, 5555–5567 (2011).

395. Wu, T. T. *et al.* Construction and characterization of an infectious murine gammaherpesivrus-68 bacterial artificial chromosome. *J. Biomed. Biotechnol.* **2011**, (2011).

396. Pelletier, J., Thomas, G. & Volarević, S. Ribosome biogenesis in cancer: new players and therapeutic avenues. *Nat. Rev. Cancer* **18**, 51–63 (2017).

397. Arkin, M. R., Tang, Y. & Wells, J. A. Small-molecule inhibitors of protein-protein interactions: Progressing toward the reality. *Chem. Biol.* **21**, 1102–1114 (2014).

398. Hughes, D. J. *et al.* Generation of specific inhibitors of SUMO-1- and SUMO-2/3-mediated protein-protein interactions using Affimer (Adhiron) technology. *Sci. Signal.* **10**, 1–14 (2017).

399. Celis, S. *et al.* Query-guided protein-protein interaction inhibitor discovery. *Chem. Sci.* **12**, 4753–4762 (2021).